

Experimental Characterization

of

Effervescent Atomization

HAMED FARSHCHI TABRIZI

A Thesis

In

The Department of

Mechanical and Industrial Engineering

Presented in Partial Fulfillment of the Requirements

for the Degree of Master of Applied Science (Mechanical Engineering) at

Concordia University

Montreal, Quebec, Canada

July 2013

©HAMED FARSHCHI TABRIZI

**CONCORDIA UNIVERSITY
SCHOOL OF GRADUATE STUDIES**

This is to certify that the thesis prepared,

By: **HAMED FARSHCHI TABRIZI**

Entitled: **“Experimental Characterization of Effervescent Atomization”**

and submitted in partial fulfillment of the requirements for the degree of

Master of Applied Science (Mechanical Engineering)

complies with the regulations of the University and meets the accepted standards with respect to originality and quality.

Signed by the Final Examining Committee:

Dr. M. Chen _____ Chair

Dr. H. D. Ng _____ Examiner

Dr. F. Haghghat _____ Examiner
Building, Civil & Environmental Engineering External

Dr. A. Dolatabadi _____ Supervisor

Approved by: _____

Dr. S. Narayanswamy, MASc Program Director
Department of Mechanical and Industrial Engineering

Dr. Christopher Trueman, Interim Dean
Faculty of Engineering & Computer Science

Date _____

Abstract

The atomization is a process widely used in aerospace, combustion, or thermal spray coating, and is controllable by adopting different fluids as well as by retrofitting nozzle geometry. Desired characteristics of atomized fluid radically depend on the application of the spraying process which could be achieved by the appropriate selection of the nozzle, as well as changing the operating conditions. The objective of this study is experimental investigation of the atomization process by an effervescent nozzle for a variety of fluids where there is a lack of experimental knowledge.

Four different liquids were taken: distilled water, pure glycerol, water-glycerol aqueous solution and suspensions. The suspension is prepared by an optimized proportion for each case in order to mitigate the sedimentation and clogging of suspended beads. We determined the properties of the atomized fluids in accordance to the commonly used quantities in practical applications. Beside the rheology analyses of the fluids, three types of characterization experiments such as shadowgraphs, PIV and PDPA were conducted. Firstly, shadowgraphs were captured and the overall structures of spraying regions were observed. Accordingly, PIV and PDPA data were provided, consisting of a velocity profile in different operating conditions as well as distributions of a droplets' diameter.

The main characteristics of atomized fluids are velocity profiles, droplet size distributions, spray cone angle, and breakup lengths. These characteristics with dimensionless variables, namely Gas to Liquid Ratios (GLRs), are calculated and compared. It was found that varied values of dynamic viscosities and surface tension values have effects on the atomization affecting breakup lengths and droplet size distributions. Various recommendations were provided regarding the experimental results and future works.

Acknowledgments

I would like to express my sincere thanks to my research supervisor Dr. Dolatabadi for patiently and constantly encouraging me throughout the entire program of my master degree. His advices and suggestions during my studies were always helpful. I also would like to express my thanks to NSERC for financially supporting this thesis.

I consider myself very fortunate that I got opportunity to work with other professors namely: Dr. Wood-Adams, Dr. Mulligan and Dr. Wüthrich. They authorized me to use their lab and even asked their staff namely Ms. Claire Therrien or former students to help me while conducting my experiments. I shall always cherish my association with them.

I visited and did a few experiments at University of Toronto under supervision of Dr. Ashgriz for a short period of time. I would like to thank Prof. Ashgriz and Prof. Chandra for their collaborations in fulfillment of my thesis.

I am grateful to KEYENCE incorporation of Canada who provided their Digital microscopy system for analyses of the complex fluids used in this thesis. I wish to thank to their helpful staff and their department for being incorporation with me. I also wish to thank to PerkinElmer incorporation of Toronto for doing PDPA test in Dr. Dolatabadi's multiphase lab which led to improvements of my experiment methodology.

Lot of credit for making this period golden goes to my dear family, specially my Mother who paved the path for me to be able to come to Canada and resume my studies here. Furthermore, my dear fiancée Ms. Lily Tandel and her helpful family who stood behind me as a strong support and their encouragement were really helpful for me to concentrate on my work. I owe much of my success to them.

I thank all my friends namely Niyusha Samedi, Khalid Koraitem, Ehsan Farvardin, Mohsen Najafi, Hamze Nattaj, and all others whose names might be missing, for helping me during my work. I hope they will accept my apology if I have hurt anybody knowingly or unknowingly during this period.

Hamed Farshchi Tabrizi

Table of Contents

| | |
|---|------|
| Abstract..... | iii |
| Table of Contents..... | vi |
| Table of Figure: | viii |
| Nomenclatures..... | xi |
| 1. Introduction | 1 |
| 1.1. Background and Motivation..... | 1 |
| 1.2. Atomization | 5 |
| 1.3. Classification of Twin-Fluid Atomizers | 8 |
| 1.3.1. Twin-fluid Atomizer..... | 8 |
| 1.3.2. Air-blast and Air-assist Atomizers | 8 |
| 1.3.3. Effervescent Atomizer..... | 10 |
| 1.4. Effective Parameters in Effervescent Atomization | 12 |
| 1.4.1. Geometry..... | 12 |
| 1.4.2. Viscosity and Surface Tension..... | 13 |
| 1.4.3. Suspension Fluids | 17 |
| 1.5. Objectives | 23 |
| 2. Experimental Methodologies..... | 24 |
| 2.1. Atomizer Apparatus and Setups | 24 |
| 2.2. Fluids' Properties..... | 26 |
| 2.2.1. Suspension Preparation & Analyses | 27 |
| 2.2.2. Viscosity | 31 |
| 2.2.3. Surface Tension | 33 |
| 2.3. Operating Conditions of Atomization..... | 36 |
| 2.4. Shadowgraphs..... | 37 |
| 2.5. Optical Patternation | 38 |
| 2.6. Particle Image Velocimetry (PIV)..... | 41 |
| 2.7. Phase-Doppler Particle Analyzer (PDPA)..... | 49 |
| 3. Results and Discussions..... | 61 |
| 3.1. Internal Flow Visualizations..... | 61 |
| 3.2. External Flow Visualizations..... | 68 |
| 3.3. Optical Patternation | 73 |
| 3.4. PIV and PDPA Analyses..... | 76 |
| 4. Closure..... | 88 |

| | |
|---|----|
| 4.1. Summary..... | 88 |
| 4.2. Conclusions | 91 |
| 4.3. Future works and Recommendations | 92 |
| Bibliography | 95 |
| Apendix | |

Table of Figures:

| | | |
|-------------|---|----|
| Figure 1-1 | Various atomizations a) rain droplets [2], b) shower flow [3], c) agriculture spray [4], d) AP&W JT15D turbofan engine [5], e) Gas turbine engine [6] | 2 |
| Figure 1-2 | Suspension Plasma Spray coating setup (SPS) [7] | 4 |
| Figure 1-3 | Various swirl-fluid atomizers a) axial, b) tangential flow [9] | 6 |
| Figure 1-4 | Rotary nozzle spray plume [9] | 7 |
| Figure 1-5 | Twin-fluid atomizer, a) schematic and b) industrial version [9] | 9 |
| Figure 1-6 | Various external flow patterns by twin-fluid atomizers with different nozzle geometries, a) full-cone, b) shear jet and c) hollow cone spray [9] | 9 |
| Figure 1-7 | Inside-out type of Effervescent nozzle design; generates bubbles by aeration into mixing chamber, and bursts of trapped bubbles at the nozzle exit [7] | 11 |
| Figure 1-8 | Atomizing gas viscosity variation effects on atomization features [23] | 13 |
| Figure 1-9 | Effects of viscosity and gas flow rate on atomizing properties [25] | 15 |
| Figure 1-10 | Suspended particles chaotic dynamics due to changed viscosity at each time interval: wakes behind the particles affects particle's motion (t =time unit) [30] | 18 |
| Figure 1-11 | Force balance of suspended solid particle in fluid; F_d : Drag, F_b : buoyancy, and F_w : Weight forces, U : Mean Velocity, R : Equivalent radius [30] | 19 |
| Figure 1-12 | Different bindings of suspension fluid affecting surface tension [33] | 22 |
| Figure 2-1 | Schematic of experimental setup | 24 |
| Figure 2-2 | a) Effervescent geometry, b) image of the transparent effervescent | 26 |
| Figure 2-3 | a) Particle size analyzer, b) Dynamic Scattering Light technique | 28 |
| Figure 2-4 | a) Micron sized spherical glass beads | 29 |
| Figure 2-5 | a) Glass beads suspended in the solution | 29 |
| Figure 2-6 | a) Motorized digital microscope, capturing 2-D images of micro glass beads suspended in solution fluid with particle sizes of b) 70-90 μm , c) 20-30 μm | 31 |
| Figure 2-7 | a) Modular Compact Rheometer model: MCR 500 by Physica, b) adjusting cylinders, c) suspension under shear forces by rotation of inner cylinder | 33 |
| Figure 2-8 | a) Tensiometer apparatus b) fluid's surface tension measurements | 34 |
| Figure 2-9 | a) Imaging setup of liquid's droplet, b) various phases affecting equilibrium contact angle and c) glass bead suspension sessile droplet | 35 |
| Figure 2-10 | a) Schematic of shadowgraphs setup, b) shadowgraphs setup by high speed camera and the nozzle installed on a stand | 37 |
| Figure 2-11 | Shadowgraphs of bubbly flow regime inside effervescent nozzle | 38 |
| Figure 2-12 | a) Optical patterning setup off-axis PIV, b) spray patterning | 39 |
| Figure 2-13 | Off-axis PIV De-warping process, a) alignment target image, b) target dots detection, c) spatial meshing of target, c) up to 99% spatial perspective corection | 40 |
| Figure 2-14 | Schematic of the PIV setup | 41 |
| Figure 2-15 | Schematic of PIV interrogation regions for velocity measurements | 42 |
| Figure 2-16 | Detection of light intensity reflected by droplets [41] | 45 |

| | |
|--|----|
| Figure 2-17 a) Light intensity contour of captured images b) subtraction of background noise by cross-correlation of the detected light contours | 46 |
| Figure 2-18 Spray velocity vector field, a) without elimination and b) after elimination of spurious vectors using Median of Median selection Algorithm | 48 |
| Figure 2-19 a) PDPA analyzing system and b) PDPA setup main components | 49 |
| Figure 2-20 PDPA velocity measurements mechanism a) probe volume, b) four laser beams focused on a point of study on spray plume..... | 50 |
| Figure 2-21 a) Optical receiver, b) probe volume fringe pattern snapshot from receiver's inside detecting dark and light zones regarding spray positive direction, c) schematic of fringe pattern motion formed by laser beams with known wave lengths..... | 51 |
| Figure 2-22 Diameter measurements by curvature radius variation of a) large volume of droplet with less curvature results in less phase angle difference, b) small volume of droplet with sharp curvature results in greater phase angle [43]..... | 53 |
| Figure 2-23 PMT voltage calibration for diameter size determination D_{10} (μm) | 56 |
| Figure 2-24 Examples of intensity validations for data cluster creating a natural curve of green dots and red dots as biased data a) water, b) suspension fluid atomization | 57 |
| Figure 2-25 Validation of droplet diameter size distributions of a) water (b) suspension atomization; with $\pm 7\%$ symmetric diameter size variation | 60 |
| Figure 3-1 Internal flow pattern transitions of a) bubbly flow b) intermittent and c) annular flow regimes as the GLR increased..... | 62 |
| Figure 3-2 Time interval evolution of Glycerol atomization analyses; bubbly regime attempting to shatter the liquid trunk ($\mu_{glycerol} \approx 1400 \mu_{water}$) | 63 |
| Figure 3-3 a) Spherical bubbles at GLR 1.1% and b) parabolic shaped bubbles at a GLR of 2.6% of glycerol atomization ($\mu_{glycerol} \approx 1400 \mu_{water}$) | 65 |
| Figure 3-4 a) Aqueous solution droplet and internal bubbly flow, b) suspension droplet and bubbly regime inside the nozzle | 66 |
| Figure 3-5 Bubble size comparison of a) water, b) solution and c) glass beads suspension operating at a GLR of 0.055% | 67 |
| Figure 3-6 Water spray patterns at various GLRs comparing Breakup length (L_b) at GLRs of a) 0.03, b) 0.055, c) 1.1, d) 1.6, and e) 2.6% | 68 |
| Figure 3-7 Various fluids atomization patterns near nozzle orifice at GLRs of a) 0.055, b) 1.1, and c) 2.6 % for water, solution ($\mu_{solution} \approx 9 \times \mu_{water}$) and c) glass beads suspension ($\mu_{suspension} \approx 10 \times \mu_{water}$)..... | 70 |
| Figure 3-8 Spray cone angle variation versus GLRs | 71 |
| Figure 3-9 Breakup length (L_b) variation versus GLRs | 72 |
| Figure 3-10 Optical patterning cross-sectional view by off-axis PIV, at various GLRs of a) 1.1, b) 1.6 and c) 2.6% with $d_{axial} = 15, 30$ and 45 cm | 74 |
| Figure 3-11 Various fluids cross-sectional patternations, operating at a GLR of 1.1%, $d_{axial} = 30$ cm, different spreading diameter for a) water, b) solution and c) suspension | 76 |

| | |
|--|----|
| Figure 3-12 Water atomization PIV analyses at GLRs of 1.1, 1.6 and 2.6% a) nearfield and b) far field | 77 |
| Figure 3-13 Velocity vector field of various fluids operating at a GLR of 1.6% | 78 |
| Figure 3-14 Water atomization PDPA analyses compared by the PIV analyses at various axial distances and GLRs | 79 |
| Figure 3-15 Droplet SMD (D_{32}) distributions st various GLRs | 81 |
| Figure 3-16 Velocity distributions at various GLRs | 81 |
| Figure 3-17 Velocity variation of various fluids (suspension, solution, water) | 83 |
| Figure 3-18 Droplet SMD distributionsfor different fluid's properties | 83 |
| Figure 3-19 Droplet RD distributions for various fluids operating at a GLR of 1.6% and $d_{axial}=200\text{ mm}$ | 85 |
| Figure 3-20 Droplet RD distributions for various fluids at GLRs of 1.6% and 2.6% and $d_{axial}=200\text{ mm}$ | 86 |
| Figure 4-1 a) Wind tunnel setup and b) effervescent elliptical orifice..... | 92 |
| Figure 4-2 Suspension flowrates of a) 200, b) 400, c) 600, d) 800, e)1000 ml/m..... | 93 |
| Figure 4-3 Suspension flow under cross-flow testing at a) 0 GLR, b) 2.6%, and flowrate of $Q=800\text{ ml/m}$, $Re_L=2574$ $We_L= 2179$, $We_G=2300$ | 94 |

Nomenclatures

Letters

| | |
|-------------|----------------------------|
| d | Diameter |
| p | Pressure |
| Q | Volumetric flow rate |
| t | Time |
| L_b | Breakup length |
| D_{32} | Sauter Mean Diameter (SMD) |
| D_{10} | Number mean diameter |
| RD | Representative Diameter |
| D_v | Volumetric diameter |
| d_{axial} | Axial distance |

Greek Letters

| | |
|-----------------|---|
| μ | Dynamic viscosity |
| σ | Surface tension |
| ρ | Density |
| ξ | Suspension constant coefficient |
| φ | Particle concentration |
| Γ | Circulation magnitude |
| κ | curvature |
| ε_a | Agglomerate porosity of suspension drops |
| σ_a | Tensile strength of suspension drop binding |

Abbreviations

| | |
|--------|---|
| PIV | Particle Image Velocimetry |
| Nd:YAG | Neodymium-doped yttrium aluminum garnet |
| PDPA | Phase Doppler Particle Analyzer |
| PMT | Photo Multiplier Tubes |
| BSP | British Standard Pipe |
| SMD | Sauter Mean Diameter |
| SCFH | Standard Cubic Feet per Hour |
| GLR | Gas to Liquid mass flow ratio |

Subscripts and Superscripts

| | |
|---|--------|
| L | Liquid |
| G | Gas |

1. Introduction

1.1. Background and motivation

Breaking a bulk liquid into smaller droplets to increase the surface area of the liquid is called “fragmentation/or atomization”. Fragmentation of a liquid is at the heart of extensive processes and automated applications such as gas turbine engines, icing phenomenon over wings of airplane, spray coatings, material synthesis and drug generation in pharmaceutical appliances. Various cases of atomization are depicted in figure 1-1. In point of fact, one could easily find the atomization in nature; rain drops being one example. Atomization is highly demanded in other applications such as automobile painting, spray drying of food production (i.e., turn coffee/milk into dried powder), and clinical drug delivery (i.e., insulin sprays into respiratory surfaces of the human body instead of liquid injections). In an aircraft gas turbine engine, atomization is used to atomize fuel and break it up into smaller droplets to reduce the output pollution and increase the thrust. Atomization is used in thermal spray coatings to inject suspended particles to a heat source for coating purposes.

Some crucially important characteristics of atomized fluid are: spray cone angle, breakup length, penetration depth, droplet size, velocity volume distributions, and droplet shape being the most important controllable atomization characteristics. Size distribution of generated droplets, for instance, determines the total performance of an internal combustion engine by means of changing surface to mass ratio of injected fuel. In other words, inside the limited space of a combustion chamber, fuel droplets have to uniformly distribute and occupy the special zones for better vaporization and ignition resolutions.

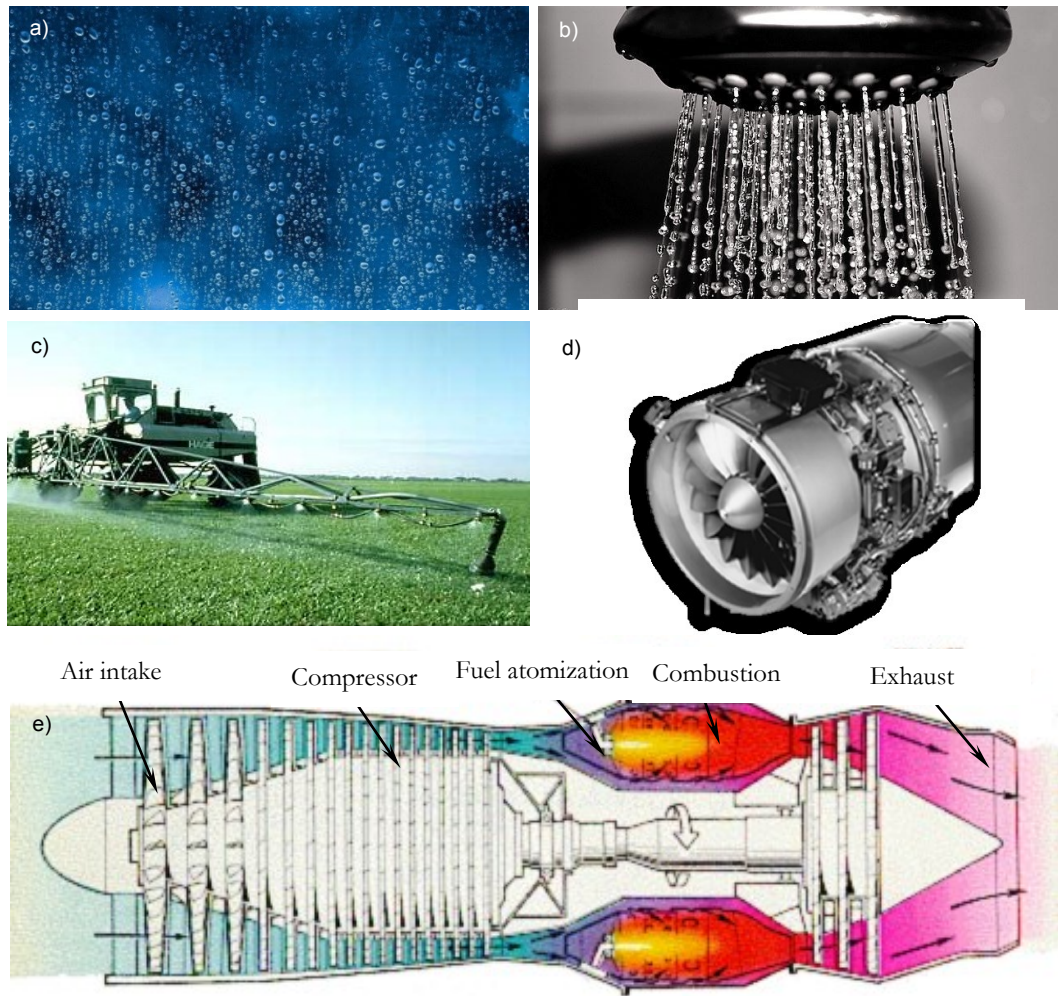


Figure 1-1 Variety of atomization a) rain droplets [2], b) shower flow [3], c) agriculture spray [4], d) AP&W JT15D turbofan engine [5], e) Gas turbine engine [6]

In cross-flow applications, such as thermal spray coating (which products are normally used in aerospace applications) it is crucial to predict the suspension fluid spray cone angle and the breakup lengths of the spray for estimating the penetration of injected fluid jet into the heat source. Due to changes of certain factors of bulk liquid properties, atomization characteristics hastily changes. Rheological properties of the bulk fluid change the droplet size distributions and the other characteristics such as spray cone angle, velocity

distributions, etc. Altering dynamic viscosity of the fluid affects the force balances, such as aerodynamic reactions on the generated droplet's surface. Moreover, design of atomizer (i.e. air-blast, air-assist) results in different out-coming spray patterns. For example, diameter size of an outlet orifice alters the generated droplets diameter sizes. If internal design of the nozzle is a rounded cone attached to a funnel cross-section, the bulk liquid experiences additional capillary disturbances in comparison without funnel cross-section due to centrifugal influences. Consequently, higher the level of disturbances, higher the breakup instabilities which results in faster and easier breakup features of bulk liquid.

In addition to geometry effects, operating conditions amongst other variables affects properties of an atomized fluid. For example, in a twin-fluid atomizer, increasing air injection pressure will result in reduction of spray droplet size leading to more refine droplets due to higher instabilities acting on the liquid by the extra injected gas. Besides, changing pressure or temperature of the ambient where the spray enters affects spray external flow pattern as well. For example, if the ambient pressure increases from standard atmosphere pressure to higher values, the extra pressure reduces spreading diameter and the spray cone angle.

As a specific application of atomization, a typical thermal spray coating is depicted in figure 1-2. The main objective of the torch in this setup is to create a flow with high temperature and momentum flux to melt and carry the injected particles, respectively. This advanced type of coating which the products are normally used in aerospace applications is capable of coating a surface with controllable features such as super-hydrophobicity, thermal barrier coatings and corrosion resistance due to the sub-micro or nanostructure of the metallic, carbide and ceramic coating on the substrate.

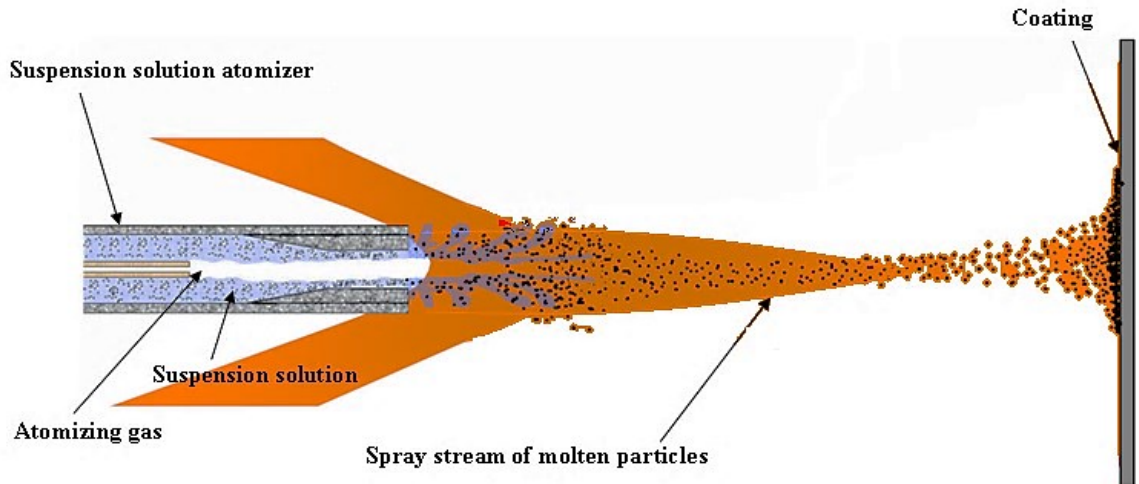


Figure 1-2 Suspension Plasma Spray Coating (SPS) [1]

The torch mostly runs by a plasma or High-Velocity-Oxygen-Fuel (HVOF) gun. The particles are fed in the torch using dry or wet injections, radially or axially. High temperature of the torch flow melts the injected particles which punch on the substrate due to high velocity and momentum leading to a fine coating structure on the substrate.

Injection of nano-submicron powders faces various inevitable problems in terms of losing time and expenditures. One of the main problems is clogging/or blockage of the powders in the injection. However, the wet injection (suspension fluid) has more advantages outweigh those of dry injection such as superior heat resistance, less erosion, and less cracking on the coatings. Nonetheless, blockage of suspension fluid in also the injection line is reported in few cases using conventional nozzles. Effervescent atomizer is in the center of focus of research institutions, because of advantages of no-blockage in suspension atomization/or injection due to self-cleaning feature and also independency from rheological properties of the fluid which is under investigation in this study to have more knowledge. Proceeding sections will shed insight to the atomization properties of the effervescent nozzle.

1.2. Atomization

Atomization is an important process in various fields and applications. Atomization of a liquid comes from the fluctuations and the disturbances acting on the surface of a liquid jet. As a primary step in combustion process of an aircraft turbine engine, atomization disintegrates bulk fuel into broken up small droplets, so it can reduce the pollution and increase the thrust as a result by increasing heat transfer [2]. Also in various effective surface material coatings, particularly thermal spray coating (shown in figure 1-2), atomization is used to inject suspended particles into a plasma flow of a heat source to melt them and to coat a substrate with a film of nano-structured surface. In other similar applications like automobile painting, surfaces are protected from corrosion by desired quality-coating. Spray drying in the food industry, for example, requires atomization to turn coffee/liquid milk to dry powder. Another sensitive application is clinical spray in drug delivery, such as insulin sprays into the respiratory surfaces of human body instead of liquid injection. Generally, fluctuations of bulk flow of jet and surface dispersions disintegrate it into smaller sizes such as ligaments or satellite droplets.

Based on the required applications and dictated operating conditions, the atomization agent varies case by case. Disturbance agents are clearly obvious while a jet exits from an orifice into another environment, such as atmospheric conditions. The disturbances could be due to design of the orifice (e.g., diameter size), fluid rheological properties and their variations associated to operating condition in which the nozzle is working. Various rheological properties will change the atomization characteristics; for example, time span which liquid jet starts to breakup into fine parts for the first time due to the suppression of the fluctuation waves on the jet surface by high viscos fluids such as glycerol liquid will be higher than the

same operating conditions for lower viscosity [3]. In the following section, each source of fluctuations/or disturbances will be described respectively based on the investigations available of last century up to the present.

Considering various applications and required spray characteristics, atomizer type-design, rheological properties of fluid, and operation conditions will be different. The atomizers from one aspect are categorized based on design of the structure of nozzle and geometry. Amongst those atomizers, the most commonly used are: hydraulic, Swirl, ultrasonic, rotary, electrostatic, air-blast and twin-fluid atomizers. In this study, last three mentioned atomizers will be covered comprehensively and the rest will be just described briefly.

The hydraulic atomizers derive atomization force by pressurizing the liquid into reservoir or supply line figure 1-3 [4]. In the swirl atomizers, high speed fluid is directed to a circular funnel shaped chamber to generate the required centrifugal force as perturbations. The perturbations created by the centrifugal force make the liquid jet to break up into small droplets to form a spray plume.

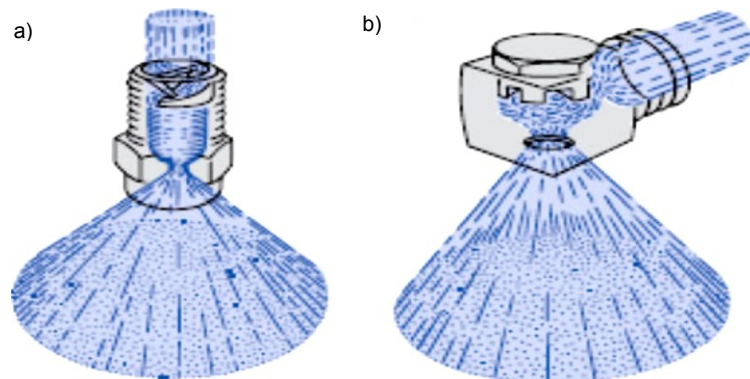


Figure 1-3 Various swirl-fluid atomizers a) axial flow, b) tangential flow [9]

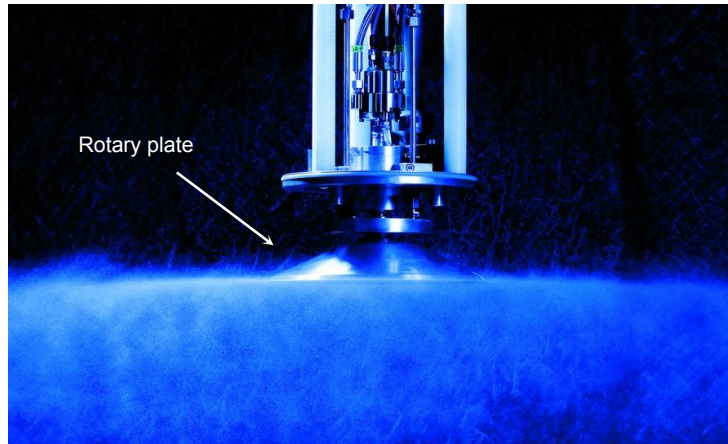


Figure 1-4 Rotary nozzle spray plume [9]

Swirl atomizers create a full-cone or a hollow-cone based on the geometry of the nozzle. The swirl atomizers have been used in wide range of applications such as gas cooling, dust removal, washing process, etc.

The rotary nozzle as depicted in figure 1-4, creates a centrifugal force for by means of a rotational part instead of geometry effects. However, the rotary atomizers have rotational parts to create the rotation of the fluid. The rotating parts are mostly disks or plates attached to the nozzle orifice which creates a sheet of liquid with a pattern much like to an umbrella shaped flow. The created flow is very uniform and the rotational part diminishes the clogging problem, if available. In figure 1-4, one common type of rotary nozzle is depicted. Another type of atomizers, which is under the electrical atomization group, utilizes vibrations of mechanical piezo-ceramic parts of the nozzle to atomize the liquid by capillary waves to disturb the liquid stabilities. The most commonplace use of the nozzle is in the electronic coatings or very sensitive medical-biomedical applications [5].

1.3. Classification of Twin-Fluid atomizers

1.3.1. Twin-fluid atomizer

As is clear from the title, two types of fluids are completing the atomization process. Twin-fluid atomizers operate at low flow rates and low injection pressures. Extensive demand for the low injection pressure and generating fine droplets made this type of atomization to reach many industrial applications such as combustion, precision coatings, thermal spray coating, spray drying, H.V.A.C. applications as well. Figure 1-5 shows a typical design of twin-fluid atomizer and the industrial version which is established by Lechler, Inc. Twin-fluid atomizer creates different pattern of exiting two-phase flow based on its internal geometry. The geometry designs mostly affect way of mixing of atomizing gas and liquid resulting in different external flow pattern. In general, the external flow could be full, hollow or flat fan pattern at the nozzle outlet illustrated in figure 1-6.

1.3.2. Air-blast and air-assist atomizers

Air-blast nozzles are commonly used in various applications of combustion fuel injection and power generation processes. This type of nozzle requires high volume of atomizing gas to be able to break up the bulk liquid into smaller ligaments and droplets. However, consuming large amount of gas flow rate makes this nozzle to be limited in some applications. For example, some atomized products are sensitive to be mixed with other substances such as atomizing gas in terms of chemical reactions and resulted in a change into the production quality of final goods. Therefore, the lower the required gas volume, the lower the reactions and more pure production of the goods will be resulted.

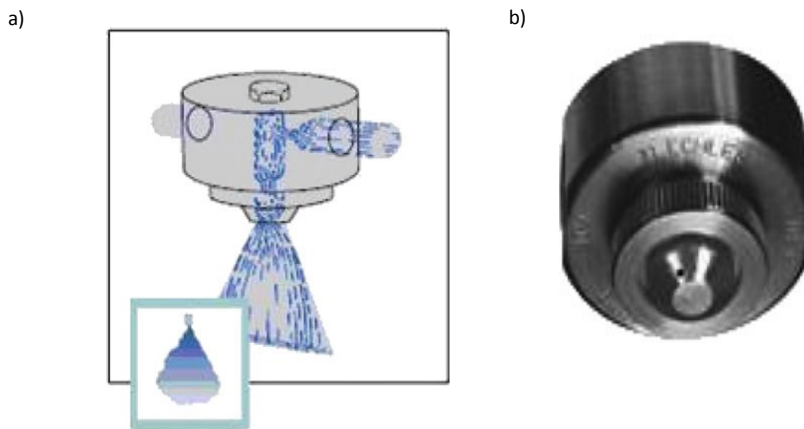


Figure 1-5 Twin-fluid atomizer, a) schematic and b) industrial version [9]

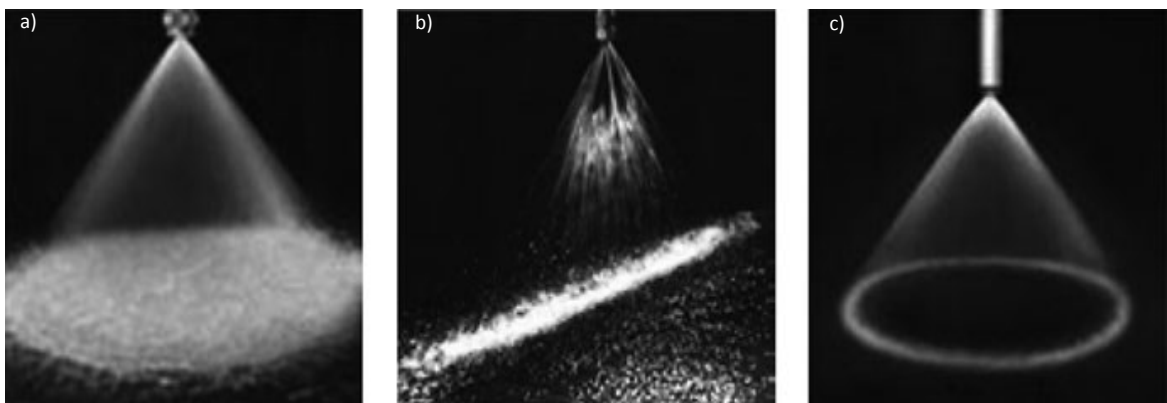


Figure 1-6 Various external flow patterns by twin-fluid atomizers with different nozzle geometry, a) full-cone, b) shear jet and c) hollow cone spray [9]

Likewise, higher the amount of the gas introduced, higher the risk of changing chemical properties of the atomized fluid will be the main disadvantage. However, there are various types of air-blast atomizer such as: pre-filming and plain-jet which are widely used. In all internal designs, the mixing chamber has one inlet for gas and one for liquid. Higher pressure difference between the atomizing gas and the running liquid is necessary for all designs.

Air-blast atomizers should not be confused with air-assist atomizers which later model requires air just to assist the atomization; although they have many similarities. The main difference between the air-blast and air-assist nozzles is the gas flow rate consumption which the air-blast utilizes far more gas flow rates than air assist nozzle. Air just assists the air-assist-nozzle in moment of a demand for higher dynamic forces for liquid breakup. For further information please refer to the Handbook of atomization by N. Ashgriz 2011. One of the most interesting types of twin-fluid atomizers is called ‘Effervescent atomization’ introduced by Lefebvre in the late 1980’s.

1.3.3. Effervescent atomizer

Another distinct type of twin-fluid atomizers is called “Effervescent atomization” introduced by Lefebvre [6], [7] and Roesler [8]. The word effervescent means bubbly liquid or sparkling environments. In this type of atomization, atomizing gas and liquid are entered into a mixing chamber where bulk liquid is aerated/or bubbled by gas. Air injection mechanism is defined in two types of inside-out in which the gas is injected into the mixing chamber as illustrated in figure 1-7, and outside-in, which the gas is mixed right close to exit orifice [9]. The later design enters the atomizing gas into the annular space attached to the liquid chamber. Therefore, the gas enters through small aeration holes into the orifice which plays the role of mixing chamber, to create the bubbly and two-phase flow at the nozzle orifice [10].

The generated bubbles with higher internal pressure in comparison with surrounding liquid are carried-out of the nozzle by liquid streams. Internal pressure of the mixing chamber is several times lower than the other conventional atomizers (i.e. air assist/or air blast) leading to higher efficiency in terms of power and energy consumption [11], [6], [7] and [8].

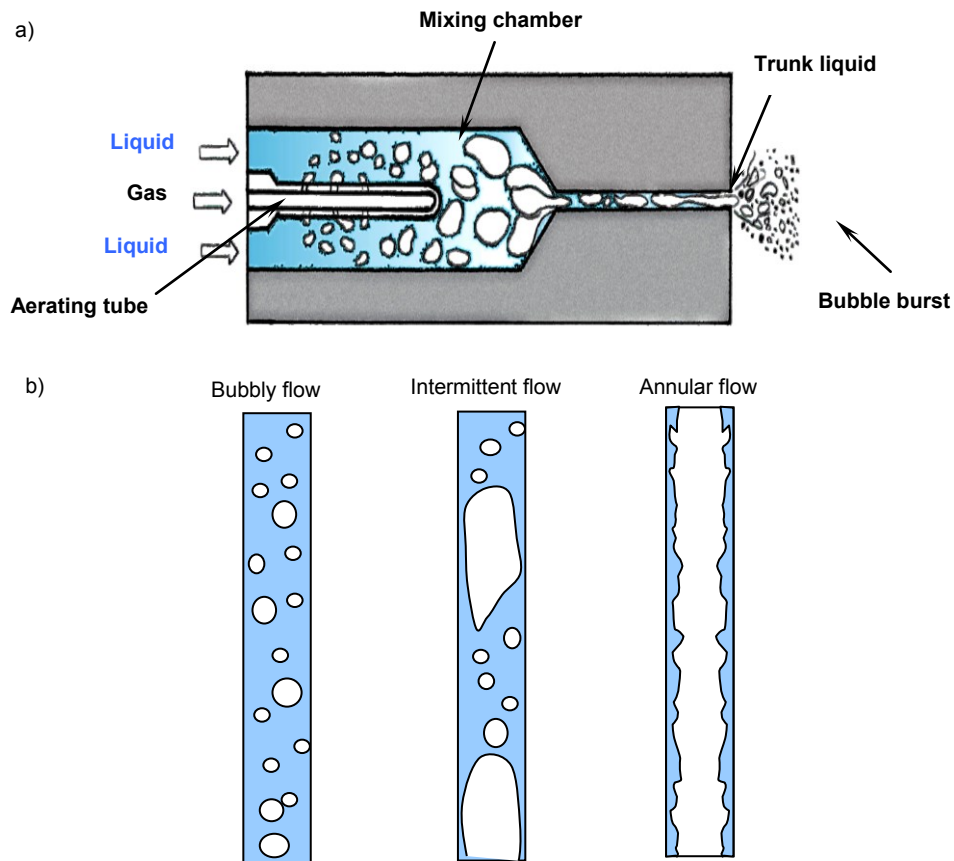


Figure 1-7 Inside-out type of Effervescent nozzle design, generating bubbles by aeration into mixing chamber and explosion of trapped bubbles at the nozzle exit [7]

The two-phase bubbly regime with slightly higher pressure than surrounding liquid attempts to overcome the surface tension forces of the liquid on the interface. [12]. The direct gas injection into the liquid chamber and generating of bubbles upstream inside the atomizer chamber is the typical procedure of an effervescent nozzle atomization mechanism. The atomization of the liquid depends on different parameters. The most important parameters are: 1) geometry, 2) Rheological properties and 3) Operation conditions. The following section is a brief summary of studies done in this field to investigate the affecting parameters during the last decay.

1.4. Effective Parameters in Effervescent Atomization

1.4.1. Geometry

As illustrated in figure 1-7, liquid from one side and atomizing gas from another port are injected into a mixing chamber to make the internal bubbly flow at upstream of the exit orifice. The bubbly regime is obtained at low GLR which represents the minimum required amount of gas for atomization; hence, this type of nozzle is appealing for various applications and research centers due to the unique operating mechanism [13].

J. Schelling and R. Lothar [14] investigated effects of mixing chamber size and its relation with flow pattern. Internal mixing chamber design affects the external spray pattern, based on the pressure variation dependency on the cross-sectional sizes of the geometry. For example, if the size is large enough, by increasing the amount of gas into the chamber, both of the fluids have time to mix. Therefore, external flow pattern could turn into different forms such as full/or hollow cone at higher gas flow rates.

Ponstein [15] examined effects of funnel section of the geometry attached to the mixing chamber. The swirl capillary instability is one of the possibilities which create more instability on the liquid flow while exiting from the nozzle orifice. The instability mostly is driven by centrifugal force of swirling flow at the funnel part of the nozzle. They have introduced equation, which is followed by Ponstein and Saffman's study [16]

$$\omega^2 = \left[\frac{\sigma}{\rho_l a^3} (1 - \bar{k}^2) + (1 - \varepsilon) \left(\frac{\Gamma}{2\pi a^2} \right)^2 \right] \bar{k} \frac{I_1(\bar{k})}{I_0(\bar{k})} + \varepsilon U^2 k^2 \frac{I_1(\bar{k}) K_0(\bar{k})}{I_0(\bar{k}) K_1(\bar{k})} \quad (1)$$

Where Γ is representative of flow circulation which could be either zero (non-swirling) or positive (as the centrifugal instabilities will be effective).

1.4.2. Viscosity and Surface Tension

Gupta et al. [17] utilized various gases with different rheological properties for atomization purposes. Due to changes in the properties of the gases, atomization characteristics such as drop size distribution and number density of atomized droplets varied; figure 1-8. Among the gases used, CO₂ is one of the most useful gases in terms of improved results in combustion process for fuel atomization by having lower pollutant exhaust gases. CO₂ has a lower viscosity in comparison with compressed air, which resulted in higher velocities of spray droplets and consequently smaller breakup lengths for liquid trunk. However, higher density of the gas creates lower velocities. This is due to the damping effects of both high density and high viscosity. Nitrogen (N₂) is another useful gas for atomization since it has similar characteristics to air, with a lower density and viscosity, which assists to produce smaller droplets. In turn, argon gas is used to compare the viscosities since it possesses high viscosity. It is found that the higher viscosities of the atomizing gas produce larger droplets, which are less in number. Hence, the results demonstrated lower energy and mass exchange of the atomized liquid with surrounded gas. Finally, lower the gas viscosity, lower the atomization efficiency and vice versa.

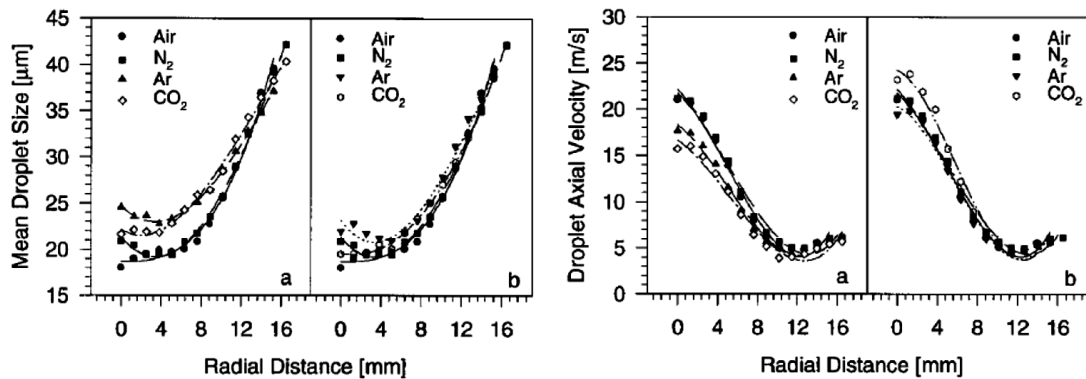


Figure 1-8 Atomizing gas viscosity variation effects on atomization features [23]

Kufferah et al. [18] found that viscosity of fluids is one of the main factors determining flow regime by changing relevant velocity. Highly viscous fluids require more dynamic forces to move faster while low viscous fluids do not. A high viscous fluid such as purified glycerol normally is conducted as a creeping flow at laminar regimes. However, low viscous fluids are normally in turbulent regimes with higher velocities at the same running gas force. The atomizing gas introduces required dynamic force for atomization and breakup of the running fluids the introduced amount of gas is limited due to choking of the fluids leading to uniform and pulsed flow at the nozzle outlet.

Higher viscosity of the liquid postpones the breakup of liquid trunk at the nozzle exit. Therefore the atomization efficiency reduces in comparison with the similar conducting parameters for atomization but for lower viscous liquids.

Lower viscosities, in turn, result in higher velocities of the running fluid. Flow regime turns from laminar to turbulent depending on the Reynolds number of the operating condition. One of the characteristics of the turbulent flow is the fluid's surface deformation. For instance, the laminar flow with a smooth interface turns into a perturbed surface with different wave lengths regarding operating velocities. These perturbations improve the breakup since the dynamic forces can easily overcome the surface tension and viscous forces. The laminar regime without interface perturbations also is depicted in the shadowgraphs image results of glycerol atomization of this study which will be discussed later.

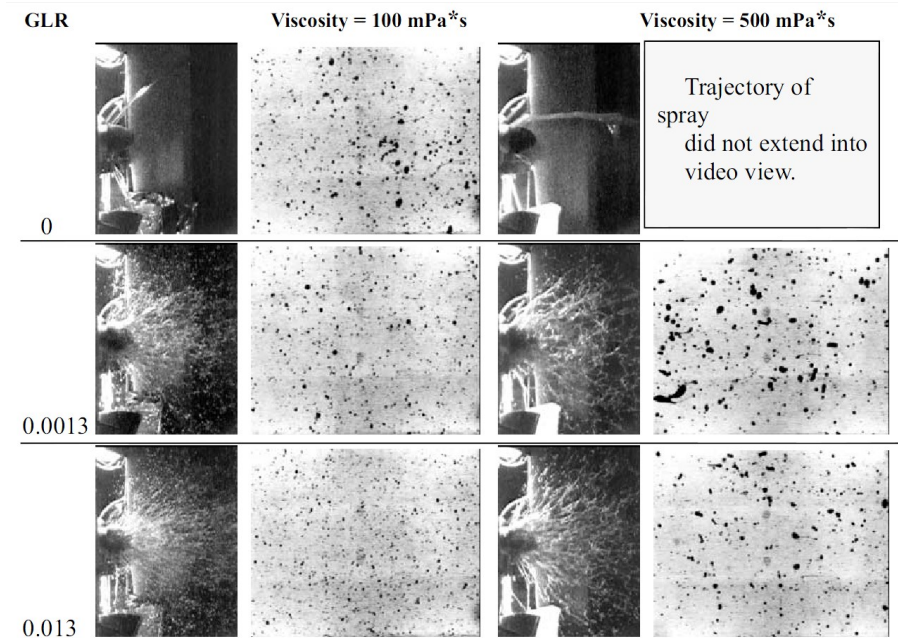


Figure 1-9 Effects of viscosity and gas flowrate on atomization features [19]

The atomization of corn syrup, which is a fairly good representative of the black liquor, is illustrated in figure 1-9. Effervescent is used to atomize black liquor by an adjustable needle to control the droplet size formation [19], figure 1-9. Black liquor containing solid fuel particles is one of the most widely used fuels for craft recovery boilers. However, since the fluid contains solid particles, the viscosity is not constant. Therefore, the atomizer must be independent from the fluid rheological properties. Since the liquor is very viscous liquid, one attempt is to increase the temperature for better atomization. However, the risk of explosion due to the high pressure of atomizing gas and high temperature makes the effervescent ideal for its atomization. Low pressure of the mixing chamber in the effervescent makes possible to heat-up the liquor to reach to lower dynamic viscous status for atomization. Even the presence of the solid particles did not affect the atomization properties by the nozzle.

Broniarz-press et al. [20] investigated spray characteristics by comparing surface tension and viscosity effects using mineral oils atomization by digital micro-graphy as experimental methodology. Calculation of droplet diameter size distribution provides heat and mass transfer values for comparison of efficiency of various atomizers. Droplets volume versus surface distribution is defined as Sauter Mean Diameter (SMD) by following equation (2)

$$\text{SMD} = \frac{\sum_i n_i d_i^3}{\sum_i n_i d_i^2} \quad (2)$$

To include the surface tension and viscosity effects, Nukiyama and Tanasawa [21] proposed correlated by equation (3):

$$\text{SMD} = \frac{0.585}{u_R} \left(\frac{\sigma}{\rho_L} \right)^{0.5} + 53 \left(\frac{\mu_L^2}{\sigma \rho_L} \right)^{0.25} \left(\frac{Q_L}{Q_G} \right)^{1.5} \quad (3)$$

where, σ and μ are surface tension and dynamic viscosity, respectively.

Empie and Loebker [22] investigated the surface tension effects versus the viscosity by comparing the resulted SMD of the spray droplets. These comparisons included internal flow pattern inside mixing chamber which has strong effect on the atomization characteristics at external flow. Indeed, both surface tension and viscosity affect the internal flow pattern. Based on the power law investigation they did by comparing various components of various fluids with different viscosities and surface tensions the found out the surface tension effects outweigh those of viscosity. They concluded that the surface tension, depending on density of the fluid, is more dominant than viscosity in atomization of the fluid. Therefore, smaller droplets may be formed from viscous fluids having smaller surface tension.

1.4.3. Suspension Fluids

Suspension fluid as a representative of complex fluids has unpredictable, chaotic and complex dynamics behavior. The complexity comes from density, viscosity and surface tension variations in the fluids dynamics. They are mainly divided into Newtonian and non-Newtonian fluids based on the viscosity variation versus shear stresses. Practical examples of complex fluids are paint colors, variety of foods such as milk products, oils, and various aerosols used in clinical drugs.

A micro suspension fluid is formed by adding micron-sized solid particles into a Newtonian or a non-Newtonian liquid. The liquid which the particles are added into is generally called “base fluid”; with high or low dynamic viscosity. A fluid which contains suspended particles and is running in a tube (vertical /or horizontal) has different rheological properties (i.e. viscosity, surface tension and osmotic pressure) in comparison with the same fluid but motionless. The added solid particles significantly alter the dynamics of the base fluid.

According to Einstein 1905 [23], dynamic behaviors of suspended particles, detectable by optic devices as shown in figure 1-10, are chaotic due to the thermal molecular interactions, or “Brownian Molecular Motion”. Owing to this phenomenon, classical thermodynamics is not applicable for the problems in this scale. In addition, if the concentration of the suspended particles is relatively high (10 Weight% of liquid or higher), the result is a non-Newtonian behavior of the suspension. Moreover, with the same amount of the base fluid and the same operating condition, Osmosis pressure, surface tension and viscosity will be different for the same case of suspension only by changing the diameter size or shape of added solid particles.

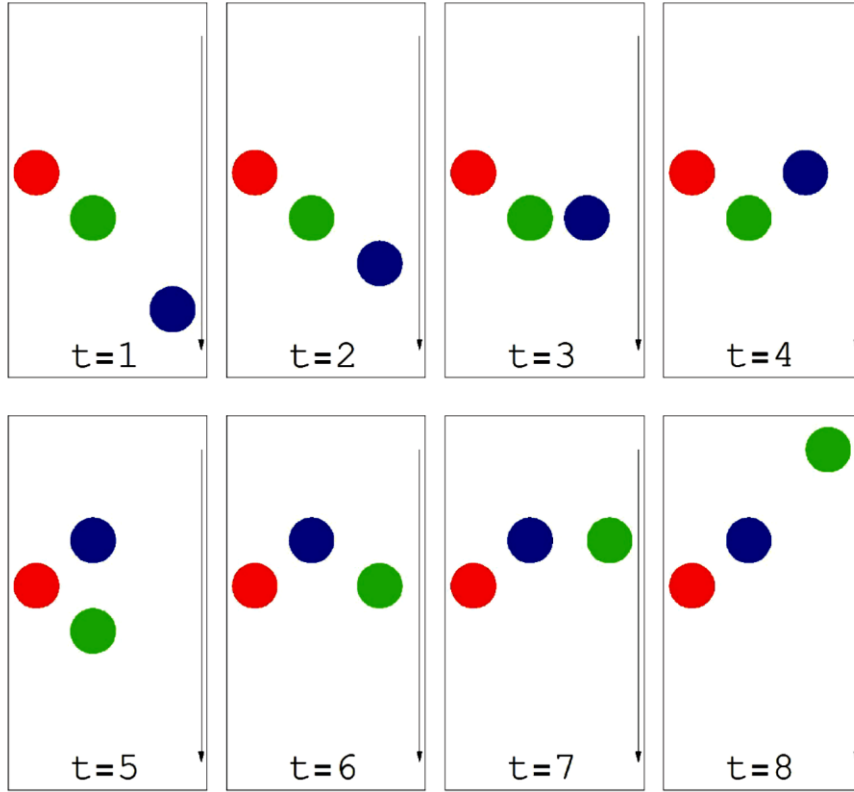


Figure 1-10 Suspended particles chaotic dynamics due to changed viscosity at each time interval, wakes behind the particles affects particle's motion (t=time unit) [30]

The surface tension and viscosity of the suspension are different in comparison with the base fluid. The properties of the suspension are also affected by the shape, size, and concentration of added particles. The concentration of the suspension is defined as the weight of added particles versus the weight of a base fluid in percentage. The concentrations above 10wg% of the base fluid will be non-Newtonian fluid in micro suspensions (relevant viscosity of the suspension defined by Einstein is: $\mu_r = 1 + \xi\phi$, where ξ is suspension constant coefficient and ϕ is the particle concentration). The irregular motion and the diffusion in the dynamic equilibrium of the complex fluid come from presence of added particles to dissolved portion of the total fluid. The changes in the properties are due to the

thermal molecular motion of the solid particles in the fluid. However, in very low concentrations, the behavior is mostly representative of the base fluid (10wg% or less).

Non-spherical particles are highly affected by drag forces which are not considerable in spherical particles dynamics. In the non-spherical particles, the unbalanced drag force and arbitrary rotation of the particles force the particles to migrate rapidly towards the pipe walls. However, in the spherical particles, the balance of the forces does not force the particles to migrate towards the wall causing agglomeration and sedimentation beside the hedge, depicted in figure 1-11, [24]. Therefore, shape of the particle is highly important in the motion and consequently in the pressure drop of the flow due to agglomerations and sedimentations of the particles. The pressure drop is not only due to the agglomeration but also to the added weight of the particles. Higher the concentrations, higher the added weight, and higher the pressure drop.

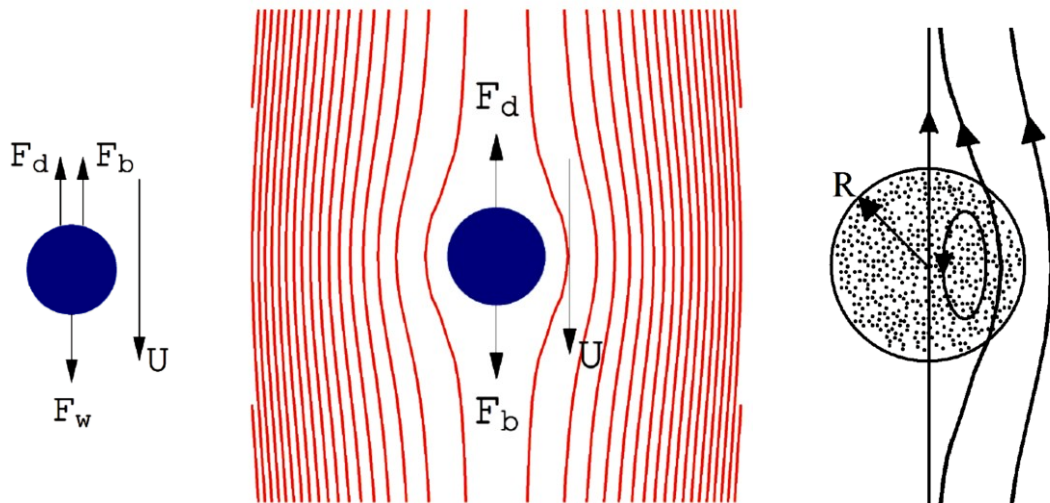


Figure 1-11 Force balance of suspended solid particle in fluid; F_d : Drag, F_b : Buoyancy, and F_w : Weight forces, U : Fluid's mean velocity, R : Equivalent radius [30]

In addition to the effects of shape and the concentration of the particles, the size of added particles in comparison with the surrounding tube and reservoir size is also important for the velocity and viscosity variations. Close to the wall, where available data are limited, viscosity highly depends on the size of the particle. Larger particles in comparison with smaller tube diameter make this viscosity dependency more effective. If the particle size is large enough in comparison with the tube, the suspension fluid will act as same as a high viscous fluid.

Furthermore in a laminar flow, the particles tend to stay in a sole streamline, however the turbulent flow with fluctuations does not support this assumption and the particle crosses the streamlines. Crossing the streamline could be due to density difference between the particle and liquid as well. For example, if the particle density is smaller than liquid density, the particle in an upward flowing direction will move towards the wall and vice-versa. Therefore, the flow will experience higher pressure drop due to sedimentation close to the wall representing a high viscous fluid.

Above all, the clogging and the agglomeration of the particles make movement of suspension flow more chaotic (as they stick to each other and form a larger equivalent diameter). While one particle is moving in front of the other particles, the following particles attempt to stick to the frontier (due to the attraction of the molecules), and also wake behind the frontier particle. Larger the equivalent diameter, larger the wake behind the particles is ensued. Equivalent diameter size of the particles grows while the particles agglomerate [25]. Besides, the wake behind the particles with larger effective surface area results in a dominant dragging force to the other particles to follow the dominant wake and finally attach to each other and form a larger sole particle. This attraction is more noticeable considering the molecular meniscus effect.

Schmidt and Mewes [26] investigated spray drying of suspension fluids which is widely used among industrial atomization applications by twin-fluid atomizers. They provided pressure gradient by atomizing gas, as running force, into the nozzle to obtain spray characteristics of the suspension fluid. The characteristics such as breakup length and spray structure were conducted by utilizing a laser scattering system. The laser introduced to a certain point of interest, close to the nozzle discharge and recorded the fluctuations and changes on the suspension fluid dynamics due to the introduced solid particles. The fluctuations are obtained by altered signal with a premium fixed frequency passing through two points of interest with a known distance. When the laser light passed through a suspension liquid jet, light intensity of introduced laser vanished due to: reflection, absorption, diffraction and refraction with both the liquid and solid particles. Another change in the introduced laser light intensity was due to the presence of bubbles, in bubbly regime inside the nozzle chamber. Therefore, it was revealed that the added particles fluctuates the received laser frequency. The higher the particle concentration, the higher the fluctuations observed. In general, these fluctuations enhance the atomization qualities.

Mulhem et al. [12] investigated the breakup and disintegration of the suspension fluid. The fluid fragmentation using a twin-fluid atomizer to disintegrate and breakup a suspension fluid by varying solid particle sizes was the aim of their study. By increasing the particle size, separation of the generated small liquid droplets from larger particles occurred. In turn, the separation of liquid droplets and solid particles was not observed while the liquid droplet size was almost the same or larger than solid particle. Therefore, the separation of the liquid droplets from solid particles (SLS) depends on the diameter size ratio between the droplets versus the solid particles. In addition, the size of the particles weakened the effect of viscosity and surface tension. The higher dis-integration rate of suspension was due to the

shear thinning effect of the added particles that improves the breakup in comparison with the base fluid's breakup. However, the particle presence normally should increase the dynamic viscosity. It should be taken into consideration that the balance between the shear thinning effects (which help for easier dis-integration and increase in viscosity which delays the breakup) both are due to the added particles.

Capes [27] investigated binding of solid particles in a liquid droplet. Balance between tensile and adhesion forces of the liquid-liquid versus particles-liquid is the dominant factor in binding. Adhesion force depends on binding of the solid particles and liquid volume portion. The binding is categorized into two main states as shown in figure 1-12, Capillary and Pendular state. In each binding, separation of the particles is different. One of the main applications of the separation of the particles is widely used in dry powder formation in various industrial processes (i.e. coffee grain and detergent powder production). To reach totally single particle separation, one requirement is to avoid agglomeration of the particles in the feed line. To facilitate the separation and obtain free single separation, free stream crossing flow is one of the usual methods. In this manner, the atomized suspension liquid is exposed to a crossing free stream of a gas, with a possibly higher temperature.




| | |
|--|---|
| Particles in liquid droplet  | The surface tension of a continuous liquid drop holds the particles captive σ_L |
| Capillary state  | $\sigma_a \approx 6 \frac{1 - \epsilon_a}{\epsilon_a} \frac{\sigma_L}{(D_{32})P}$ (5) |
| Pendular state  | $\sigma_a \approx \frac{9}{4} \frac{1 - \epsilon_a}{\epsilon_a} \frac{\sigma_L}{(D_{32})P}$ (6) |

Figure 1-12 Different bindings of suspension fluid affecting liquid surface tension (σ_L) and tensile strength (σ_a) [33]

1.5. Objectives

The objective of this study is to characterize effervescent atomization by analyzing four types of fluids fragmentations from bubbly to annular flow. Compressed air as atomizing gas is used to influence various flow patterns from individual separated bubbly regime to annular flow for atomization purposes (i.e., from GLR 0 to 2.6%). The various liquids are water, purified glycerol, aqueous solution of water plus glycerol and suspension fluids. Experimental study is conducted by Shadowgraphs, Optical patteration, PIV and PDPA techniques for the effervescent atomization analyses to characterize and compare the results by investigating:

Internal and external atomization patterns.

Breakup lengths, spray cone angle, spreading diameter.

Generated droplets size, velocity distributions in various locations.

2. Experimental Methodologies

2.1. Atomizer apparatus and Setups

The investigations and approach for this study aims at comparing the different fluids atomization features in an effervescent atomizer. The tailor-made nozzle is a standard typical effervescent atomizer proposed first by Lefebvre in the late 1980's [7]. Schematics of the tools and all controlling systems used for this purpose are depicted in figure 2-1. Experimenting circuit consists of air supply line from a central pressurizing compressed air (to be used as atomizing gas). In addition, the air is used to pressurize a pressure tank in which the various liquid are filled in. The tank is connected to a pressure gauge to indicate the pressure inside the tank.

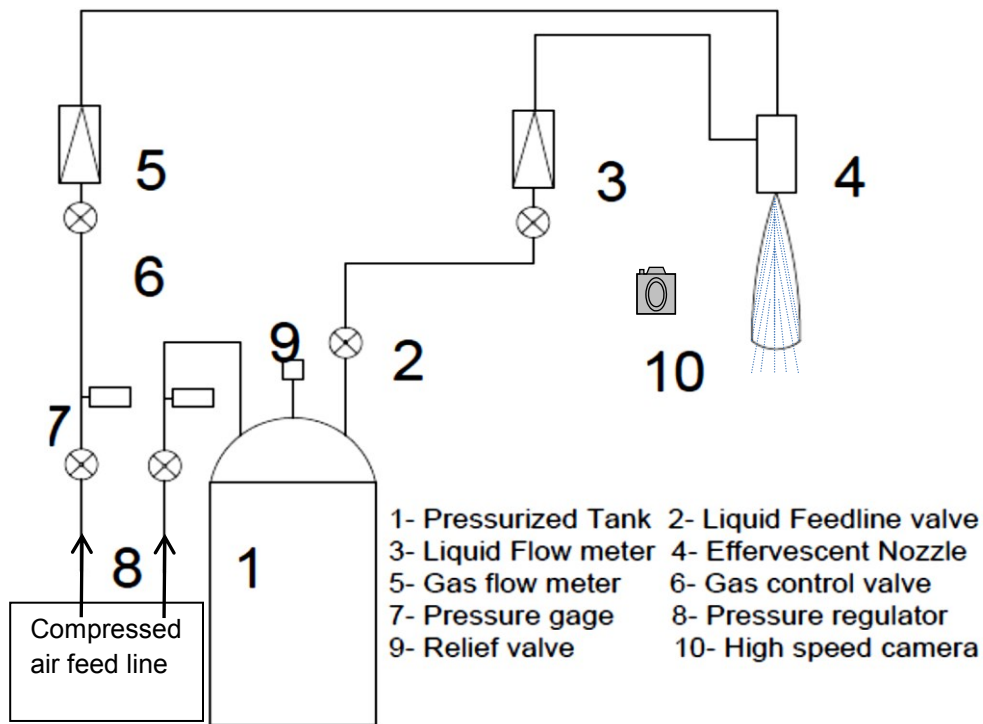


Figure 2-1 Schematic of experimental setup

The pressure tank is a stainless steel tank that has a capacity to store 30 liters. The filled liquids were pressurized by connecting the compressed air feed line into the tank, and a pressure regulator controlling the pressure inside without considering consumption of liquid for testing. All the valves used in the circuit are globe valves. The pressurized liquid varying from $P=0$ to $P=1.40$ MPa would feed the nozzle's liquid port after passing through a flowmeter and control valves. From another tube, pressurized air passes through a float type air flowmeter, control valves, and then goes to the top air connection of the nozzle. The flowmeter, according to the supplier claims, has an uncertainty of $\pm 4\%$ and provides air in SCFH. The air flowrate varied from 0-36 SCFH by keeping the liquid flowrate constant and making various GLRs. The atomizer connected to the air and liquid tubes and mounted on a stand with a sliding plate.

The effervescent atomizer is referred to the tailor-made effervescent proposed by Lefebvre in 1980's. The assembly, details of injector, and dimensions in "mm" are shown in figure 2-2. The geometry used in this study is inside-out mode in which the aeration tube is surrounded by a bulk liquid in a mixing chamber where the pressurized air enters by two small aeration holes. The liquid connection is a M8×10 BSP threads fitting to liquid hose. The bottom portion of the main body consists of a converging cone and an exit orifice where the pressure changes apply to the fluids while passing through the cone part. Internal body of the nozzle plays role of a mixing chamber. The air entering by two diametrically opposite aeration holes aerates bulk liquid and forms bubbly or annular flow based on the injected gas amount. Nonetheless, the larger volume of the mixing chamber does not easily allow the creation of a bubbly regime, even though the air flow rate is very low.

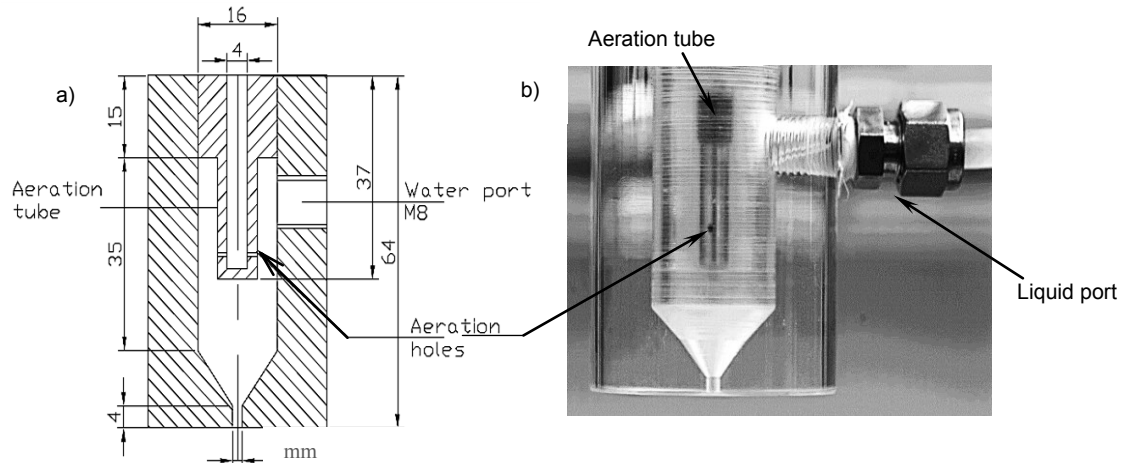


Figure 2-2 a) Effervescent nozzle [all sizes in mm], b) image of the transparent effervescent nozzle

2.2. Fluids Properties

Compressed air for atomization is used to atomize four different commonly used liquids by the effervescent nozzle. The different fluids are: distilled water, pure glycerol, an aqueous mixture of water and glycerol, and suspending micro glass beads in the aqueous solution of the distilled-water plus glycerol called solution in the proceeding sections. The aim of characterizing the spray is to gather experimental data which will be used as a benchmark to compare the atomizer's performance with various fluids in various applications, specifically in Thermal Spray Coating (TSC).

Water atomization analysis was the primary liquid source for the experiments using air as atomizing gas. The compressed air was supplied externally to the laboratory through the building's air supply system which is brought to ambient conditions. The second fluid was pure glycerol. The third case was the aqueous solution of water plus the pure glycerol, mixed 50 % by volume of each fluid, respectively. Afterwards, keeping the solution at the same volume fraction of 50 Vol%, solid particles were added to the solution (as base fluid) to form suspension fluid.

2.2.1. Suspension Preparation & Analyses

The solid particles are micron-sized spherical Silicon-glass beads with size distributions of 20-30 μm , and also 70-90 μm , as second set of suspensions, purchased from Discovery Scientific Canada. “The glass beads are produced from pure raw materials and have a homogeneous, smooth and shiny surface with a density of 2.5 g/cm^3 ” according to the supplier. The size distribution of the provided particles is examined using a Particle Size Analyzer provided by HORIBA Scientific illustrated in figure 2-3. The model used is Partica Model LA-950 which is laser-diffraction based particles size distribution analyzer. The advanced optical design of the machine provides a measurement range varying from 0.01 to 3000 μm at the same instant.

Dynamic scattering light technology (DLS) of the HORIBA system detects random changes of scattered light intensity from a suspension or solution. The system uses tracking the random motion of particle known as of “Brownian motion”, and does the calculations based on the famous equation of Stokes-Einstein. This system is widely used in industry to measure fine particles even smaller than a nano-meter, such as nano-gold, protein and collided particle sizes. By throwing laser scattering light to a sample of particles flowing into a measuring cell, the scattered light intensity while hitting the cell containing particles alters the back scattered light intensity to a receiver. The collected scattered light intensity by the receiver provides random frequency changes of the refracted laser light (due to random motion of the particles inside the measuring cell). Therefore, by signal processing of the altered frequency from the original laser light frequency, the particle size will be known.

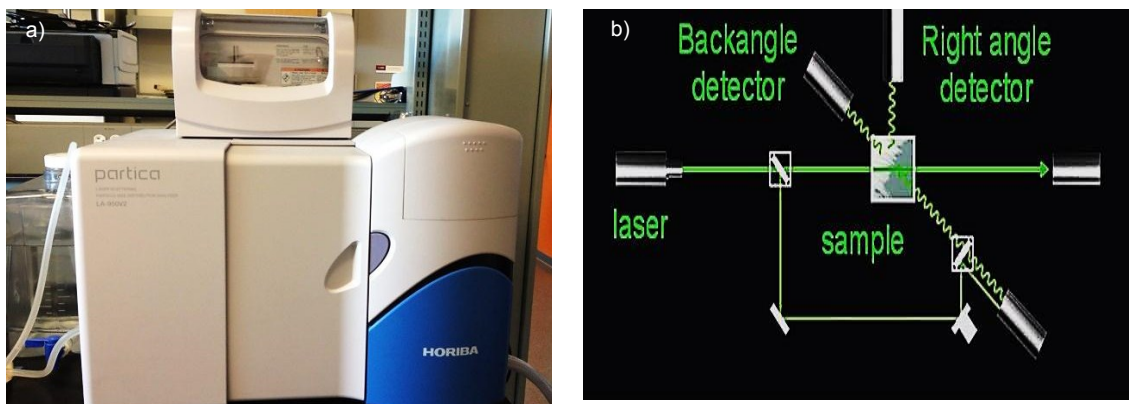


Figure 2-3 a) Particle size analyzer, b) Dynamic Light Scattering technique

After the particle sizes were measured, they were added to the solution to create suspension fluids. Glycerol is a colorless and odorless liquid soluble in water. The suspension is mixture of water-glycerol solution plus solid particles added by 10 weight percentage of the total solution's weight. For example, for a sample solution consisting of 500 g of water and 500 g of pure glycerol, 100 g micro glass beads were added. Figure 2-4 shows particles used in the experiments. However, making a suspension fluid is not as simple as mentioned above. It requires finding optimum way of a preparation of a specific type of suspension. In other words, it is not easy to suspend heavy solid particles in a liquid without having sedimentation. In this study, conditions such as having stable suspension without having sedimentation for 40 hours are gained.

First of all, one of the important factors of suspension preparation is the mixing method of solid particles with base fluid. The first step called wetting of the solid particles. For this purpose, a centrifugal mixing blade was used to provide high rotation mixing to ensure the particles to be fully covered by solution. Hence, the particles were mixed in high velocity blade mixer with small amounts of water.

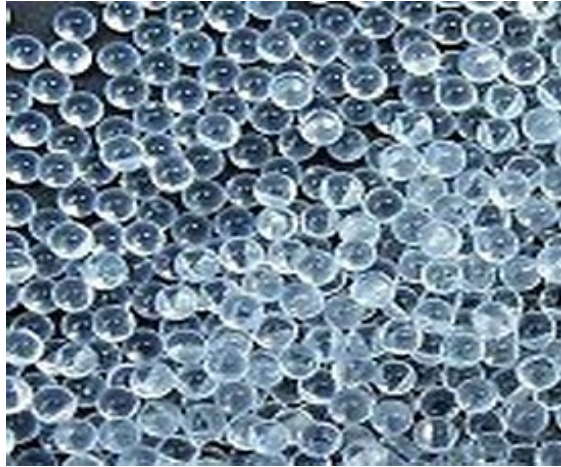


Figure 2-4 Micron sized spherical glass beads

Then, the wetted particles were added to the solution. Later on, the preliminary prepared suspension was mixed by a low power ultrasonic mixer for about 30min. Finally, the suspension is prepared in a way to ensure the minimum sedimentation, which takes about 40 hours to sediment.. Figure 2-5 is a sample of prepared glass beads suspension before filling in the pressure tank.



Figure 2-5 Glass beads suspended in solution

The prepared suspensions are examined by a digital microscopy system to assess characteristics such as an agglomeration and a homogenous distribution of particles suspended in the base fluid. The digital microscopy made by “KEYENCE” has a magnification of 500-5000 times larger than the actual dimensions (using optical lens VH-Z500R/500W). By scanning a sample at any angle needed, the software is able to distinguish edges and boundaries of the very fine bodies, such as particles suspended in a liquid. It also accomplishes calculations, such as maximum or minimum diameter sizes of the particles. The captured images could be either 3D or 2D, depending on required data from the experiments. For our experiments, 2D images were used. Figure 2-6 shows setup of the motorized digital microscope while capturing images of a suspension droplet.

The motorized digital microscope has ability to provide large depth of view, versatile and highly accurate in dimensional measurements. The experiments done for the thesis were using sample of suspensions under the magnification lens capturing the images. The images shown in figure 2-6 belong to a very small droplet of glass beads suspension of both sizes (20-30 μm and 70-90 μm) with a droplet diameter of 1 mm placed in a white vessel under the optic lens. The vessel is put on a motorized plate with a 3D free axis to move and provide the scanning of the sample by the magnification lens. For more information regarding the microscope, please visit the company’s website.

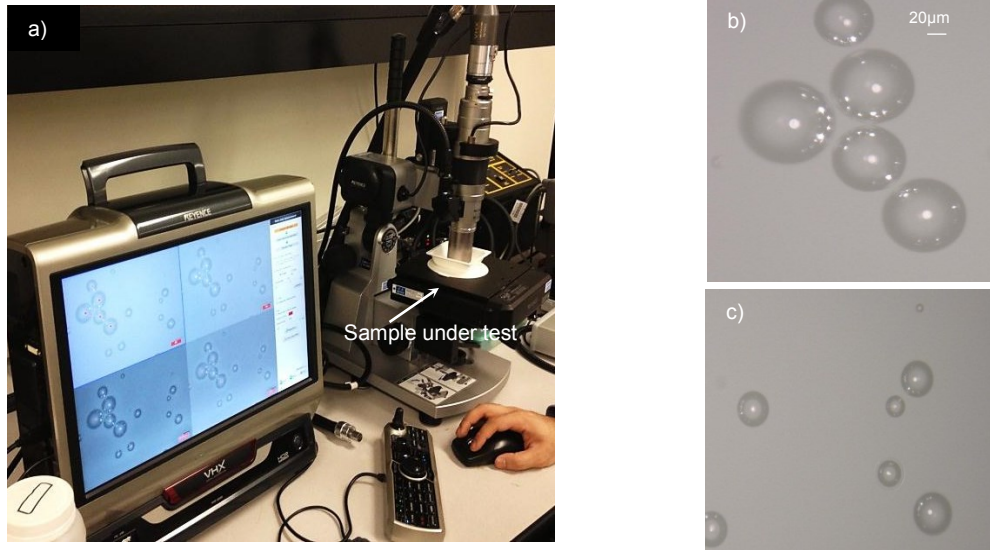


Figure 2-6 a) Motorized digital microscope, capturing 2D images of micro glass beads suspended in solution fluid with particle sizes of b) 70-90 μm , c) 20-30 μm

2.2.2. *Viscosity*

The next step is to obtain rheological properties of the prepared suspensions. Rheological properties of the running fluids play a dominant role in the atomization characteristics. Investigating simple fluid is a starting point while the next step is testing more complex fluids containing suspended solid particles. A complex fluid is a mixture of two or more substances which can be physically distinguished and separated. A simple example of a complex fluid could be a mud puddle where the water containing dirt particles creates the suspension fluid. Furthermore, lubrication oils containing silicate microspheres are used widely in the lubricant system of cars engines. However, the mystery behind how this complex fluid reduces the friction inside the engine is still under investigation. Behavior predictions of complex fluids are done mostly qualitatively or empirically, and are another encouragement for this study.

In this thesis, viscosity of the suspensions is tested using a highly sensitive viscometer. The Rheometer MCR 500 illustrated in figure 2-7 is the system used to conduct the measurements to obtain rheological properties of the fluids. According to the supplier (Physica Inc.), it is sensitive to the changes of the properties of the fluids, allowing for the detection of any variation in the properties of the fluids. The Physica rheometers are adaptable via easy-to-use and high performance software called “Rheoplus”. Rheoplus used in this study is able to cover the whole range of tasks, from a simple control of the rheometer to the creation of professional diagrams and plots.

The procedure of the experiment was followed based on the instruction provided by the Physica Company, the supplier. As depicted in figure 2-7, concentric cylinder geometry with two common axes was used to measure the viscosity by applying adjustable shear forces. The shear forces are applied, starting from a high to a very low rotational velocity (minimum values: torque $\pm 0.1 \mu\text{Nm}$, 10^{-9} s per sample, angular velocity 0.001 rad/s with accuracy of 10^{-7} rad/s, viscosity resolution 10^{-4} Pa.s with accuracy of $\pm 10^{-6}$ Pa.s). The inner cylinder is defined as inside geometry and the outer cylinder is defined as outside cylinder by providing a hollow gap ($\pm 0.01 \mu\text{m}$) while is entered to the outside geometry. The inside cylinder applies the adjustable shear forces by rotation, and the outside cylinder is like a cup container holding the sample fluid for experimenting, and both are made of hydrophobic Teflon. For the first step, 30 ml of water (at 20 °C) was the first fluid to be measured. Its result was compared with the existing standard value which the result was with more than 98% accuracy in comparison with standard values. Later, the same amount of aqueous solution of water and glycerol were examined in the know 50V%. Finally, the various suspensions were examined and the obtained results are tabulated in table 1.

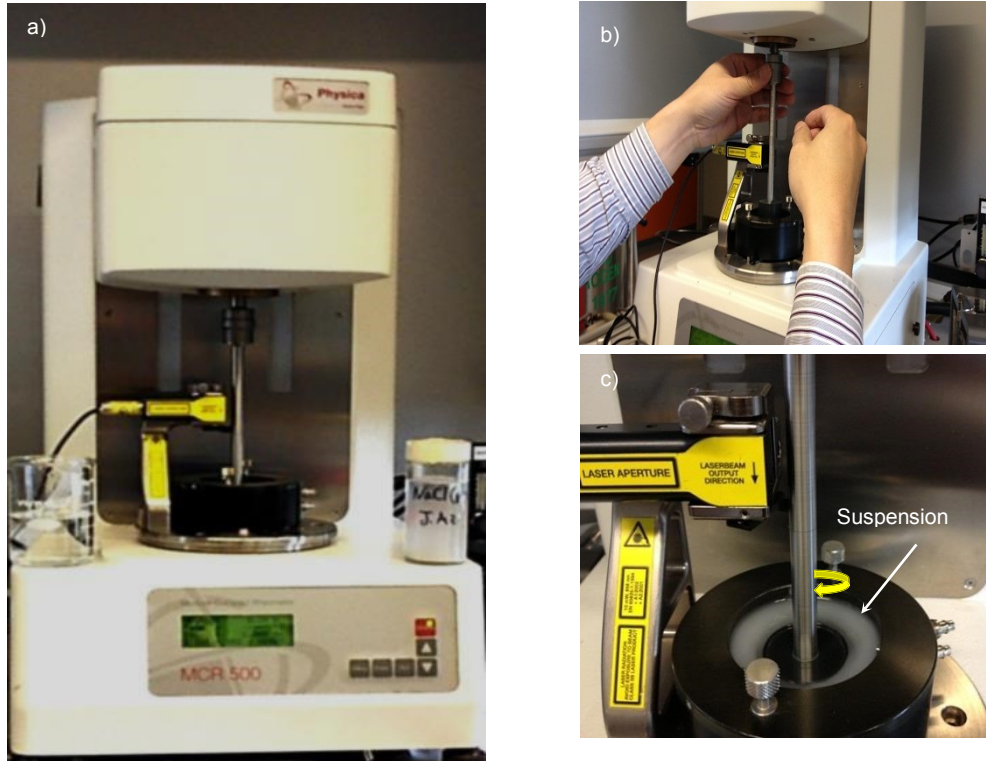


Figure 2-7 a) Modular Compact Rheometer model: MCR 500 by Physica, b) adjusting cylinders, c) suspension under shear forces by rotation of inner cylinder

2.2.3. Surface Tension

After particle size analyses, digital microscopy and viscometry of the fluids, it is vital to measure the surface tension of the fluids specially the suspensions. First, the surface tension is measured for water at 20 °C. To make sure about the calibration, water was tested and compared with the literature, where the standard surface tension of water at 20 °C is $7.3 \times 10^{-2} \pm 0.2$ N/m. The machine used in the experiments is Fisher surface tensiostat Model 21 made by Fisher Scientific, illustrated in figure 2-8. This machine is made to measure apparent surface tension, interfacial tension of liquids, and provides the surface tension value in [dynes/cm] (calibration and conversion of the system is provided in appendix c). The mechanism is built on the effect of surface tension in the platinum-iridium ring. The most important part is determination of accuracy of the measured values.

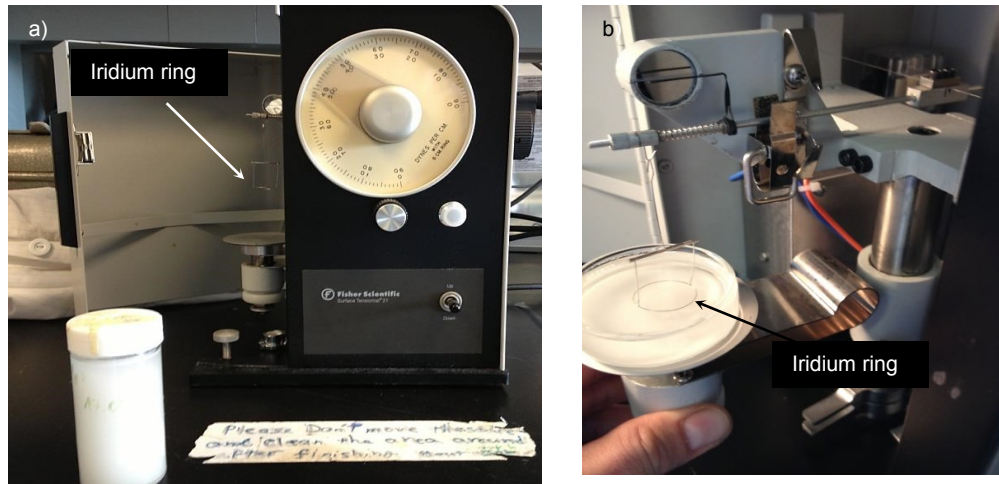


Figure 2-8 a) Tensiometer apparatus b) fluid's surface tension measurements

Based on the instructions provided by the supplier, and considering ASTM Method D-971, all the details and calculations were done with very accurate results (99.5 % accuracy in agreement with the standard tabulated values [28]).

Through the procedure of testing, after filling a beaker by suspension fluid, the platinum-iridium ring should be beneath of the liquid surface about 1/8 inch and immersed in liquid. By adjusting the knob to zero, the ring is brought to the surface of the sample fluid by lowering the adjustable table. A distended thin film of the liquid will be appearing inside the ring. This is done by simultaneously lowering the table and turning the knob until the distended film at the surface of the ring reaches to a breaking point. The point where the breaking of the liquid film is observed is the measuring point. Therefore, the apparent surface tension is obtained by the mentioned procedure, and the same procedure was applied to the other fluid samples. Table 1 provides values of the rheological properties of the four types of fluids used in the atomization experiments.

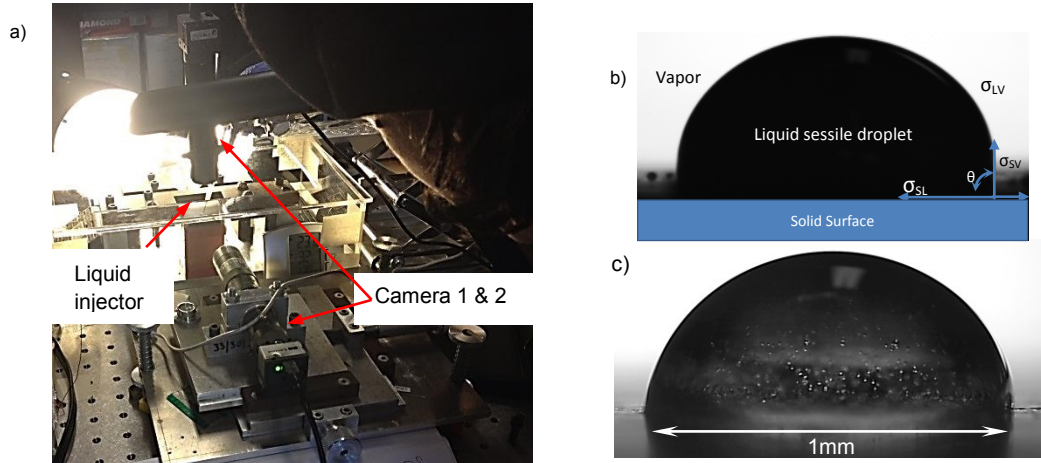


Figure 2-9 a) Imaging setup for liquid's droplet, b) various phases affecting equilibrium contact angle and c) glass bead suspension sessile droplet,

Table 1: Rheological Properties for various fluids

| At 20°C | Distilled water | 99% pure Glycerol | Solution | Glass beads Suspension |
|---------------------------------|----------------------|----------------------|-----------------------|------------------------|
| ρ (kg/m ³) | 999 | 1263.9 | 1146.6 | 1273.2 |
| μ (N.s/m ²) | 1.1×10^{-3} | 1.47 | 8.39×10^{-3} | 9.17×10^{-3} |
| ϑ (m ² /s) | 1.0×10^{-6} | 0.0011 | 7.32×10^{-6} | 7.25×10^{-6} |
| σ (N/m) | 7.3×10^{-2} | 6.7×10^{-2} | 6.8×10^{-2} | 5.7×10^{-2} |

For validation of the surface tension measurements, contact angle of the fluids as another form of surface tension measurements was done using Young equation [29, 30] as shown in figure 2-9. The equilibrium contact angle, is defined as the angle formed by interior angle of droplet surface in contact with other phases. Due to the surface tension and the intermolecular interactions of the liquid with other phases, an angle is generated at the interface of the solid substrate. Thus, the liquid and environmental air contact angle will be different from another fluid having a different surface tension.

The contact angle was measured while a droplet of a liquid with known properties is injected on a regular Teflon plate; since the specification could be found elsewhere for the Teflon

surface. After injecting a droplet with a known diameter, the contact angle was measured by Matlab image processing tool box. A suspension droplet with contact angle of 78°, water 82°, solution 84.5° and finally glycerol 89° were calculated and recorded. The suspension revealed more hydrophilic features in comparison with other fluids. Lower contact angle of the suspension droplet is indication of lower surface tension which is in good agreement with the previous surface tension measurements.

2.3. Operating Conditions of Atomization

Atomizing gas flowrate in twin-fluid atomizers plays dominant role in nozzle performance to breakup liquid into ligaments and fine satellite droplets. However, different applications require limited range of gas flow rates considering spray characteristics at nozzle outlet. For this study, thermal spray coating applications and their requirements was the main subject to arrange the flowrates.

The air flow rate varied from 0 to 0.0169m³/min (36 SCFH), while constant flowrate of liquid 0.0008m³/min (1.69 SCFH) applied for all of the running fluids. Gas to liquid ratio is defined as a ratio of the gas mass flow rate to liquid mass flow rate (GLR), provided in table 2. Details on the controlling devices for the measurement systems and the calculation of GLR are discussed in Appendix A. Further explanations regarding the various fluids and their rheological properties have been reported in the previous section. The following sections provide experimental methodology of atomization analyses.

Table 2: List of various gas flowrates used to atomize four different fluids

| Air Flow Rate (m³/min) | No Air | 0.011 | 0.056 | 0.084 | 0.0169 |
|--|---------------|--------------|--------------|--------------|---------------|
| Gas to Liquid Ratio (GLR %) | 0 | 0.055 | 1.1 | 1.6 | 2.6 |

2.4. Shadowgraphs

Shadowgraphs or known as Shadowgraphy is a flow visualization method used to take and analyze inclusive images of high speed flows. The method is widely used for the visualization of spray droplets where usual imaging systems are not practical enough to qualitatively compare the characteristics of fine droplets.

Background is illuminated by a diffused light source to provide a homogeneous intensity histogram distribution for behind the captured images. Experimental setup is illustrated in figure 2-10, where a diffused light was imposed on a secondary light diffusion object, (i.e., an opaque glass or velum paper) to make the background light more homogenous. The homogeneity of the lighting system was also adjusted by two lighting intensity controllers installed in parallel with each other. For a better visualization of the nozzle inside, one small LED lighting system was also used to provide forward illumination of the nozzle mixing chamber. FASTCAM (Photron, USA Inc.) is a high speed camera equipped with CMOS image sensor is used to provide excellent light sensitivity allowing high speed recording.

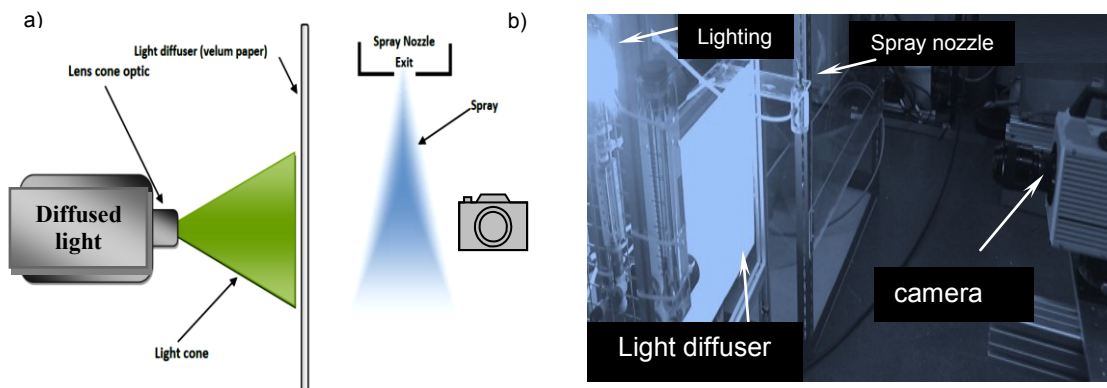


Figure 2-10 a) schematic of shadowgraphs setup, b) shadowgraphs setup by high speed camera and the nozzle installed on a stand

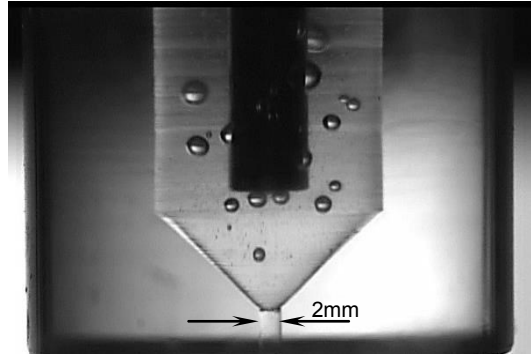


Figure 2-11 Shadowgraphs image of bubbly flow regime inside the effervescent nozzle

By using the method, high contrast gray scale images are provided revealing important details that could have not been observed elsewhere by today's common imaging methods. Typical example of shadowgraphs image is presented in figure 2-11. The image belongs to inside visualizations of effervescent nozzle atomization where one could find very sharp edges of the bubbles in bubbly regime that is very rare to be able to detect those edges or boundaries by other imaging setups.

2.5. Optical Patterning

Optical patterning is another flow visualization method used to picture the spray patterns on the horizontal plane perpendicular to spray centerline. The main advantage of this method is using a scattering laser light source to illuminate the cross-sectional spray area. In this manner, flow stream is not interrupted. Therefore, it is known as a non-intrusive way of patterning in comparison with mechanical patterning, where spray distribution patterns are determined by the volume of the liquid accumulated in tubes, placed at specified heights below the atomizer discharge. The optical method is widely used for patterning, since it uses mie-scattering laser light to illuminate the cross-sectional spray plume without interfering in the natural flow of the spray [31, 32, 33].

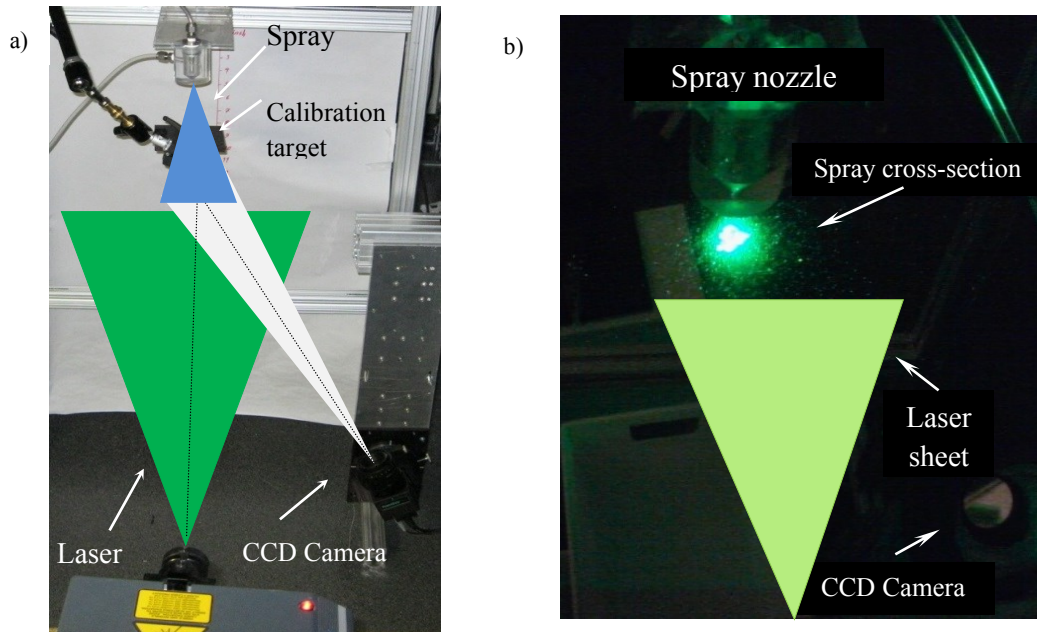


Figure 2-12 a) Optical patternation setup Off-axis PIV, b) spray patternation image

Figure 2-12 illustrates an optical patternation setup, also known as Off-axis PIV which uses Nd:YAG scattering laser to fire an illumination sheet horizontally, perpendicular to the spray axes. Figure 2-12-b is a snapshot, while the laser is fired and CCD camera is capturing the patternation images. A horizontal laser sheet was fired to illuminate the spray plume on its plane. The CCD camera and the laser were synchronized with each other in order to capture the images simultaneously while the laser is fired.

The CCD camera was located in an angle in order to keep the point of view undisturbed. It is important to note that it is not possible to install the camera at the top or bottom view due to view obstruction. Therefore, captured images have an off-axis angle and a distortion of the images is expected. This acquires resorting to an image post-processing technique called “De-warping Correction Algorithm” available in pre-processing toolbox inside the PIV software (Insight3G).

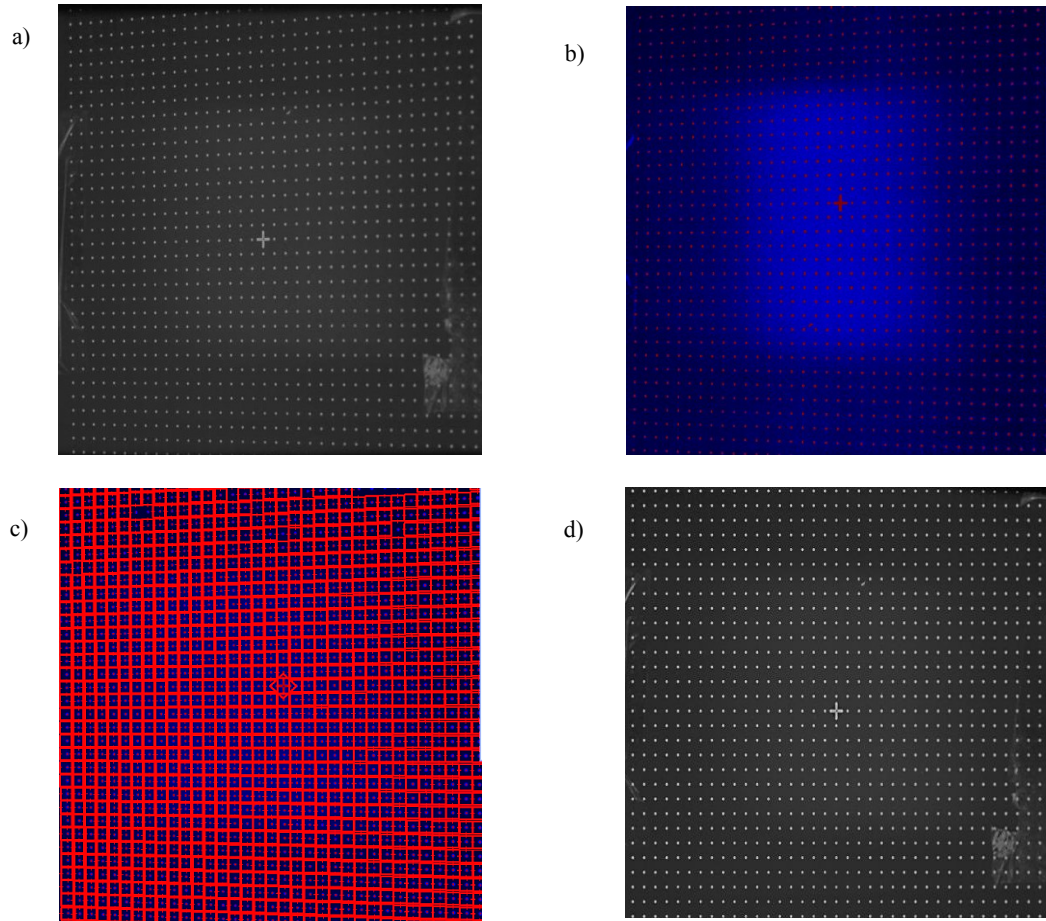


Figure 2-13 Off-axis PIV De-warping process, a) alignment target raw image, b) target dots detection, c) spatial meshing of the target, c) up to 99% perspective spatial-tilt correction

“De-warping the images from camera plane to the light sheet plane uses perspective calibration involved pixel intensity interpolation” [34]. Figure 2-13 illustrates the procedure of the de-warping in a nutshell. First, an image of the calibration target is taken by the CCD camera, then the taken image of the target is detected spatially by the software and special calibration to mesh the recognized dots is applied. Finally, the distorted image having angle respect to the camera is mapped in a position that the distortion is eliminated up to 99%.

2.6. Particle Image Velocimetry (PIV)

The Particle Image Velocimetry (PIV) also is a non-intrusive laser diagnostic technique used to attain velocity vector field of various fluids. The vector field could be obtained in a 2D or 3D domain which is called “Stereo PIV”. The 2D-PIV technique was first developed in the early 1980s and has become an indispensable tool for experimentally analyzing various fluid flows. In addition, this technique is frequently utilized to validate and improve on numerical simulations of fluid dynamics [34]. The classic 2D PIV system setup used in this study is illustrated in figure 2-14. The system is made up of an Nd:YAG laser, a CCD camera (Charge-coupled device with two frames of A and B), a pulse synchronizer, and a high performance PC for processing the digital imaging data. The PIV measurements relies on capturing two successive pair of images by the CCD camera and simultaneously illuminating the fluid body by a high power Nd:YAG laser. For further information about the setup, specifications and calibration are provided in appendix B.

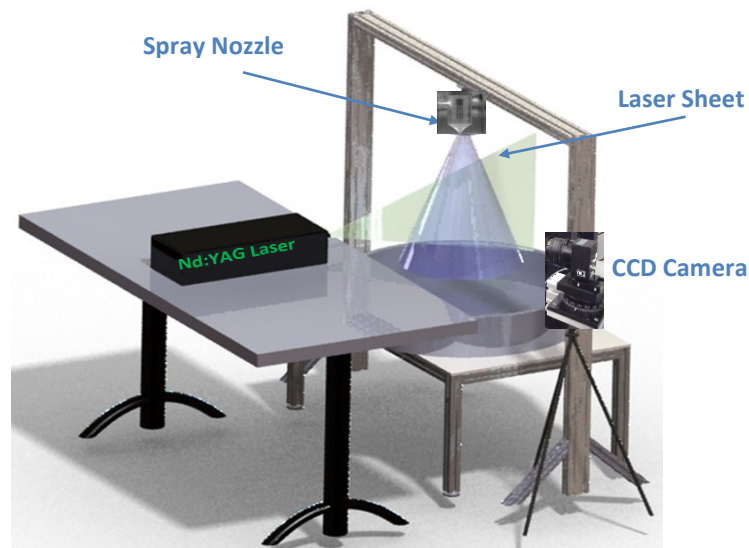


Figure 2-14 Schematic of the PIV setup

A synchronizer controls the timing of the triggers of the laser and the camera. Through the velocity assessing process as schematically shown in figure 2-15, first the laser fires a single pulse at t_0 to illuminate the spray droplets. A short time later (in the order of a few microseconds), the camera opens its iris to capture the first illuminated spray image by the frame A. Second pulse of the laser light is fired at $t_0 + \Delta t$; then, once more the camera opens its iris to capture the second image by the frame B. Above all, only a few milliseconds have passed and two images have been captured by the frame A and B with a known time delay between the frames. The droplet velocity is determined by cross-correlation using Fast Fourier Transform (FFT) algorithm as illustrated in figure 2-15. The FFT algorithm was incorporated to compute the displacement of the detected droplets with regard the time delay. Hence, the velocity components of submerged droplets are attained, since the Δt is known.

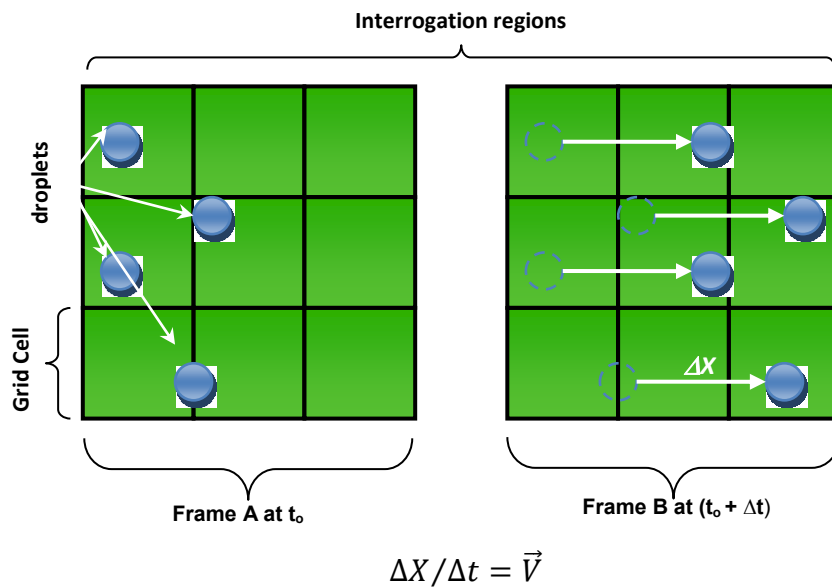


Figure 2-15 Schematic of PIV interrogation regions for velocity measurements

The captured images are referred to as frame A and B for the first and second pair of images, respectively. Each frame is divided into cells known as “Interrogation Regions” illustrated in figure 2-15. The frames are pre-processed, processed and post-processed as digital signals, whereby the illuminated droplets are displayed in their respective grayscale intensities of tracked spray droplets in the entire domain of study.

Depending on the flowrate and the GLRs, the PIV settings were also reconfigured during the whole experiments. These changes mainly include the camera aperture setting, laser source power and synchronization time snaps- classified in table 3. These changes are required due to the changes of the spray velocity where the measuring system settings will be affected. For example, if the spray is running with a high GLR, the timing should be lowered for tracking the droplets without losing them within the created grids due to higher velocities of injected atomizing gas.

In addition to the FFT cross-correlation, several rules of thumb are considered in the data acquisition system. First of all, the interrogation domain was selected to be as small as possible in order to attain meticulous details in the flow, such as swirling regions and spray back flow. There is, however, a limit to the size of the created cells /or meshes. Small cells were proven to affect the credibility of the applied correlation algorithm since fewer numbers of tracking particles were involved in the calculations. It was suggested in many studies, M. Wernet et al. 2007 [35] to select the cell size in a way that at least 5-10 particles are captured in each frame. Accordingly, for this study considering the spray and atomization pattern, the cell size was selected as 32×32 pixels equals to $2.8 \times 2.8 \text{ mm}^2$.

Another matter of concern is proper selection of the time delay Δt . If the time delay is very small, it would result in estimating lower velocity magnitudes. On the other hand, time steps

that are too large may adversely affect the PIV's capability in tracking the targeted particles. It is suggested the time step should be selected in regards of the moving particles with the highest speed gradients (at least could sweep around 25% of the interrogation region). For example, if a 32×32 cell size is used, then the time step should be selected not more than 8 pixels for a maximum displacement of the particles, L. Liu 2008 [36]. Table 3 illustrates the time step settings used for this study regarding the interrogation grid size and various GLRs.

Table 3: Setup of the PIV system

| GLR % | 0 | 1.1 | 1.6 | 2.6 |
|---|----------|------------|------------|------------|
| Δt (μs) | 100 | 80 | 60 | 40 |
| Lens Focal Length (mm) | 50 | 50 | 50 | 50 |
| Lens Aperture ($F\#$) | 8 | 11 | 11 | 16 |
| Camera Distance mm | 800 | 800 | 800 | 800 |
| Grid Size (pixels) | 32X32 | 32X32 | 32X32 | 64X64 |
| Spatial Resolution mm | 2.8X2.8 | 2.8X2.8 | 2.8X2.8 | 5.6X5.6 |

There are combinations of several factors involved in total errors and vague results detection by the system. However, it is inevitable to omit individual sources of errors completely. Therefore, several practices are available that benefit to lower the overall error rate to enhance accuracy of the analyses. As mentioned earlier, several rules of thumb must be applied and taken into account to ensure that the obtained PIV data has more than 95% accuracy in the representation of the flow characteristics.

It is clearly depicted in figure 2-16 that the background noises play a crucial role in the computational domain in the FFT cross-correlation by detecting faint low intensity particles. One of the main sources of the background noise is saturated images. The saturated images should be avoided in order to lower the background noise. On the other hand, low intensity particles in the images also could be detected as a noise. In addition, a secondary reflection

of the laser light by the surrounding material of the setup is another important noise basis which could affect the captured images by the CCD camera with high intensity images as over saturated points. Hence, it is critical to select the accurate laser power, and the correct camera aperture to come up with minimal background noise images.

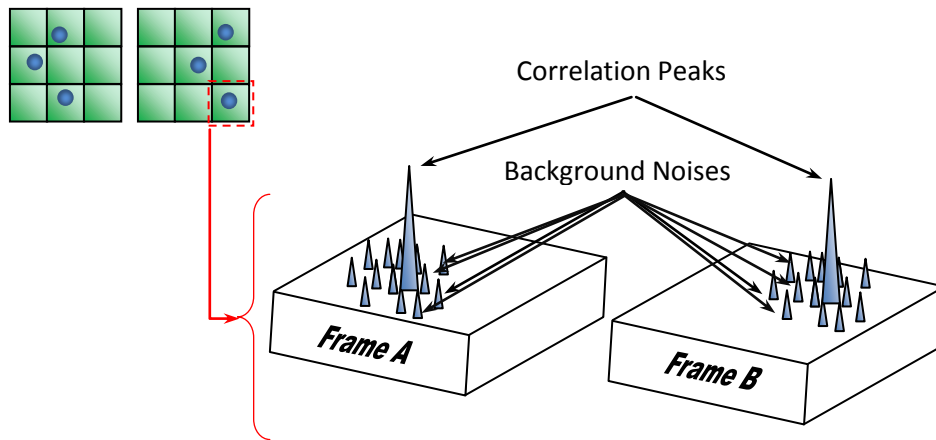


Figure 2-16 Detection of light intensity reflected by droplets [41]

The first solution for ensuring minimum noise could be the reduction of background noise in the source. For example, in the setup, the shiny objects should be cover by laser protection covers to avoid the high intensity saturated reflections captured by the camera. Secondly, by calibrating the camera in the first image and also for each GLR during the experimenting, one could come up with appropriate laser power for calibration images with the least background noise.

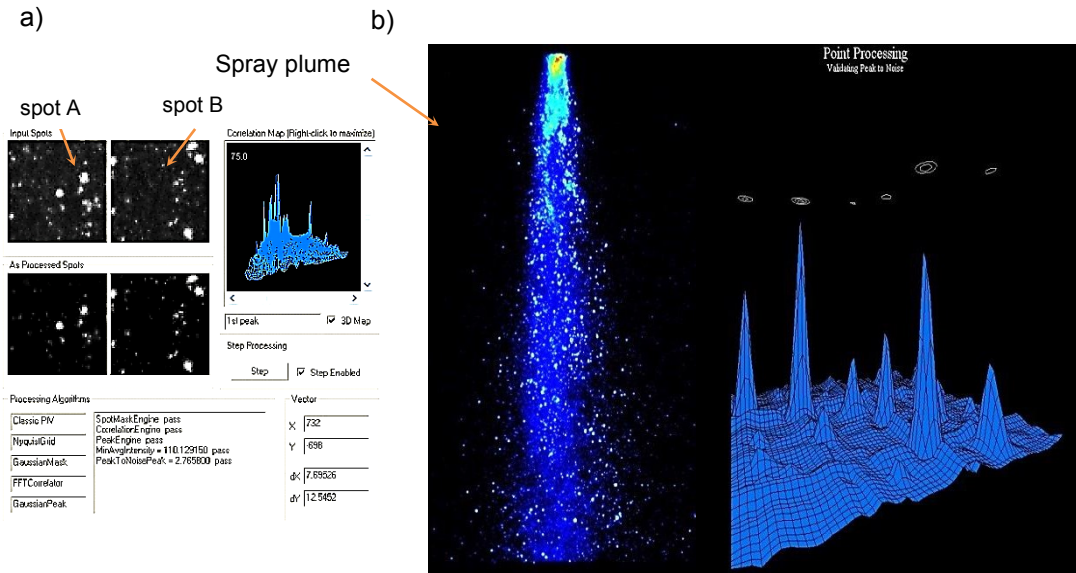


Figure 2-17 a) Light intensity contour of captured images b) subtraction of background noise by cross-correlation of the detected light contours

As explained above, the captured images will certainly have noises. These noises can be eliminated by Background Subtraction (BS) technique. Figure 2-17 is an illustration of an effervescent spray flow while monitoring point-processing method as required for BS. In figure 2-17-a, spot A and B before and after background subtraction are depicted, and the related reflected correlation light intensities are provided in figure 2-17-b. The noticeable point is spots A and B after BS in which fairly clear backgrounds are obtained.

For the background noise elimination, it is necessary to capture more than 1000 images of the whole actual spraying setup. The images without spray flow will be stored. By using the PIV's processing toolbox, they will be analyzed and computed to obtain average intensity of the individual images by super-imposing the each computed image. The result is a new image with the total average intensity of the entire captured raw images from the setup, called

“background images”. Then the images of the spray flow will be captured and stored. For this study, 1000 pairs of images are captured for each GLR and each fluid. Then, the background images are subtracted from the actual images of the experiments. This provides a clear background and high contrast image which is more optimized in terms of processing time, accuracy of the processing and post processing. However, not all the noises (faint particle observed in each frame) have been removed from the images (including the correlation algorithm itself). Hence further post processing and point processing are required for extra validations.

One of the post-processing validation methods used is called “linear general selection algorithm”. This is a specific algorithm used in PIV for the elimination of background noise, and also for the back-flow effects using Median of Medians algorithm. The method functions by looking at the whole domain to remove spurious vectors raised as a result of errors in the correlation plugins. Each individual targeted spray droplet vectors is considered in this algorithm. The particles intensities are compared with the neighboring detected vectors by ranking the vector magnitude and removing the spurious vectors.

For instance, in a field of computation, if detected particles show velocity magnitude of 3, 5, 4, 5, 3.5, 4.2, 25, -32 m/s, their average will be 2.21. However, the median of medians algorithm will be 4.11. Note how the difference is considerable where the value obtained applying the median is almost two times larger than mean value. As noticed, the vague numbers such as 25 or -32 are omitted in the median selection algorithm due to the significantly high or low ambiguous values, respectively. Therefore, the median selection algorithm eliminates spurious vectors affecting the results to provide more accuracy.

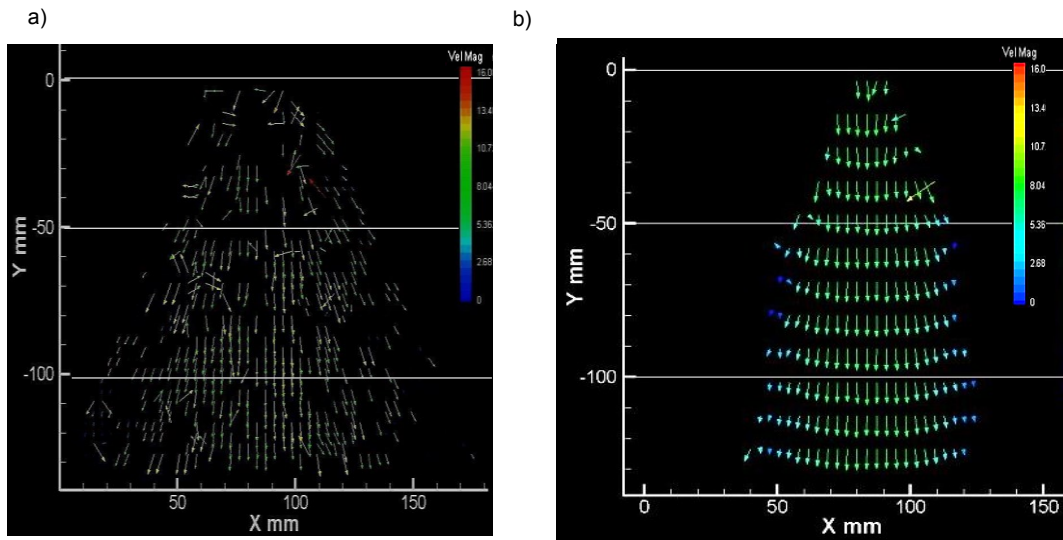


Figure 2-18 Spray velocity vector field, a) without elimination and b) after elimination of spurious vectors using Median of Median selection Algorithm

Figure 2-18 illustrates processed vectors, detecting spurious vectors and elimination of them after post-processing. Resolving the ranges in which the eliminations of the spurious vectors or magnitudes are considered is critical while setting up the post-processing toolbox features. As provided in the setting manual, comparing the range for determining the neighboring cells is provided by cell numbers. For example, a reasonable choice will be comparing neighboring in 5×5 or 7×7 cells; where comparing a vector is done by the 7 cell of the neighborhood cells. In other words, each detected droplet is compared with neighboring cells in which the closer, the more accuracy will be obtained; however, the computational time will be increased significantly. In turn, a choice of 3×3 is not acceptable, especially for dilute sprays since it considers only 3 of the surrounded grids.

2.7. Phase-Doppler Particle Analyzer (PDPA)

Phase Doppler Particle Analyzer (PDPA) is known as a non-intrusive laser diagnostic measuring technique. The system utilizes essential basics of Doppler Shift, or the Doppler Effect named after Austrian physicist Christian Doppler, who proposed the change of frequency of wave observed by a photo-electric receiver and called Doppler Effect [37]. The basic concept behind the development of the PDPA system is evolved from the Laser Doppler Velocimetry (LDV). The main difference between LDV and PDPA is capability of droplet size determination by the latter method.

Figure 2-19 demonstrates the PDPA setup used in the study of the effervescent spray consisting of four fundamental components including illumination system (converging laser beams Argon-ion based Class IIIB transmitter with maximum power of 560 milliwatts), an optical receiver (made of optical components inside), a signal processor, and a high performance PC to receive and analyze the data.

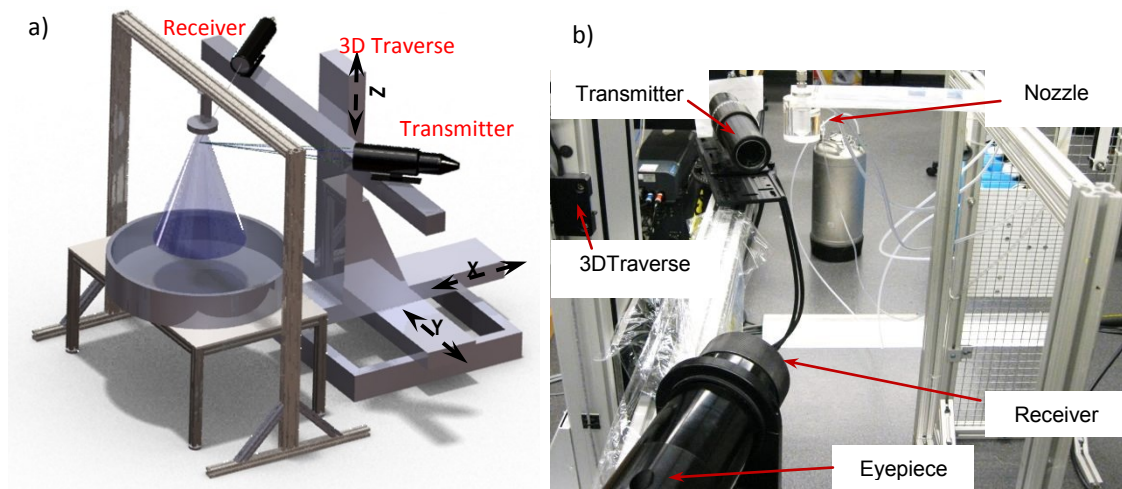


Figure 2-19 a) PDPA schematics & b) a snapshot of PDPA main components

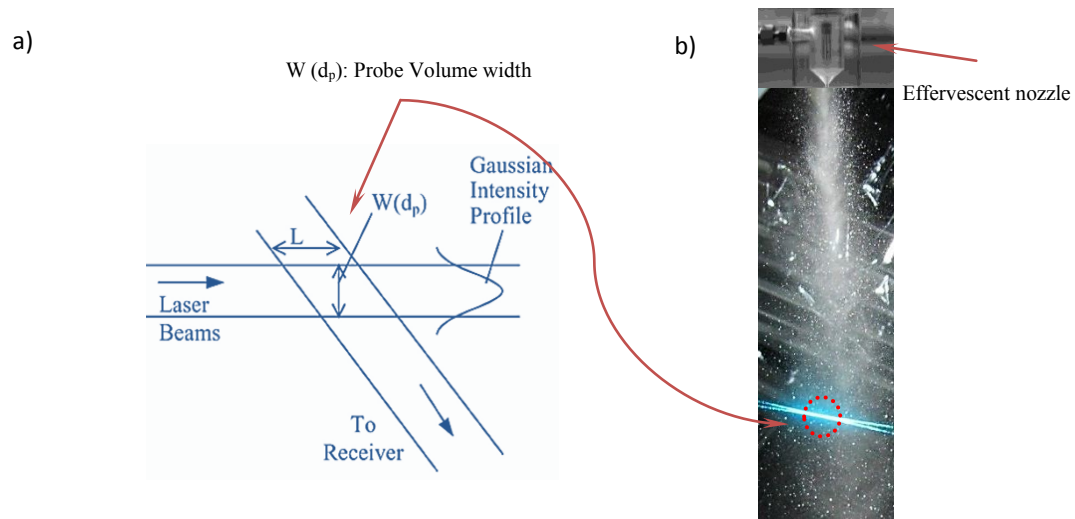


Figure 2-20 PDPA velocity measurements mechanism a) probe volume, b) four laser beams focused on a point of study on spray plume

Figure 2-20 provides detailed information of the PDPA computation method for velocity and diameter size measurements. Fired laser is consisting of two types of laser beams, blue and green for each component of velocity (u , v). The convergence of the totally four transmitted beams into a point creates a point of study where is subject to gain the required data. The point of study creates a volume known as “Probe Volume” as illustrated in figure 2-20-a. The converged laser beams to a point known as point of study is illustrated in figure 2-20-b while the beams are focused into the point in front of the optical receiver.

The main concept behind the PDPA measurement is considered as an Eulerian coordination where the assessing system studies a specific point in space and resembles the point as a control volume to measure any passing through particles. The main reason of using the converging laser beams in the illumination system is the Eulerian coordination requirements of point-wise measurements. For measuring droplets all over the spray plume, a 3D traverse, having a minimum of 1mm spatial is used to sweep captured the data based on a user defined positioning matrix.

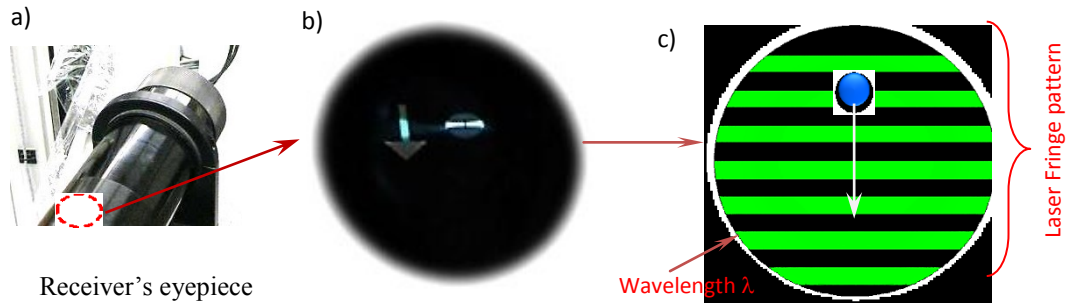


Figure 2-21 a) Optical receiver b) probe volume fringe pattern snapshot from receiver's inside detecting dark and light zones regarding spray positive direction, c) schematic of fringe pattern motion formed by laser beams with known wave lengths

The probe volume is formed of a series of dark and light zones at the intersection of the two laser beams. The dark zone with lined arrangement creates a fringe pattern inside the probe volume illustrated in figure 2-21. The dark lines possess known distances from each other. They make it possible to detect the light zone from dark fringes. A light sensitive receiver where probe volume is captured by, made of Photomultiplier Tubes (PMT), is located normal to the plane of dark fringes as illustrated in figure 2-21-b which is an actual receiver inside image taken through the receiver's eyepiece. Creation of a 90 degree intersection between the light and dark fringes is due to the capability of the receiver to detect the refraction and off-reflection of wave lengths scattered by particles while passing through the probe volume, generated by converged laser beams on the spray plume.

The reflected light is detectable by the receiver due to the presence of the light and dark zones with known spacing δ_f from each other. When a droplet passes through the probe volume, refraction of the distorted light is mirrored into the receiver where the altered signal is transported to a multibit digital processor by fiber optic cables. The signal processor

converts the reflected light signals into digital signals before they are displayed as measured data on a computer processor.

“The fringe pattern is calibrated in a method that light rays possess a specific wavelength λ in the order of nanometers” as previously shown in figure 2-21 [37]. The signal processor measures the time (inverse of signal frequency) that takes for a refracted wave of a droplet with known wave length to pass through the probe volume. Afterwards, velocity of the subject droplet by multiplying the fringe spacing δ_f to the frequency of the detected signal f_D is calculated by $u = \delta_f f_D$. Therefore, the velocity of the droplet passing through the probe volume creating a signal reflected to the receiver is calculated by the data processor.

The advantage of PDPA in comparison with the conventional LDV system is the diameter measurement of seeded particles or droplets representing flow velocity via PDPA. For better understanding, a simple example of a large and a small droplet passing the probe volume transferring the refracted laser light to the digital processor as an example of the measurement method is illustrated in figure 2-22. The photo-sensitive receiver is made up of three PMT face plates, known as channel A, B and C with regard to the X, Y and Z directions, respectively.

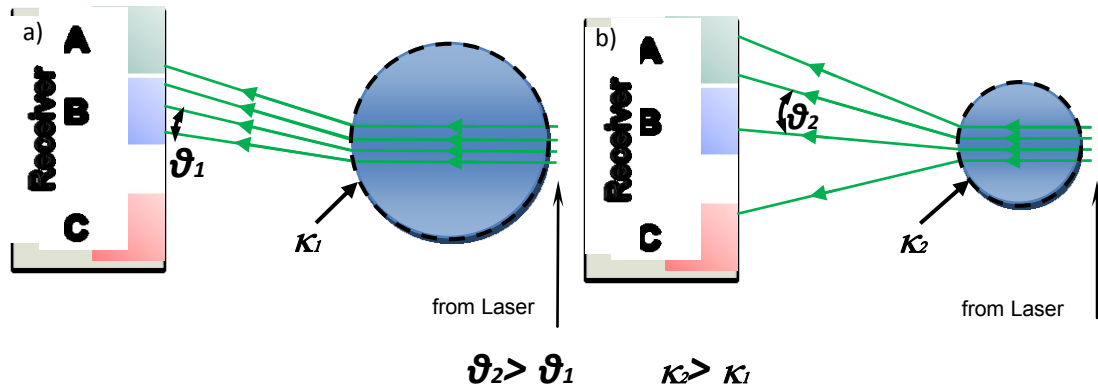


Figure 2-22 Diameter Measurement by curvature radius changes: a) large volume of droplet with smaller curvature (κ) results in smaller phase angle (ϑ) difference, b) small volume of droplet with sharp curvature results in greater phase angle changes [38]

“The PMT plates are placed at a specific distances from each other, where each plate detects the refracted light at slightly different angle [37]”. In figure 2-22, a larger droplet passes through the laser light to alter the original wave length and its path. It is clarified in the image that a large droplet in comparison with a small one has shallower curvature, resulting in the angle between each light ray to deviate slightly. However, if the targeted droplet size becomes smaller, the refracted rays detected by the PMT plates will be wider between each ray.

A smaller droplet with a sharp refracted ray angle in comparison with the large droplet with shallow ray angle refraction will provide different shifted phase angle. The face plates will detect the altered degree known as a shift in phase angle to determine how large or small a droplet is. In other words, the smaller droplets provide sharper phase angle causing the rays to deviate significantly. This angle or phase shift relies on the laser beam properties and the setting of the PDPA measurements during the calibration and experiments. The parameters used in the experiments are presented in table 4.

Table 4: Laser beam properties of PDPA system

| | Channel 1 (Green Laser) | Channel 2 (Blue Laser) |
|--|-------------------------|------------------------|
| Laser Power (mW) | 500 | |
| Transmitter Focal Length (mm) | 512 | |
| Max Diameter Difference | 7% | |
| Beam Expander (ratio) | 1.0 | 1.0 |
| PMT Voltage (V) | 525-550 | 525-550 |
| Max Number of Samples | 10,000 | 10,000 |
| Band Pass Filter (MHz) | 2-20 | 1-10 |
| Downmix Freq (MHz) | 38 | 37 |
| Time Out (s) | 30 | 30 |
| Burst Threshold (mV) | 200-300 | 200-300 |
| Wavelength (nm) | 514.15 | 488 |
| Focal Length (mm) | 363 | 363 |
| Laser Beam Diameter (mm) | 2.65 | 2.65 |
| Fringe Spacing (μm) | 3.7441 | 3.7441 |
| Beam Waist (μm) | 84.93 | 80.55 |
| Bragg Cell Frequency (MHz) | 40 | 40 |
| Scattering Mode | Refraction | |
| Polarization | Normal to beam | |
| Scattering Off Axis Angle ($^{\circ}$) | 37 | |

For the entire spray plume and the characterization of the total spray droplets, one should scan different points in space. Using a 3D-traverse, different locations based on the matrix of defined positions on the spray plume were scanned. For this reason, 9 radial points of interest at 3 axial distances resulting in 27 measurement locations for each fluid was examined. Three different GLRs multiplied by the 27 points, resulted in a total of 81 points for the spray characterization of each fluid type.

The PDPA technique is able to study droplets with diameter sizes varying between 0.5 up to 350 μm and having velocities up to 200m/s. In a nutshell, the PDPA technique is accurate in measuring wide ranges of spray characteristics in various operating conditions spatial resolution in comparison with the PIV measurements. For more information regarding the software, details of chosen points and the hardware components of the PDPA system, sufficient information is provided in appendix B.

One important issue occurred with the suspension atomization diameter measurements, where the presence of suspended solid particles with different refractive indices could result in biased data. The scattering domain selection where reflection or refraction mechanisms should be identified for the PDPA system was the main subject in order to select the proper diameter optic settings considering refractive indices, standard polarization, and attenuation level of each fluid. To take into account the effects of various refractive indices of multiphase flow such as suspension fluid, averaging of the refractive indexes of material is applied. One could find different refractive indexes of various materials used in table 5. Considering the refractive index of glass beads which is suspended into the solution, the refractive index of 1.46, with off-axis angle of 37 degrees, and a standard polarization, the domain 11 is selected for the suspension atomization.

Table 5: Refractive indices of different materials

| Material | Distilled water | Solution: | Glass Beads |
|-------------------------|------------------------|------------------|--------------------|
| Refractive index | 1.33 | 1.42 | 1.52 |

The PDPA measuring technique similar to the PIV has certain error sources. The randomly captured errors may cause biased data. One of the main sources of errors is derivate from PMT (photo multiplayer tubes) voltage settings. The PMT voltage setting is used to determine the receiver's optical-sensitivity to the refracted/or reflected lighting signals. In general, the higher the PMT voltage, the more sensitive the receiver will be. If the receiver sensitivity becomes too high, the PDPA system mainly receives and measures noise rather than the actual droplets reflections; and the recorded results will be affected dramatically.

To adjust the PMT voltage for a specific test setup, with different GLRs and different fluids, the PDPA laser has to be focused at the densest region of the spray plume in order to calibrate for the most complex condition. For this goal, a 25mm axial distance from the nozzle exit (the location of a dense spray with many satellite droplets) was chosen for the calibration purposes.

Figure 2-23 is a demonstration of PMT voltage variation for each channel versus mean diameter (D_{10}) size by varying the PMT voltage from low to high. Number mean characteristic diameter (D_{10}) is based on averaged value of the counted droplets. Lower values of the voltage where the least noise is captured –that is 350 V- is a good point to start. As the PMT voltage is increased, the receiver sensitivity becomes higher and the PMT plates are able to detect the smaller D_{10} values. The increase in the voltage should be continued until D_{10} is almost constant and does not decrease anymore. The settled value is the most optimum PMT voltage. Because of the higher refractive indices associated with the solution and suspension, the PMT voltage of 525V used for water spray analyses increased to 550V for solution and suspension fluids.

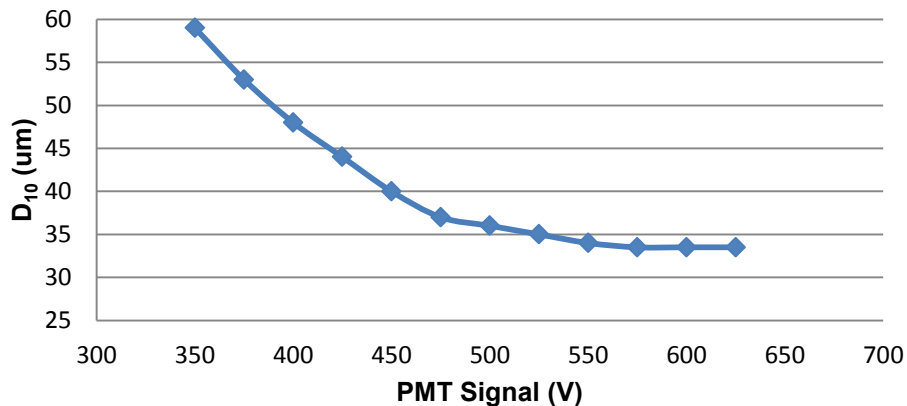


Figure 2-23 PMT voltage calibration for diameter size determination D_{10} (μm)

“One of the characteristics in the PDPA measurements is that the fringe pattern of the converging laser beams takes on a Gaussian distribution where the light beams are almost thicker in the center and weaker at the outer edge” [37]. In other words, Gaussian light signals distributions are obtainable if the detected droplets pass at center of the fringe. In many cases, larger droplets while passing through the fringes, even if they pass on the center have tendency to reflect non-Gaussian distributions in comparison with the smaller ones. This could affect the results since they will not be counted as examined droplets at the specific point.

Similar to the PIV, reflection of laser light from surrounding shiny objects is detected by the receiver PMT plates- biasing the results. Therefore, it is recommended to avoided generation of the noise at the source. To avoid these reflected high intensity signals, Flowsizer (PDPA’s software) has the ability to monitor the received light intensity for validation reasons called “Intensity Validation”. That not only affects the diameter measurement, but also volume flux calculations. Figure 2-24 illustrates two different cases for the intensity validation of the acquired data.

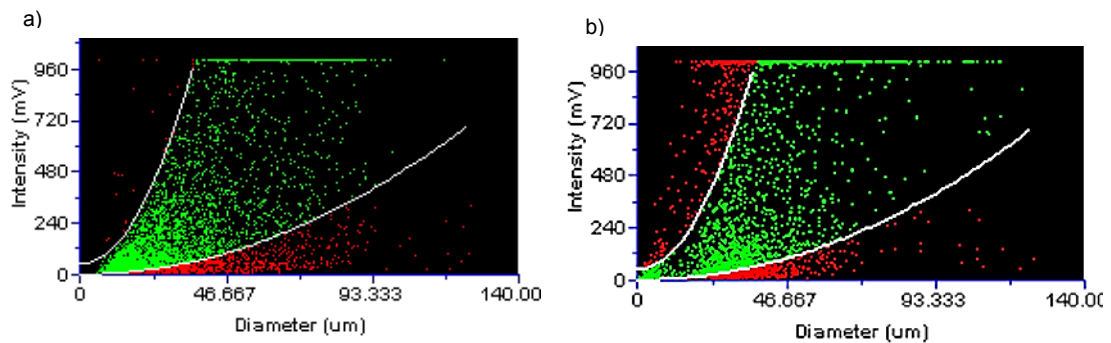


Figure 2-24 Examples of intensity validations for data cluster creating a natural curve of green dots and red dots as biased data a) acceptable domain, b) fairly acceptable

The intensity validation method provides a differentiation boundary for selecting cut-off data; in which the data beyond a certain limit are not considered in the calculations. In figure 2-24, the entire data detected by the receiver is plotted by dots, red and green. The red and green dots illustrate individual diameter measurements of the detected droplets passing through the fringe motion versus their respective signal intensity (mV). It is noticeable how a cluster of green dots corner themselves within a certain average size and create natural parabolic curve. Green and red colored dots represent accepted and rejected data, respectively. The red dots could be representative of those not passes through the center of the fringe, and created faint intensity signals picked up by the receiver. Therefore, this technique provides more accuracy in the PDPA computations. For example, for a point of interest, if a SMD of $52.31\mu\text{m}$ is obtained with no intensity validation, the value could be reduced to $43.33\mu\text{m}$ when the intensity validation procedure is applied. This means improving the accuracy up to 25% which shows the importance of this type of validation. In figure 2-24-b, the detected dots on the left side of the curve are not included in the calculations. Consequently, the results will be biased in a way that larger sizes will be obtained for the diameter values.

Not only the intensity validation procedure is required to validate the data acquisition, but also other validations such as diameter difference versus diameter. Figure 2-25 is an illustration of acceptable case versus a case which needs improvements. Based on the experience have been obtained through two decades conducting the PDPA technique, rejection of any droplets whose mean diameter exceeds $\pm 7\%$ of the recorded diameter size is recommended [37, 39]. In other words, to validate the recorded data, the method uses elimination of the droplets whose size is out of $\pm 7\%$ expected mean diameter size. For instance, if the range of expectation of SMD size is between 30 to $70\mu\text{m}$, the software will

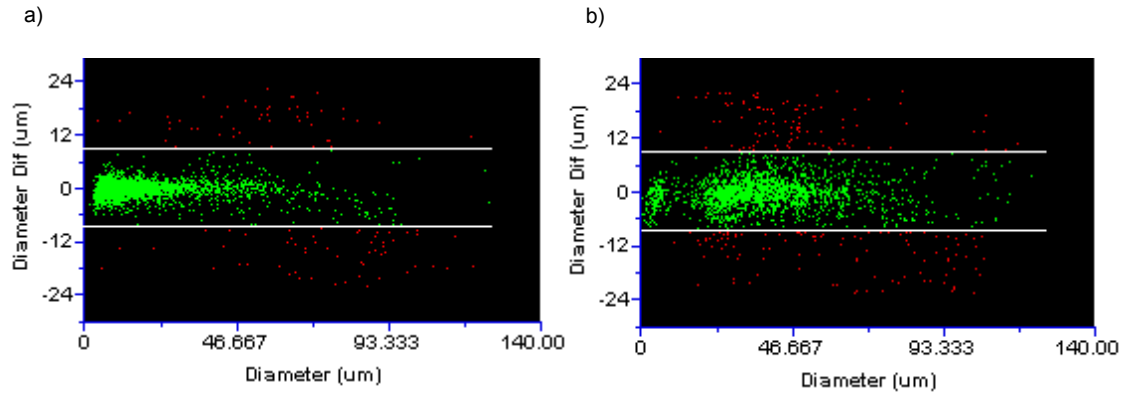


Figure 2-25 Validation of droplet diameter size distributions with $\pm 7\%$ symmetric diameter size variation of a) acceptable b) fairly acceptable

-reject those who have size larger than 74.9 or less than $27.9\mu\text{m}$. Nonetheless, as operating condition changes, the resulted plots will be different though.

Plotting diameter size difference versus diameter has another advantage which provides information about how the spray is spread. For example, one could find the symmetric distribution of the generated spray plume by this method. In addition, it is feasible to estimate mass flux at different locations.

Diameter versus velocity should be examined. The category of the diameter versus velocity could be found comprehensively by Westerwheel and Schwarzkopf et al. [40, 39] where the effect of floating small mist droplets surrounding the spray versus their velocity had been examined. In the case of spray flow, there is always floating fine droplets surrounding spray plume that a receiver detects as passing particles. These small droplets have very low velocity and often are in contrary with the spray positive direction-respecting gravity. Therefore, the acquired data will be affected while averaging the counted valid data. However, based on

their investigations, it is revealed that in a dense spray diameter versus velocity validation effects is not more than 3% of the total value for diameter size values- which is negligible.

3. Results and Discussions

The first set of results consists of Shadowgraphs of different fluids associated with the nozzle internal flow pattern and an external atomization as the main subject of the visualizations. For temporal variation studies of the aeration process, continuous spray motion is imaged by the high speed camera for particular time intervals. The parameters measured from the imaging are: spray cone angle, breakup length through primary and secondary. To establish a benchmark, one should qualitatively compare the possessions of rheological variations of the fluids behavior by the visualization. Afterwards, PIV and PDPA as the secondary measurement tools providing quantitative information dealing with velocity field, droplet size and their distributions at various locations from the nozzle discharge orifice. Finally, the provided information will shed light for insight and comparison of the recorded and computed data.

3.1. Internal Flow Visualizations

Upstream internal flow governs characteristics of the external spray plume, such as breakup length through primary-secondary, and spray cone angle. Mixing of base liquid via aeration gas inside the mixing chamber leading to two-phase or multiphase flow regime (by adding solid particles), makes the internal flow copiously complex. Bubbly flow as an inherently random phenomenon has more convolution due to evolution of the generated bubbles upstream while passing through the converging chamber and nozzle discharge orifice. The generated bubbles considerably undergo a significant amount of stretching in the converging section to accommodate larger sizes of the bubbles inside the liquid trunk jet. This is highly affected by the injection method of the aeration gas into the chamber and the operating conditions such as air injection pressure drop, GLR and aeration tube structure.

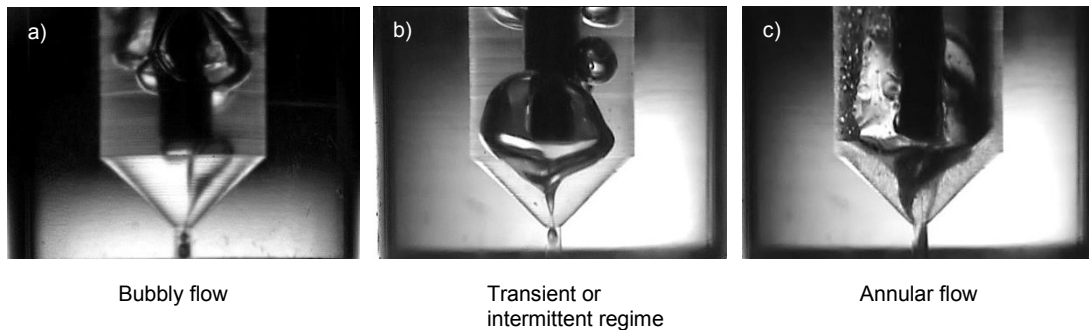


Figure 3-1 Internal flow pattern transitions of a) bubbly flow b) intermittent and c) annular flow regimes as the GLR increased

Figure 3-1 is a demonstration of various GLRs creating bubbly regime and the pattern transition into slug and annular flow by increasing the gas injection rate. At the low GLR (0.055%), individual bubbles are carried by the liquid from the mixing chamber through the converging section and the nozzle discharge orifice. A noteworthy point is the necking of large bubbles trapped in the liquid at the vicinity of the circular discharge orifice due to local pressure changes. At the low GLR of 0.055% (figure 3-1-a), rather large bubbles with an average diameter of 3.5mm are formed near the aerating port. The bubble is disintegrated into smaller bubbles due to the pressure drop at the converging section. Consequently, the sequence of smaller bubbles passing the discharge section is increased. Increased bubble numbers will result in continued bubble burst at the nozzle exit where the pressure of the air bubbles overcomes the surface tension force at the interface of the liquid trunk.

Further increase of the gas flow rate, bubbly regime gradually transits to the consequent regimes called “intermittent and annular flow” (figure 3-1-b) where the bubbles no longer exist and the discharge section of the nozzle is occupied with a round gas jet surrounded by thin liquid sheet. This is in good agreement with other reports, T. Roseler and Lefebvre 1989 [8]. Furthermore at the maximum GLR (2.6% figure 3-1-c), separated annular jets observed.

Separation of the gas jets exiting from the aeration holes at the converging section, despite merging and forming a single air jet, occurred due to higher gas injection rates. The higher the gas flow rate, the better the atomizer performance, leads to a larger spray cone angle and a faster breakup of the liquid trunk. These improvements are due to the extra injected pressure by gas to the carrying fluids to breakup the liquid trunk at the nozzle exit.

Purified Glycerol (99%) representing an extreme viscous liquid was conducted for atomization purposes and the results is demonstrated in figure 3-2. Increased viscosity of the glycerol has significant tendency to prevail at the bubbly regime for the GLRs up to 2.6%. This is in good agreement with the findings of Chin and Lefebvre 1993 [41].

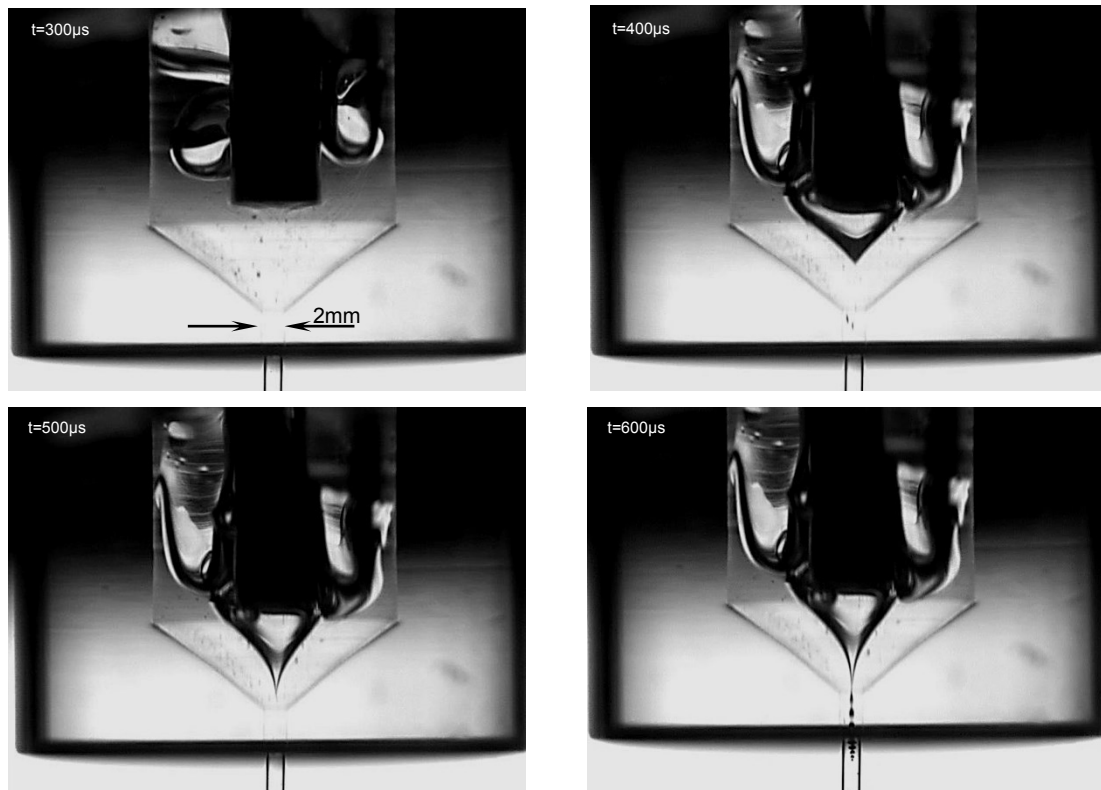


Figure 3-2 Time interval evolution of Glycerol atomization analyses; bubbly regime attempting to shatter the liquid trunk ($\mu_{\text{glycerol}} \approx 1400 \times \mu_{\text{water}}$)

Figure 3-2 is a temporal evolution of the glycerol atomization taken at particular time duration of 550 μs . At the first step, it is clear that the generated colossal air bubbles are incapable of coalescence and form voids at the nozzle mixing chamber. Despite, the bubbles continued separated from each other. Alternatively as the time passes with 100 μs delay of each image shown, the bubbles surrounded by the glycerol are carried downstream through the converging section where the velocity of the local fluid was increased due to smaller confined cross section of the nozzle geometry. As the velocity is increased at the converging section of the nozzle, the local pressure is dropped; therefore the bubbles merge and form larger single bubbles. The single bubbles at the vicinity of the discharging section disintegrate into smaller spherical bubbles trapped by the glycerol liquid trunk.

Fluid rheological properties control the atomization process of the effervescent atomization, as well. The trapped bubbles incapable to overcome the surface tension strong damping force of the surrounding viscous glycerol; hence, they are not capable of bursting at the nozzle exit and fragment the bulk fluid into smaller droplets as depicted in figure 3-3-a. As the GLR is further increased up to 2.6%, the immersed bubbles into the glycerol film remain inside the liquid jet without bursting. However, the only difference by means of extra injected air results in altered shape of the bubbles having semi parabola mode as shown in figure 3-3-b. the extra gas attempts to stretch the bubble by extra injected pressure forces. However, the balance of force between the bubble inside pressure and surface tension pressure is in a way that surface tension and viscous forces outweigh the bubble internal pressure. Therefore, the bubble is not to burst, hence the shape is changed to parabola with the extra injected gas. Note that smooth surface of the glycerol trunk without exterior perturbations due to viscous damping forces of high viscosity.

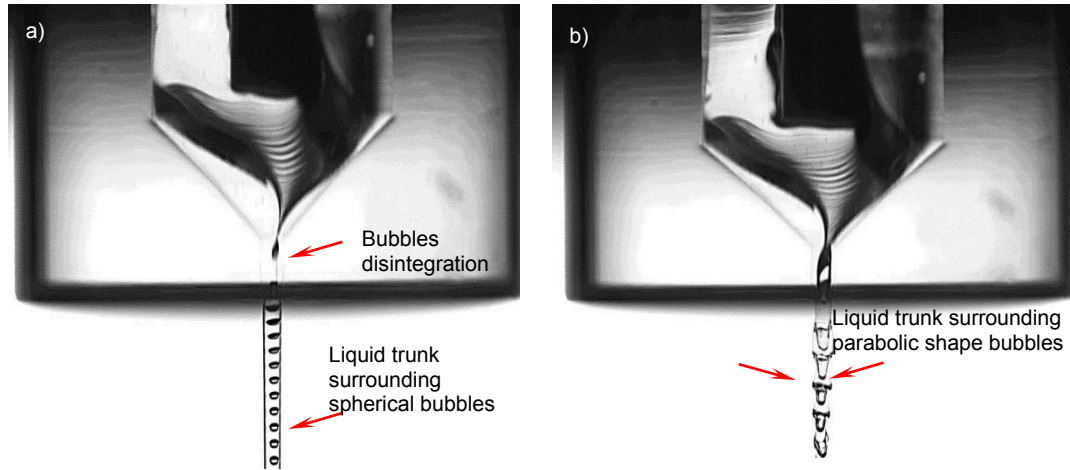


Figure 3-3 a) spherical bubbles at a GLR of 1.1% and b) parabolic shaped bubbles at a GLR of 2.6% of glycerol atomization ($\mu_{\text{glycerol}} \approx 1400 \times \mu_{\text{water}}$)

Furthermore, suspension fluids rheological properties also affect the effervescent internal flow pattern. By adding solid particles into the solution (water+glycerol 50% Vol), the properties of the base fluid has changed (table 1). Visualization of spherical sessile droplets and a bubbly internal flow are given in figure 3-4. The first set of the images belong to sessile droplets as representative of each fluid of solution and the suspension, respectively. Noteworthy point is the presence of spherical particle homogeneously distributed in the 1mm diameter sessile droplet.

In the second set of images of figure 3-4 randomly generated air bubbles in the suspension fluid portrayed another feature of bubble size dependency on the surface tension due to the shear force effects of the suspended solid particles. The main difference between the solution and the suspension flow at a bubbly regime is the presence of the solid particles. These particles create shear force to the surrounded bubbles. Hence, the shear forces applied on the bubbles halts the bubbles' evolution; despite breaking them into smaller sizes. Therefore, the bubble size is much smaller in comparison with solution

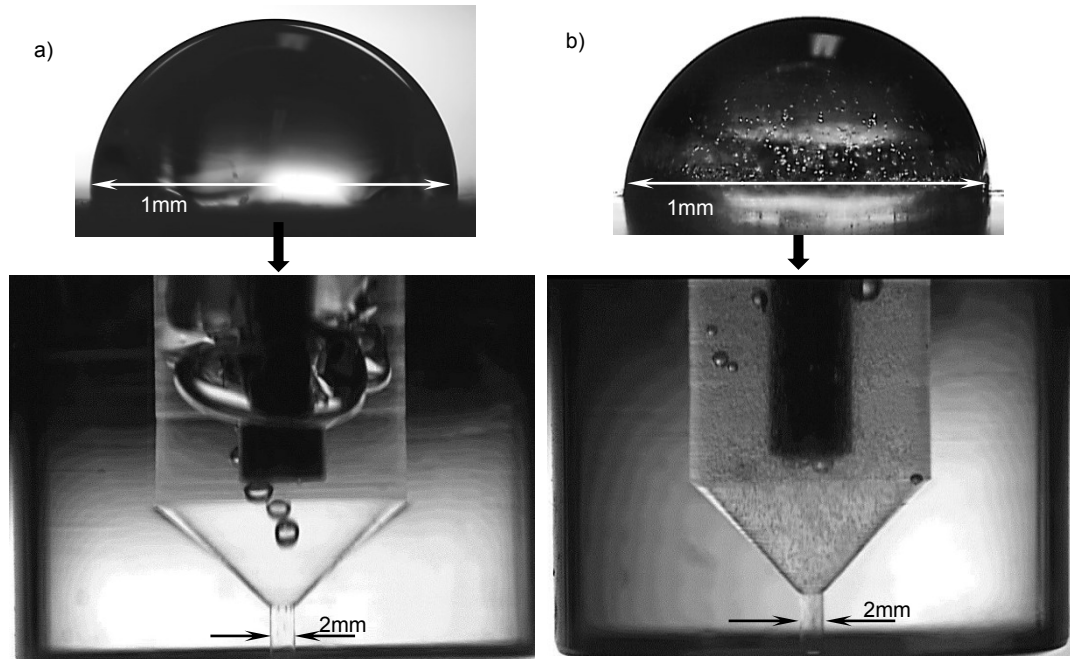


Figure 3-4 a) Aqueous solution droplet and internal bubbly flow, b) suspension droplet and bubbly regime inside the nozzle

Lastly, figure 3-5 is a comparison between three fluid types bubbly flow running at similar operating conditions. However, as reported by Bai and B. Thomas 2001 [42], the bubble sizes are not constant at particular operating conditions. Figure 3-5-a belongs to water aeration where the larger bubbles with an irregular sequence are formed by air injection at the nozzle mixing chamber. After coalescence and forming a void, the bubbles are disintegrated at the vicinity of the discharge orifice, creating a higher frequency rate of bubble generation. The second fluid is the aqueous solution aeration, where smaller bubbles experience the same trend for atomization. However, due to the higher viscosity, the bubble sizes are decreased, figure 3-5-b. Finally, suspension aeration similar to the other fluid types contains bubbles immersed into the suspension fluid, illustrated in figure 3-5-c. Nonetheless, the decreased surface tension and shear forces applied by solid particles to the generated bubbles forces them to be smaller than the other fluid type's bubbles.

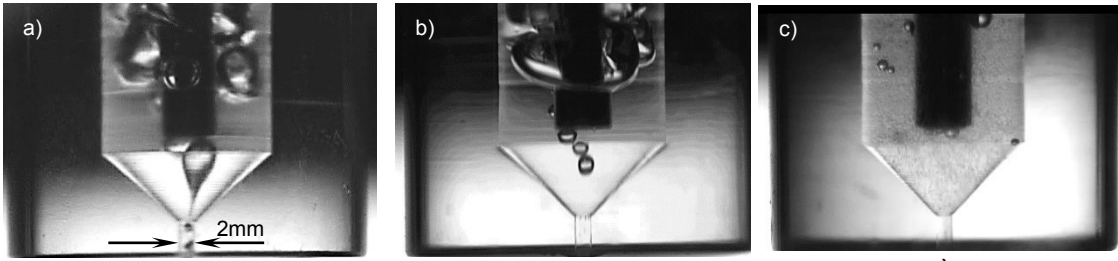


Figure 3-5 Bubble size comparison of a) water, b) solution & c) glass beads suspension operating at a GLR of 0.055%

3.2. External Flow Visualizations

Qualitative and parametric analyses of the diverse atomized fluids and operating conditions at the nozzle exit is the scope of the external flow visualizations. The relationship between the internal flow patterns with the resultant external flow will be likewise portrayed in this section. Then, studies of the near orifice of bubble bursting mechanism and spray characteristics (i.e. spray cone angle and breakup lengths) will be comprehensively discussed.

Similar to the internal flow visualizations, the first set of images shown in figure 3-6 represents the effect of GLR on the atomized fluid pattern. For small GLRs (up to 0.055%), separated bubbles (i.e. bubbly flow) at the nozzle exit ensued the bubbly trunk liquid. Specifically at GLR of 0.03%, the bubbly liquid trunk discharged from the nozzle expands, bursts the surrounding liquid into fine shreds and satellite droplets due to pressure variance amongst surrounded bubbles by the trunk jet. The bubbles burst, and the consequence is an undesirable disparate continuous liquid column. The non-continued flow is the result of the delay between the individual bubble bursts. The bubble bursting continues until GLR reaches 1.1%, where the transition from bubbly regime to intermittent flow happens.

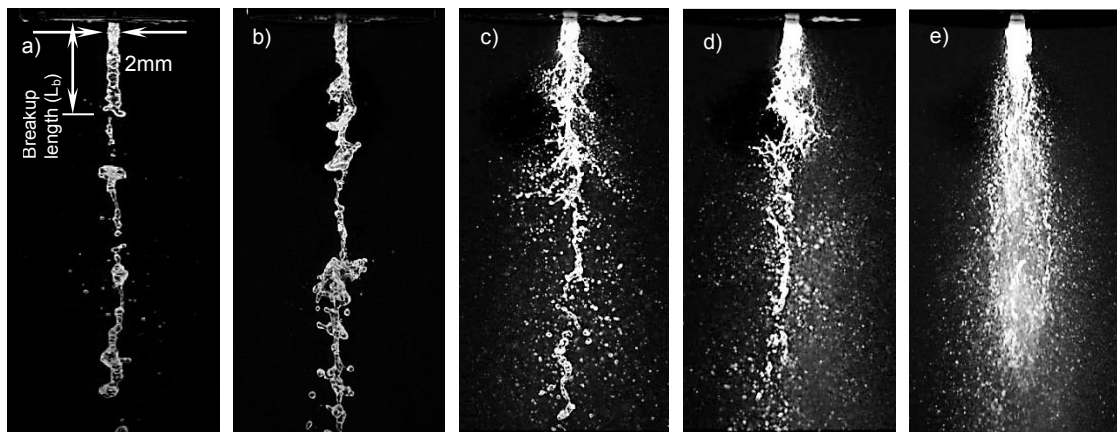


Figure 3-6 Water spray patterns at various GLRs comparing Breakup length (L_b) at GLRs of a) 0.03, b) 0.055, c) 1.1, d) 1.6, and e) 2.6%

By increasing the gas flow rate (from GLR of 1.1 to 2.6%) the bubble random burst at the nozzle orifice no longer exists and the spray unsteadiness which is mainly due to the erratic motion of the bubbles upstream as well as in the discharge orifice is omitted. In other words, further increase of the gas flow causes the formation of an annular gas core surrounded by a ring of liquid film as shown figure 3-6-e. This pattern transition is in good agreement with the studies of Sutherland et al. 1997 [43].

Properties of the atomized fluids significantly influence the inherent unsteadiness feature of the effervescent atomization as illustrated in figure 3-7. The flow unsteadiness has been perceived as the disparate continuous liquid column, J. Luong and P. Sojka 1999 [44]. The images of first row at figure 3-7-a compares averaged breakup length (L_b) of the bubbly regime for the various fluids operating at a GLR of 0.055%. The primary breakup length and its pattern vary due to the rheological variation amongst the fluids. The evident point is the increase of the primary breakup length of the solution caused by augmented viscosity leading to superior intermolecular adhesion; hence, delayed expansion of the bubble bulges. The delay causes the bubble travels further downstream for bursting purposes (figure 3-7-b).

In one hand, higher viscosity of the solution consequences smaller bubbles by thicker liquid film across the interface necessitate delay in the burst, figure 3-7-a. On the other hand, the reduced surface tension at the suspension bulk fluid [$\sigma_{water} = 7.3 \times 10^{-2}$, $\sigma_{solution} = 6.8 \times 10^{-2}$ $\sigma_{suspension} = 5.7 \times 10^{-2} \pm 0.2(N/m)$] demonstrates reverse behavior on the breakup distance. Shear stresses applied by means of the added solid particles on the base fluid (aqueous solution) with the same viscosity perform as a truncated inter-molecular force; therefore, breakup shifted upstream distance closer to the exit orifice by the multiple discrete bubbles burst, figure 3-7-a.

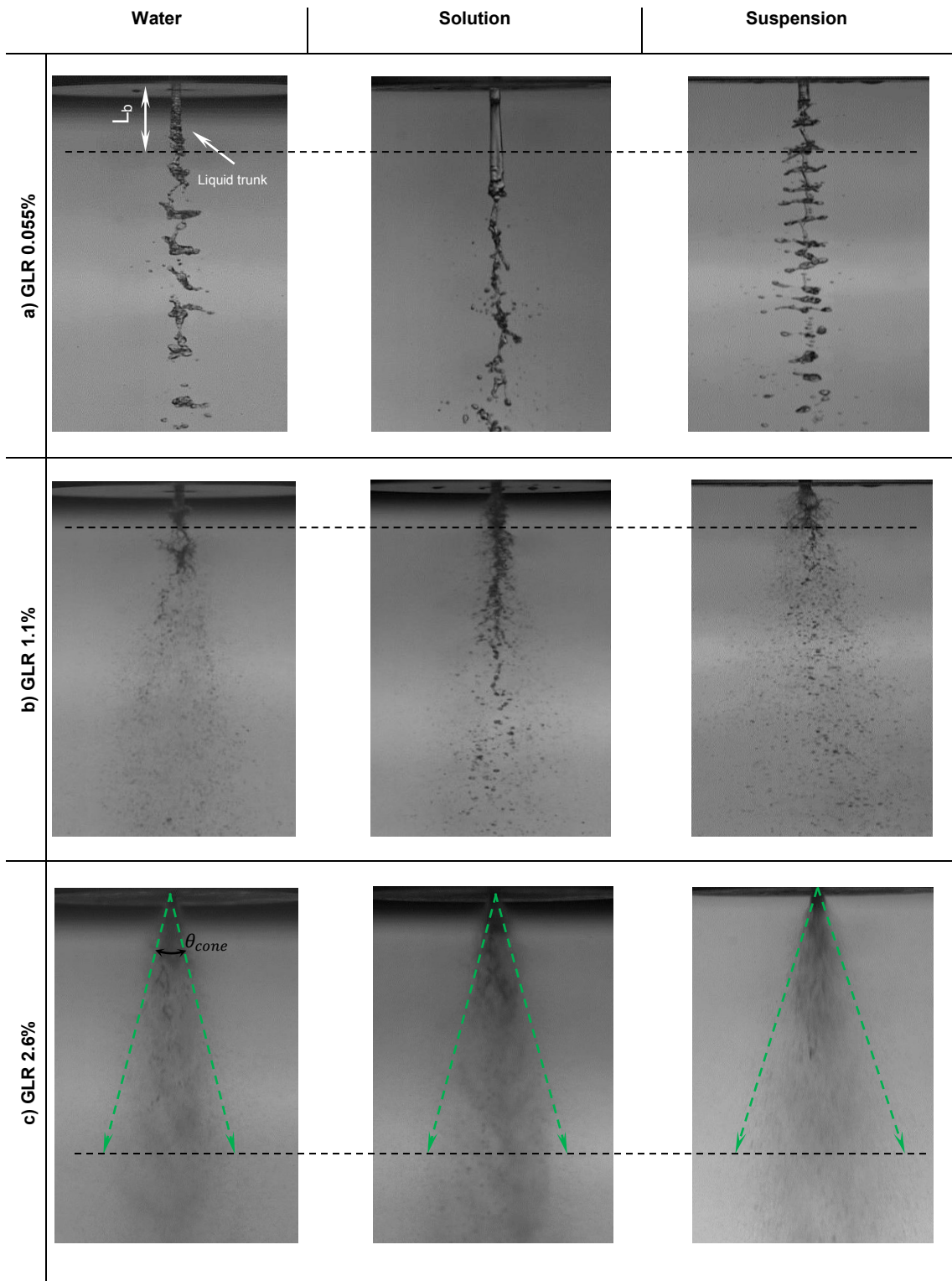


Figure 3-7 Various fluids atomization patterns near nozzle orifice at GLRs of a) 0.055, b) 1.1 and c) 2.6% for water, solution ($\mu_{solution} \approx 9 \times \mu_{water}$) and c) glass beads suspension ($\mu_{suspension} \approx 10 \times \mu_{water}$)

Spray cone angle as another critical atomization feature is demonstrated in Figure 3-8. Increasing the amount of atomizing gas (i.e. from GLRs 1.1 to 2.6%) leads to wider spray plume and higher mass exchange exposed to the nozzle exit environment. The data in figure 3-8-b are calculated from processing of one thousand images using averaged mean values. As explained above, the higher the GLR, the greater the spray cone angle. Spray cone angle of atomized water and aqueous solution varies from $\theta_{cone} = 7.5$ to 20.5 and 6.7 to $18.5 \pm 0.5^\circ$ respectively for the minimum and maximum GLRs. However, the atomization of suspension illustrated larger spray cone angle values varying from 10 to 30.2 ± 0.5 due to the lower surface tension and solid particles separation- as discussed earlier.

The main reason for the spray dispersion (i.e. increase of the spray cone angle) is the transition of the bubbly regime to annular flow. The higher dynamic force of the annular flow through the nozzle discharge orifice easily shatters the liquid phase (trunk) owing to developed aerodynamic forces acting on the trunk flow. In addition, the spray cone angle is highly dependent on the fluid rheological properties; as depicted in figure 3-8.

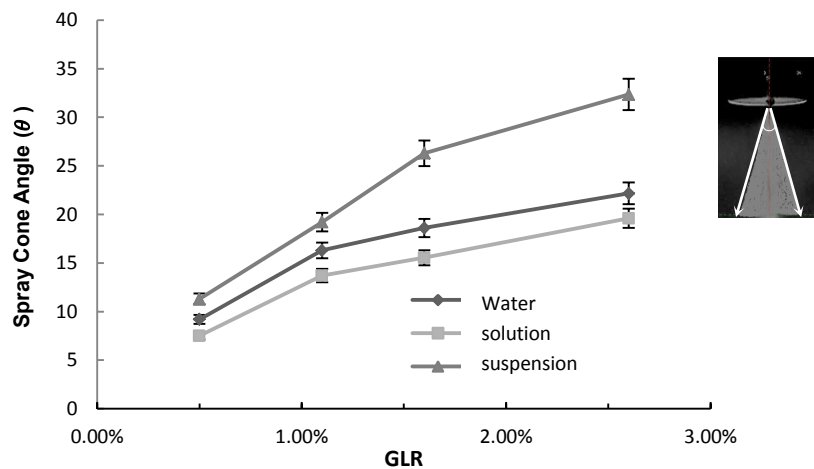


Figure 3-8 Spray cone angle variation versus GLRs

Similarly, the averaged breakup length (L_b) reduced by increasing GLR as shown in figure 3-9. The L_b values are obtained using image processing techniques and considering the mean values of the distance where the first bubble bursts and shatter the surrounding liquid trunk. Similar to the spray cone angle of suspension, the breakup length (L_b) of the suspension was conspicuous; since at the minimum GLR (0.055%), the L_b was 5.4 ± 0.2 mm compared to 8 ± 0.3 and 13 ± 0.5 mm for water and solution, respectively. Upstream internal flow structure due to the presence of solid particles and shear stress applied by the particles to the generated bubbles, and the lower surface tension are the most rational reasons for the variation of the values of the suspension L_b in comparison with the other fluids.

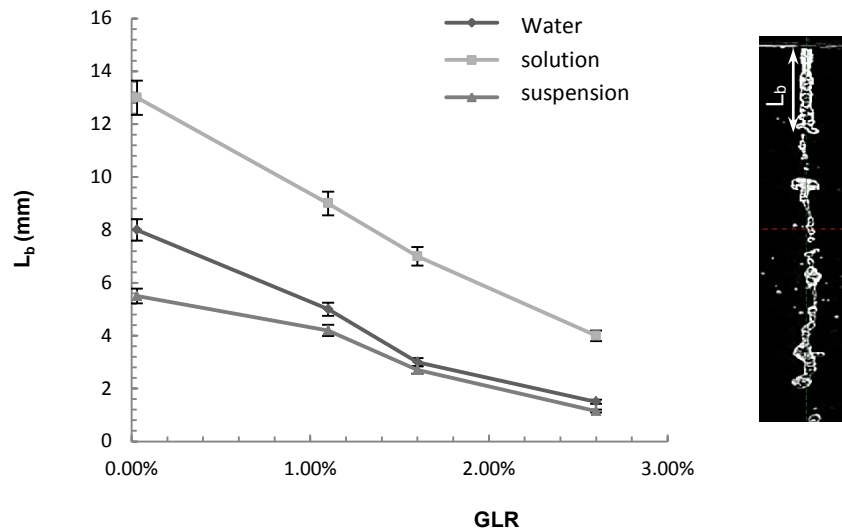


Figure 3-9 Breakup length (L_b) variation versus GLRs,

3.3. Optical Patterning

The spray cross-sectional pattern amongst supplementary features of atomization is one of the unavoidable aspects in studying mass distribution patterns at cross-sections of the spray plume. For example in combustion applications, the large concentration of local heat release and the concentration of species are contingent on the radial distribution of atomized fuel. Importantly to fulfill the main objective of this study, the radial spreading of suspended particles determines the final quality of the coated substrate in suspension thermal spray coatings. Thereby, cross-sectional patterning plays a crucial role in the spray characteristics in different applications and is necessary to study in more details.

The optical patterning is known as a non-intrusive process without hindering the spray droplets streamlines. This technique primarily illuminates one plane (horizontal or vertical) across the spray plume and depicts information of spray cross-section by capturing the cross-sectional images. Resulting images are five hundreds of processed instantaneous images captured by the CCD camera to attain the average intensity images. To record the information of the cumulative mass distribution pattern of the spray, the instantaneous images are superposed on a single de-warped image where the perspective calibration is applied to acquire the normal view of the spray plume.

The illustrated results in figure 3-10-a belong to a side view (containing spray axis) of water atomization. Figure 3-10-b,c,d are at various axial distances (d_{axial} =15, 30 and 45 cm) from the nozzle discharge orifice representing normal-plane visualizations. It should be noted that the images- in the second, third and the last rows- are representative of 15, 30 and 45 cm axial distances from the nozzle, respectively.

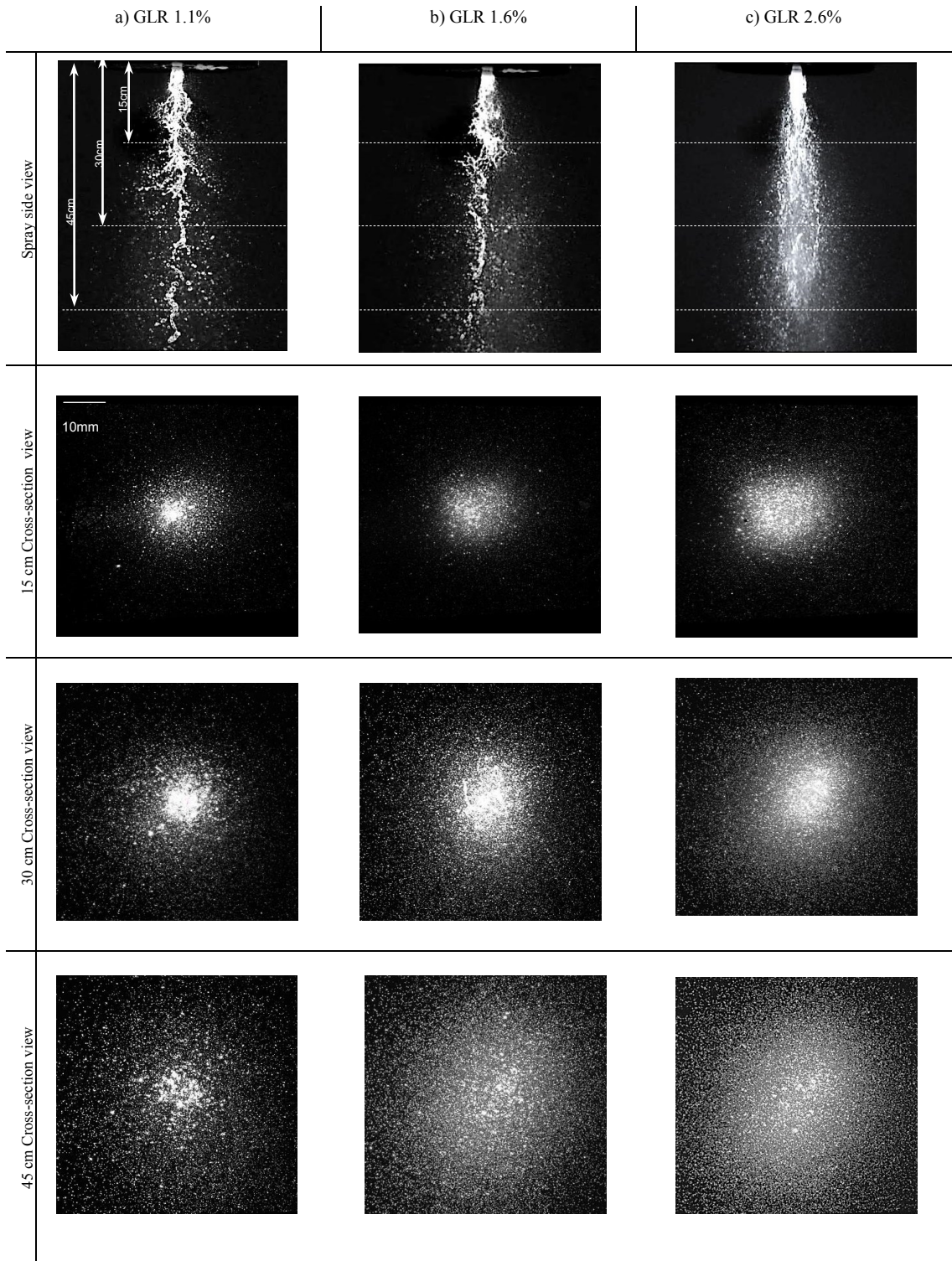


Figure 3-10 Optical patterning cross-sectional view by off-axis PIV, at various GLRs of a) 1.1, b) 1.6 and c) 2.6% with $d_{axial}=15, 30$ and 45 cm

Qualitative and quantitative comparisons of the results in figure 3-10 could be an additional sort of validation for the spray cone angle values, where the suspension elaborated a slightly higher spray cone angle. A similar trend has been observed by the off-axis PIV for the suspension. At a low GLR of 0.055%, the indication of liquid lumps at the core of the spray is the symbol of bubble blasts. A shattered liquid trunk by the bubble bursts, and its transition to evenly fine droplets at a fully developed conical spray by increased GLRs (1.1% and more), is clearly elaborated in the images. Further downstream is the result of the distances in wider spread diameter for all of the atomized fluids at the various GLRs.

Figure 3-11 demonstrates the various fluids atomized at equal operating conditions (GLR of 1.1%) and at the same axial distance of $d_{axial}=30$ cm. Due to the inferior surface tension of the suspension (as a consequence of solid particles applied shear thinning effect on the liquid trunk flow) the spray is wider at its developed radial distance from the spray axis. In addition, the lower spray cone angle of the solution is due to the larger viscosity depicted in more liquid lumps at the core of the spray axis. For instance, in this figure, water atomization is concentrated mostly in a spread diameter of 13.7 ± 0.3 mm from the spray core. However, this value diminishes to 7.8 ± 0.3 and increases for the suspension fluid to 17.6 ± 0.3 mm. Therefore, the values obtained by using shadowgraph technique are in good agreement with this method.

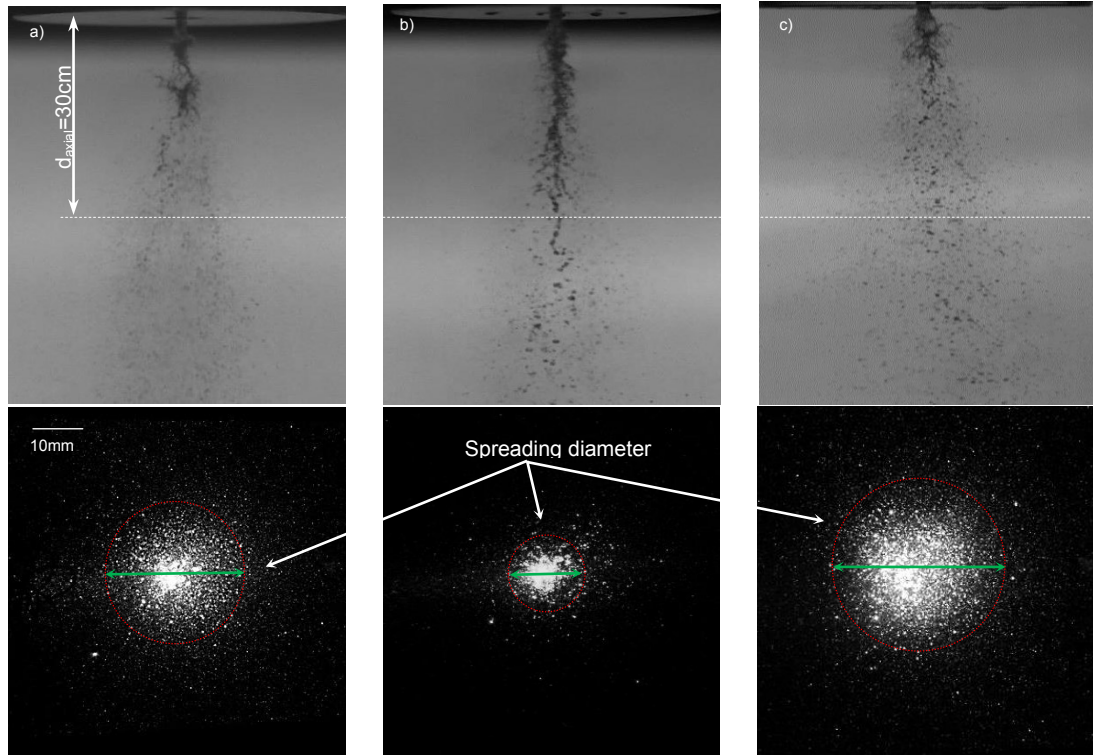


Figure 3-11 Various fluids cross-sectional patterning, operating at GLR of 1.1%, $d_{axial}=30\text{cm}$, with different spreading diameter due to rheological difference of a) water, b) solution and c) suspension {Note: spreading diameter boundaries is defined by light intensity variation}

3.4. PIV and PDPA Analyses

The PIV analyses of water atomization with various GLRs and domain of interest are shown in figure 3-12. It is important to mention that, nearby the nozzle exit where the presence of trunk and/or very dense spray flow, the PIV results could be biased due to over saturated images. Therefore, upstream domain has a 15 mm axial distance (d_{axial}) below the nozzle that is required to avoid the biased results. The velocity magnitude increased by increasing the gas flow rate where the average lowest velocity and highest velocity were 7.6 and 14.4 ± 0.4 m/s at GLR of 0.5% and 2.6% and the axial distance of 50mm below the nozzle exit, respectively.

By increasing the gas flow rate (i.e. at GLR 2.6%) uniform axisymmetric velocity vector distribution was observed and is shown in figure 3-12-a. Spray centerline showing smaller vectors is indication of hollow cone spray at GLR of 2.6% which is in good agreement with outcomes of Santangelo et al. 1995 and Sovani et al. 2001 [45, 46]; reported a hollow ring shaped spray cone at greater GLRs (1.1% and more). As discussed earlier in the optical patternation, by increasing the gas rate, the core of the spray plume gains less liquid lumps at the centerline of the spray and the spray cone expands until reaches to annular regime with a hollow cone spray mode.

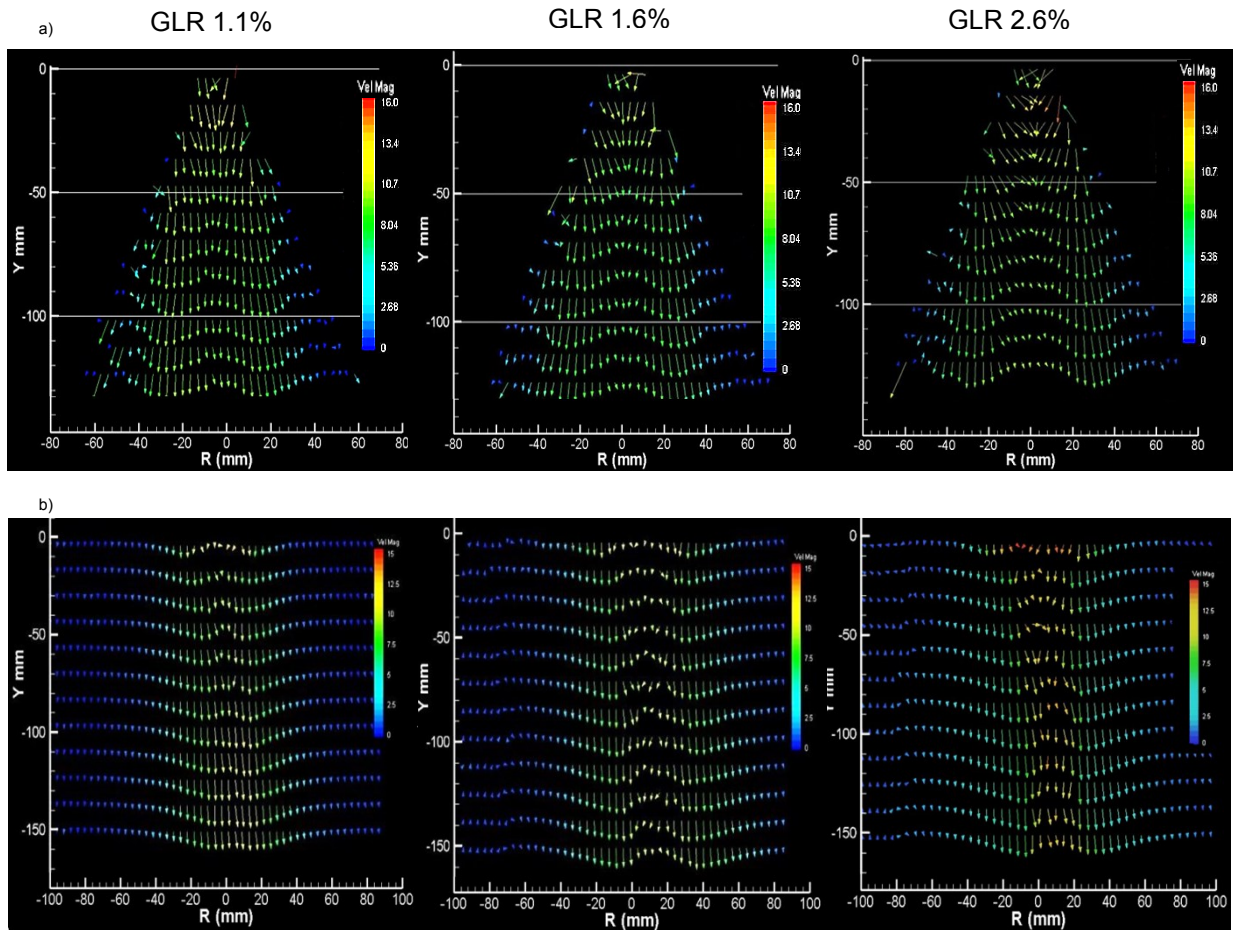


Figure 3-12 Water atomization PIV analyses at GLRs of 1.1, 1.6 and 2.6% a) near-field ($D_{axial}=15mm$), and b) far-field ($D_{axial}=300mm$)

The second set of the PIV analyses examines further downstream distances as depicted in figure 3-12-b. The PIV alignment target was placed at $d_{axial} = 30\text{cm}$ below the nozzle orifice. In the view of the shadowgraphs and of the optical patterning images where the extra cone spreading diameter was captured downstream, now PIV analyses also represented the same pattern figure 3-12-b shows downstream velocities of water atomization at GLRs of 1.1%, 1.6% and 2.6%, respectively. Downstream domain, lower velocities are seen due to the frictional decelerations. However, the symmetry pattern of the vector field as an important factor of the spray velocity distributions remained unaffected for all cases.

A comparison of velocity vector field of various fluids is portrayed at figure 3-13. It displays velocity fields of the water, solution, and suspension operating at the similar GLR of 1.6% and at axial distance of 15 mm. The velocity magnitude and the spreading of the spray plume variations are the noticeable variances. Clearly, the smallest velocity vectors belong to the solution with the averaged magnitude of 11.3 m/s, and the highest is 13.52m/s belonging to the suspension at the centerline near the orifice. Fairly higher spreading diameter of the suspension agreed well with the earlier discussed optical patterning results.

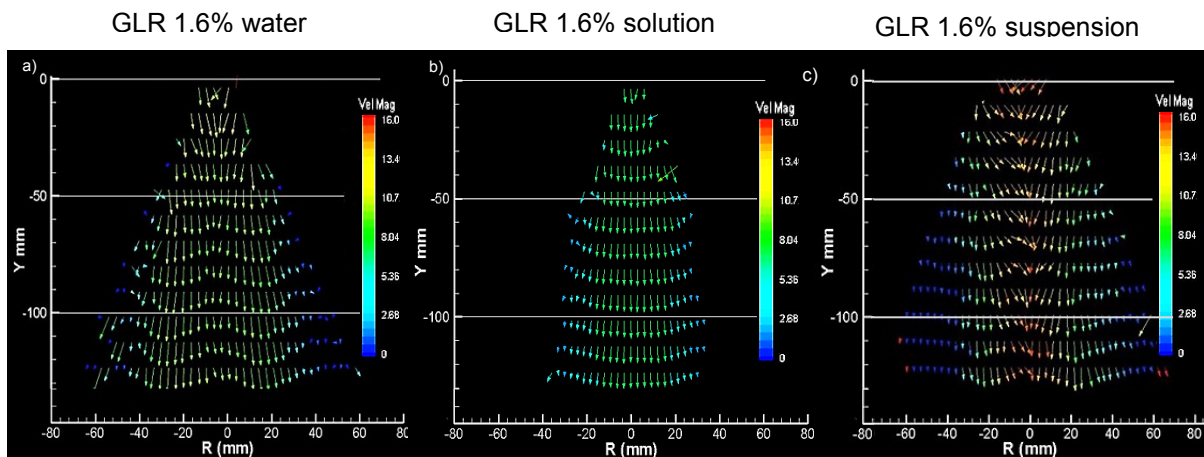


Figure 3-13 Velocity vector field of various fluid operating at GLR of 1.6% a) water, b) solution, c) suspension

The PIV velocity vector fields and the spray patternation clearly confirmed the symmetric pattern of the spray plume for almost all spraying conditions. Point wise measurement will provide more detailed understanding of the spray features. Hence, it is rational to scan the spray across one radial line passing through the spray axis using the PDPA. The PDPA radial scans have been done for the various fluids at different stand-off distances and GLRs to compare the recorded data via the PIV and finally estimate the nozzle’s performance.

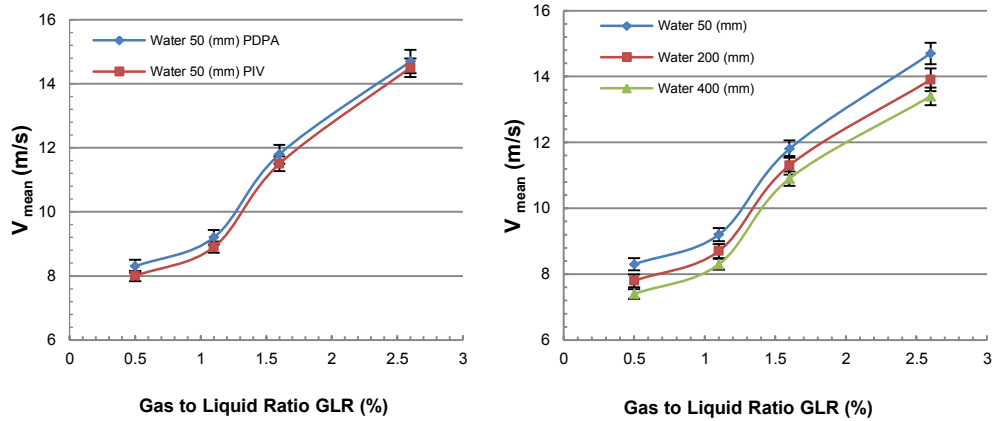


Figure 3-14 Water atomization PDPA analyses compared by the PIV analyses at various axial distances and GLRs

The nozzle’s performance is directly associated to key characteristics such as droplet velocity and droplet size distributions. The smaller the droplet, the higher the mass exchanges and higher the velocity lead to further penetration of the spray are the most important features of a high performance nozzle. In figure 3-14 velocity values acquired by the PIV are compared with the values of the PDPA analyses. The compared velocity of the PIV is calculated at $d_{axial}=50$ mm with averaged value of the cross-sectional velocity obtained by Tecplot; as post processing calculations. For example, with GLR of 1.6% and 50mm distance the droplets velocity is 11.5 ± 0.2 m/s; where this value is 11.8 ± 0.2 m/s as recorded by the PDPA at the

same distance and the GLR. The difference between the values is less than 6% which is highly acceptable.

The water spray analyses as premium running liquid is conducted at three different stand-off distances: 50, 200 and 400 mm and the GLRs varied from 0.55% up to 2.6%. It is clear from the figure 3-14 that the PDPA analyses are in good agreement with the PIV values. Similarly, the velocity is increased by increasing the GLRs. Indeed, the extra injected pressure of atomizing gas turns into kinetic energy inside the nozzle chamber to shatter and transport the droplets downstream. Furthermore downstream of the spray flow, reduced velocities were observed due to resistant aerodynamic decelerations too.

Droplet diameter size distributions as supplementary key factor of spray characteristics is plotted in figure 3-15. For simplicity of the comparison, selective GLRs of 1.6% and 2.6% will be mostly discussed in the proceeding sections. Sauter Mean Diameter (D_{32} /or volume to surface area ratio of the total droplet's diameter size) varied by changing the extra injected gas flow rate. In this plot, the D_{32} reduced from 52.3 to $40.2 \pm 0.5 \mu\text{m}$ for increased GLR of 1.6% to 2.6%, respectively at the centerline and 50mm below the nozzle. This value reduced further downstream to 44.3 and $41.1 \pm 0.5 \mu\text{m}$, respectively. In addition to that, D_{32} showed dependency on various radial and axial locations, too.

Especially, at the periphery of the spray plume larger droplets of the atomized water resulted at smaller GLR of 1.6% having a 50 mm axial distance below the nozzle. The reduced atomizing gas injection flow rate/or pressure results in lower internal aerodynamic forces in order to shatter the liquid and transfer downward. Besides, the droplets have not chance to go through the evaporation or secondary breakup at distances closer to the nozzle orifice. Hence, the droplet sizes are larger than further downstream (figure 3-15).

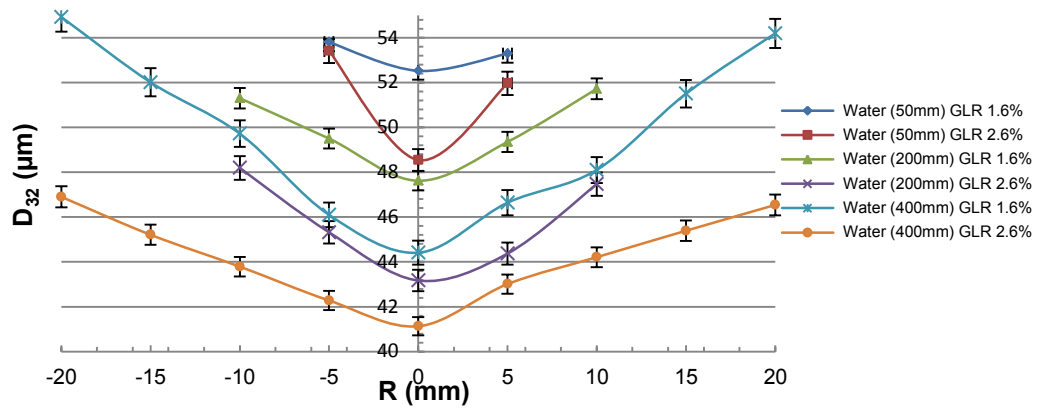


Figure 3-15 Droplet SMD (D32) distributions at various GLRs

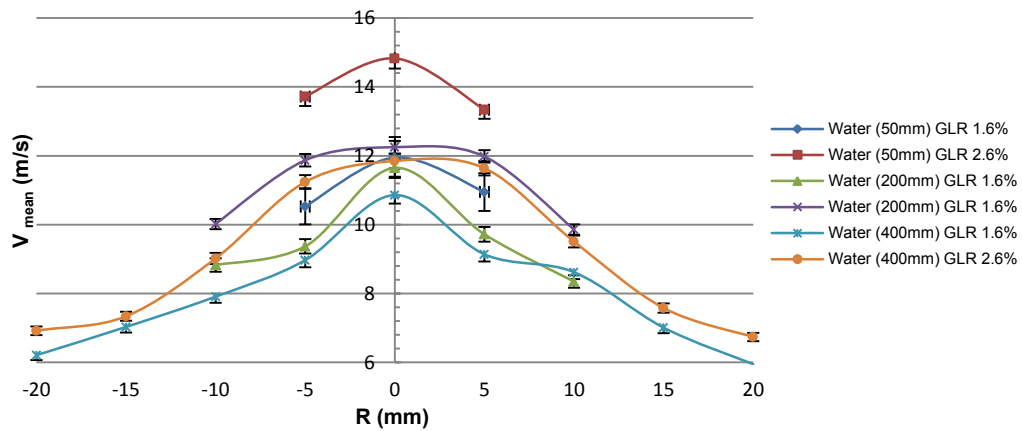


Figure 3-16 Velocity distributions at various GLRs

Figure 3-16 illustrates the velocity variation of water droplets at GLRs of 1.6% to 2.6% and various axial distances of 50, 200 and 400 mm versus radial positions. The higher mean velocity at GLR of 2.6% is $V_{\text{mean}} = 15.1 \pm 0.3$ m/s, while this value reduces to $V_{\text{mean}} = 13.8 \pm 0.4$ m/s at the same axial distance of 50 mm. Further lower velocities observed at GLR of 1.6% at farthest axial location of 400 mm with a value of 10.9 ± 0.2 m/s. At the closer distances, the droplets acquire high running force of extra injected atomizing gas into the mixing

chamber and the effects of the ambient frictional forces are not dominant yet. The velocity of the droplets become smaller (GLR 2.6%, 400mm, $V_{\text{mean}}=11.7\pm0.3$ m/s) specially at the periphery of the spray plume and further downstream due to less interactions of the droplets with the extra injected atomizing gas

Further downstream of the spray flow, the droplets decelerate due to ambient aerodynamic forces acting on the droplets. Another reason is the wider spray downstream with more effective surface area resulted in higher interaction mass with the ambient air. Therefore higher shear forces of the ambient air acting on the droplets due to larger spreading diameter of spray decelerates the spray flow ($d_{\text{axial}}=400$ mm, figure 3-15).

At further downstream of the spray flow not only the spreading diameter of the spray plume is increased, but also the fluctuation of the spray as an indication of unsteadiness of the spray is reduces at downstream (figure 3-15). This specifies the effect of the higher GLRs at further downstream of the spray assisted in the better performance of the nozzle in terms of diminished fluctuations.

Recall effect of the rheological properties on the recorded velocity distributions by the PIV vector fields where the suspension demonstrated higher velocity values (15 ± 0.3 m/s) and the solution with minimum velocity (10.32 m/s) operating at GLRs of 2.6% and 1.6%, respectively. Now, in figure 3-17 the velocity distributions of the various fluids operating at GLRs of 1.6% and 2.6% with $d_{\text{axial}}=50$ mm are depicted. The velocity peak at the spray centerline for the suspension running at $d_{\text{axial}}= 50$ mm and GLR of 2.6% is 15.4 ± 0.3 m/s. While at the same operating parameters, the value of 14.3 and 13.7 ± 0.3 m/s obtained for water and the solution droplets, respectively. Similar trend of velocity peak for suspension and minimum velocity for the solution is detected by the PDPA analyses.

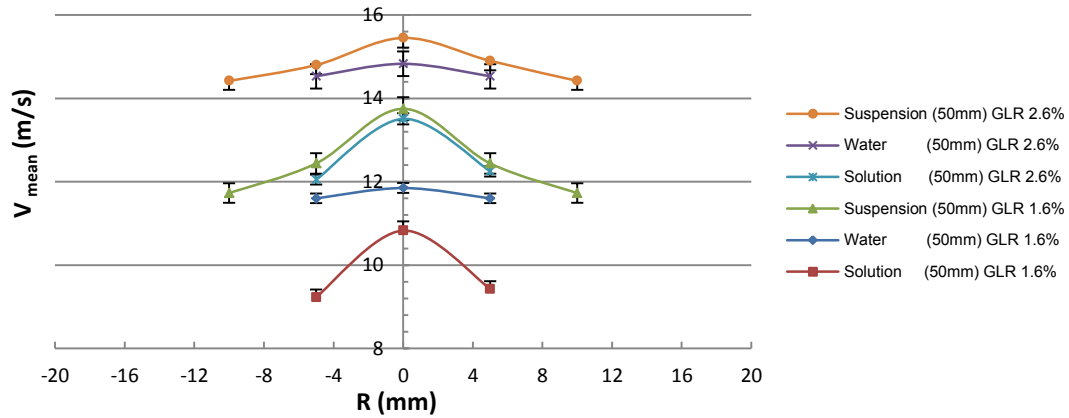


Figure 3-17 Velocity variation of various fluids (suspension, solution, water)

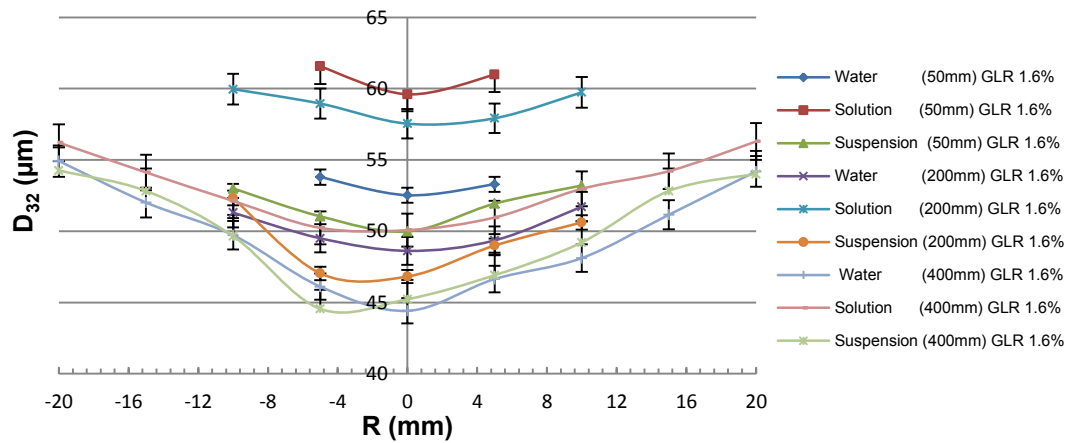


Figure 3-18 Droplet SMD distributions for different fluid's properties

Spray centerline as a dilute and fast flowing portion has the most interaction with the atomizing gas- close to the nozzle orifice. However, the ambient air reduces the velocity of the exiting flow due to applied frictional shear forces or ambient pressure on the generated droplets. This reduction of the velocity is more sensible at the edges of the spray where the generated droplets have the least interaction with the upstream atomizing gas. Therefore, the lowest velocities were detected at the boundaries of the spray flow (figure 3-17).

Sauter mean diameter (D_{32}) variation for different properties of the fluids is plotted in figure 3-18. The operating conditions are GLR=1.6% at various axial locations of 50, 200 and 400 mm from the nozzle orifice. At 50 mm axial distance with GLR of 1.6%, the D_{32} values are 49.98, 52.53 and $59.62 \pm 0.5 \mu\text{m}$ for the suspension, water and the solution, respectively. The similar trend of the smaller droplets at the spray centerline and the larger at the boundaries is noticeable. The suspension atomization with higher viscosity due to the presence of the solid glass beads has depicted superior atomization properties by the lowest values for droplet diameter and wider spreading diameters.

Similar to the previous cases, not only the fluid properties, but also the operating conditions (i.e. GLRs) alter the droplet size distributions. Further downstream- $d_{\text{axial}}=200$ and 400 mm- the droplet size vanishes due to the aerodynamic reactions of ambient air with droplets. For example, evaporation of the droplets vanish the droplet sizes. However, lower velocities of the spray peripheries reduce the frictional/or heat and mass transfer effects (lower momentum ratio between ambient still air and moving spray droplets); hence, larger droplets at the spray edges are mostly due to lower velocities of the droplets.

At last but not least, figure 3-19 and figure 3-20 illustrate “Representative Diameter” (RD) values for the sprayed fluids. Representative diameters are center of attention for many spray applications due to their importance for comparing performance of different types of nozzles running at same conditions. The RD values calculated from cumulative distribution curves of the PDPA analyses are volume based analyses where wide size range of produced droplets containing very fine ($Dv1$) and very coarse ($Dv99$) sizes are compared.

In other words, at the control volume of the PDPA system there are thousands of droplets with wide range of diameter sizes in which a specific percentage (i.e. 1%, 10%, 50%, 90%,

99%) of the total volume of the sprayed liquid is made up of droplets with diameters smaller, larger or equal to the stated specific value of the total liquid volume. For example, Dv10 (also known as Dv 10%) is a representative diameter where 10% of the total volume of the atomized liquid is made up of droplets with diameters smaller or equal to the value of the valid counted droplets.

The valid counted droplets are those fit to Rosin Rammler distribution at various operating conditions. For instance at GLR of 1.6% and $d_{axial}=200$ mm mass median diameter size of 26.4 ± 0.3 μm is representative of 10% of the total valid counted droplets. This value is the averaged value amongst the droplets passing through the probe control volume. Dv10 of the passing droplets from the total 5400 valid counted bins/or droplets has spherical shape with diameter of 26.4 ± 0.3 μm as depicted in figure 3-19. This value is increased to 47.3 ± 0.2 μm , 102 ± 0.2 μm and 106 ± 0.2 μm for the Dv50, Dv90 and Dv99, respectively.

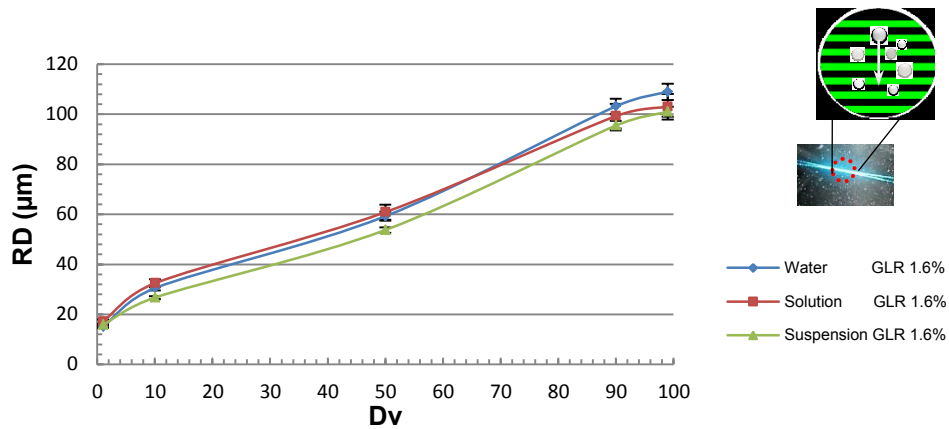


Figure 3-19 Droplet RD distributions for various fluids operating at a GLR of 1.6% and $d_{axial}=200$ mm

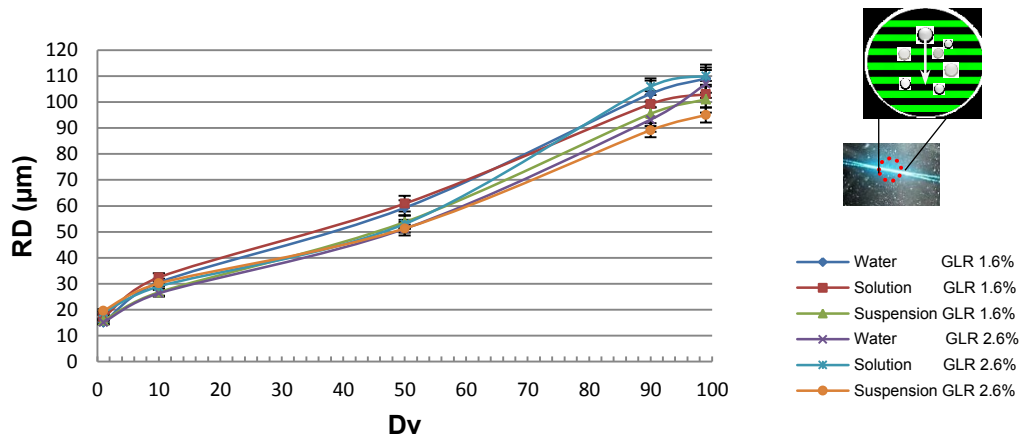


Figure 3-20 Droplet RD distributions for various fluids at GLRs of 1.6% and 2.6% and $d_{axial}=200$ mm

Suspension fluid amongst the other fluids has smaller Dv_{10} value of $23.2 \mu\text{m}$ at the similar conditions. In other expression, the suspension flow is depicting finer particles in comparison with water and the solution flow. This value did not affected significantly by increasing the GLR from 1.6% to 2.6% at the same control volume axial distances as shown in figure 3-20. The same trend is observed for Dv_{50} , Dv_{90} and Dv_{99} values. This is as another indication of consuming the atomizing gas kinetic energy for faster transportation of the droplets downstream of the spray flow. Higher velocity magnitudes is an indication of higher penetration depth in which the suspension flow will have the largest penetration into a cross flow in comparison with other fluids.

Interestingly though, the effervescent nozzle behaved as a high performance atomizer to atomize different fluids without being affected by rheological properties of the fluids. However, effervescent nozzle atomized the solution and suspension fluids without having considerable difference between the resulted droplet sizes or velocities. Moreover, clogging issue which is a severe problem in the atomization of suspension fluids didn't observed.

4. Closure

4.1. Summary

Aim of the present thesis was to experimentally characterize Effervescent atomization. For this reason, atomization features of four types of fluids with various rheological properties were compared. To acquire the fluids rheological properties, viscometer, tensiometer, particle size analyzer and digital microscopy apparatuses were used. The various fluids involved simple and complex liquids. Distilled water, 99% pure glycerol, 50vol.% water and glycerol mixture (solution) represented simple liquids. 10wg.% concentration of micro glass beads suspension represented complex fluids.

Various Gas to Liquid Ratios (GLRs) as an important dimensionless number were determined in order to compare the nozzle's performance by means of non-intrusive laser diagnostic techniques such as PIV analyses, Off-axis PIV patteration, PDPA and Shadowgraph. The reason of utilizing combination of several techniques was to shed insight on the performance of the nozzle comparing various characteristics i.e. spray patterns, breakup lengths, spray cone angle, droplet sizes and velocity distributions to fulfill required characteristics of thermal spray coating process, as the main subject of this study.

Atomization of the purified glycerol with dynamic viscosity nearly ($\mu_{\text{glycerol}} \approx 1400 \times \mu_{\text{water}}$) did not occurred in the range of determined GLRs successively used for the other liquid's atomization. However, for the remaining fluids, atomization process with the specified GLRs went through. Interestingly, though effervescent atomizer portrayed better quality of atomization for atomizing the suspension fluid amongst the others.

Suspension as a representative of complex fluids is one of the most challenging liquids to be atomized; since the other type of atomizers are incapable of easily shattering the fluid due to clogging issues through the atomization process and atomizer orifice as well.

In the first step, qualitative investigation of the spray pattern was conducted using shadowgraphs technique. Image processing tools¹ was used to process the shadowgraphs raw images to portray both the nozzle internal flows as well as external spray side views. Cross sectional view of the spray plume was captured using optical patterning of Off-axis-PIV imaging techniques. Internal flow patterns illustrated more details regarding dependency of the bubbly regime to the fluid's properties and also the operating conditions. Both imaging techniques proved the axisymmetric of the spray cone. Likewise, expansion or contraction of the conical spray plume by respectively increasing or decreasing the GLR was recorded. At higher GLRs, presence of the liquid lumps at the core of plume vanished and finer particles with higher spreading diameters were observed.

Spray cone angle which is the angle between the spray peripheries was affected by the rheology variations as wells the GLRs. The higher the spray cone angle, the better the nozzle performance. From the optical patterning it was noticed the spray plume has tendency to expand and turn into a hollow cone shape as the GLR was increased up to 2.6%; despite remaining in a full-cone shape. Amongst the fluids, suspension illustrated highest cone angle and the solution lowest values- water spray cone angle was sandwiched between.

Following the external flow patterning images, liquid trunk breakup length (L_b), as another important parameter affecting the spray penetration depth was studied. The breakup length

¹ Matlab image processing toolbox was used to generate various processing codes to post-process the one thousand raw images obtained by a high speed camera to obtain the averaged value of the images for each case. The generated codes are provided in the appendix B.

values also obtained using the image processing techniques. The smaller the breakup length, the better the spray performance is ensued. It is revealed the breakup length reduced by raising the GLR, and vice versa. Furthermore, rheology of the fluids also played role in the variation of the breakup length values. Surprisingly, the suspension was the running fluid with the lowest L_b among the others which is in contrast with other nozzles performances.

The second step was quantitatively investigating the spray characteristics such as spray droplet's velocity distributions. For this purpose, Particle Image Velocimetry (PIV) as the primary instrument analyzed features of atomization in various operating conditions such as different regions on the spray plume and various GLRs including all of the fluids. Two different regions of upstream and downstream fields were examined and the velocity vector fields were plotted depicting the various operating condition's effects on the variation of stemmed velocity. Clearly revealed the spray was wider at higher GLRs, especially downstream regions. Moreover, widest spreading diameter of the spray cone with slightly higher velocity magnitudes belonged to the suspension atomization amongst the fluids.

Further confirmation of the velocity variations was necessary to validate the obtained PIV results. For this reason, Phase Doppler Particle Analyzer (PDPA) was used to obtain not only the velocity, but also the droplet diameter size distributions simultaneously. The PDPA with higher spatial resolution is a point-wise measurement system capable of measuring various characteristics of spray including various diameter size representatives. For each fluid case, 27 radial points and 3 cross-sectional planes and the determined GLRs were scanned; resulting in 81 cases of experimenting for each fluid.

The values obtained by the PDPA were in good agreement with the velocity magnitudes analyzed by the PIV, having off-variance less than 6% shift in the PDPA values which could

be due to the averaged value of the defined position matrix² and various error sources such as low resolution of the PIV measurements compared to the PDPA. However, the suspension with slightly higher velocity and spreading diameter magnitudes had overall the highest values amongst the other type of fluid's atomization. The qualitative analyses of shadowgraphs and off-axis PIV images also showed finer droplets at higher GLRs that were confirmed by the PDPA analyses. Moreover, the diameter and velocity distributions at various axial and radial locations confirmed the symmetry of the spray cone versus its centerline.

4.2. Conclusions

Various fluids (i.e., simple and complex) atomization considered to evaluate various features of atomization. Amongst the fluids, suspension representative of complex fluids portrayed appealing characteristics such as higher velocity magnitudes and finer droplets that could be summarized in the following three points:

- 1) The clogging issue of the suspension fluid inside the nozzle is fairly resolved due to fluctuations of internal upstream flow with bubbly /or annular regime which causes self-cleaning of the nozzle leading to not clogged orifice.
- 2) The effect of shear forces of the suspended particles with different densities lowered the local interfacial surface tension and intermolecular adhesive forces leading to high frequency of fragmentation on liquid trunk.
- 3) Higher fragmentation rate obtained not only by the presence of the particles, but also existence of the various internal flow patterns (i.e., from bubbly to annular flow). The internal flow patterns governing external flow characteristics controlled the atomization features independent from fluid's properties.

² The position matrix is defined based on the locations where the PDPA measurements are done and is depicted in appendix B.

Additionally, higher penetration of the suspension fluid due to higher velocities owing to further acceleration of the suspended denser solid particles is concluded considering ongoing cross-flow experiments. The denser solid particles are highly affected by the gravity acceleration in comparison with the base fluids droplets. Therefore, the effervescent nozzle is a promising atomizer for atomization of variety of the fluids for different applications namely thermal spray coatings, regardless of fluid's rheological properties.

4.3. Future works and Recommendations

The investigations carried out in the present thesis can be considered upon as setting stones and paving the path for ongoing/or future experimental benchmark at different operating situations; such as cross-flow setup using elliptical orifice instead of previously used circular geometry of the nozzle showed in figure 4-1.

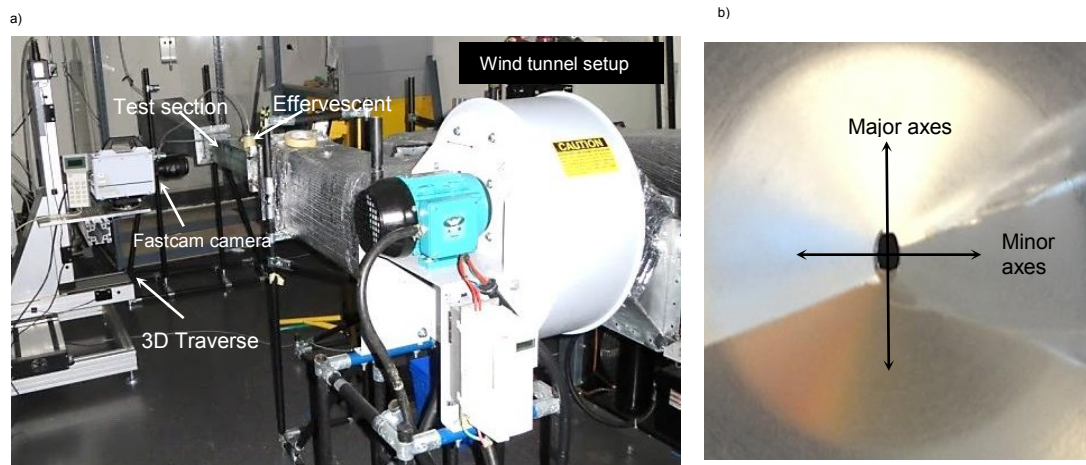


Figure 4-1 a) Wind tunnel setup and b) effervescent elliptical orifice

The obtained results lead to interesting outcomes via investigating the suspension atomization by the effervescent nozzle under cross-flow, as showed in figure 4-2. In this set of image, various suspension fluid flowrates are injected and the shadowgraphs images taken

from inside a chamber installed in a subsonic wind tunnel are illustrated. While the suspension flow is injected at zero aeration (GLR of 0), the circular flow jet portrayed interesting axes-switching pattern (or swirling) at different flow rates. The unidentified feature behind this phenomenon is not quite understood yet, whether it is axes switching or swirling flow exited from the nozzle. To make sure this phenomenon is repeatable, various suspension fluids such as Al_2O_3 suspensions were conducted and the similar trend in jet flow pattern was observed in shadowgraphs images.

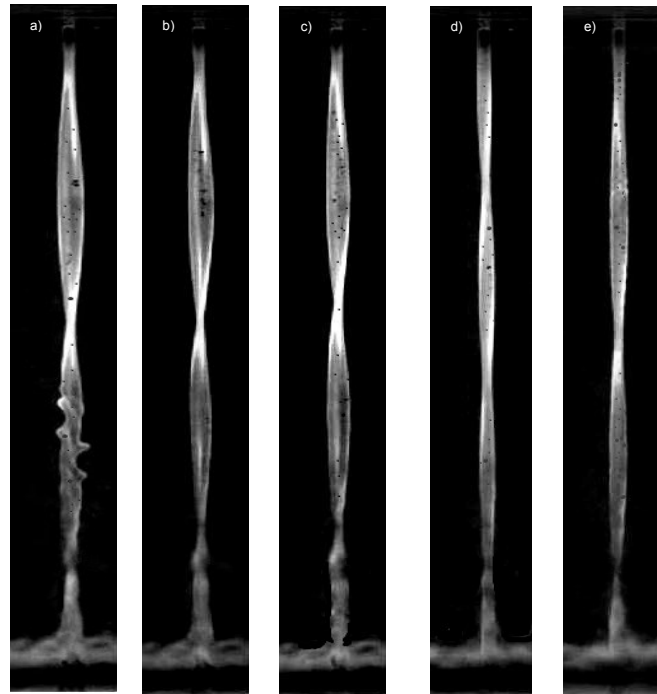


Figure 4-2 Suspension injection by circular orifice of effervescent at various flowrates of
a) 200, b) 400, c) 600, d) 800, e)1000 ml/m

Furthermore, the suspension fluids were put in expose of a free stream crossing air flow with known adjustable velocities and portrayed significantly higher penetration depths as showed

in figure 4-3. One should be wondering if the circular orifice of the nozzle is changed into elliptical, what could be the result in terms of the exit flow pattern or penetration depths. More important is to investigate these characteristic using 3-D velocity profiles by a stereoscopic PIV. Moreover, the PDPA analyses done in this study was mostly on the normal axis of the spray, however, one could wonder what if the analyses are done at the cross-section of the spray and compare the recorded data with the present study.

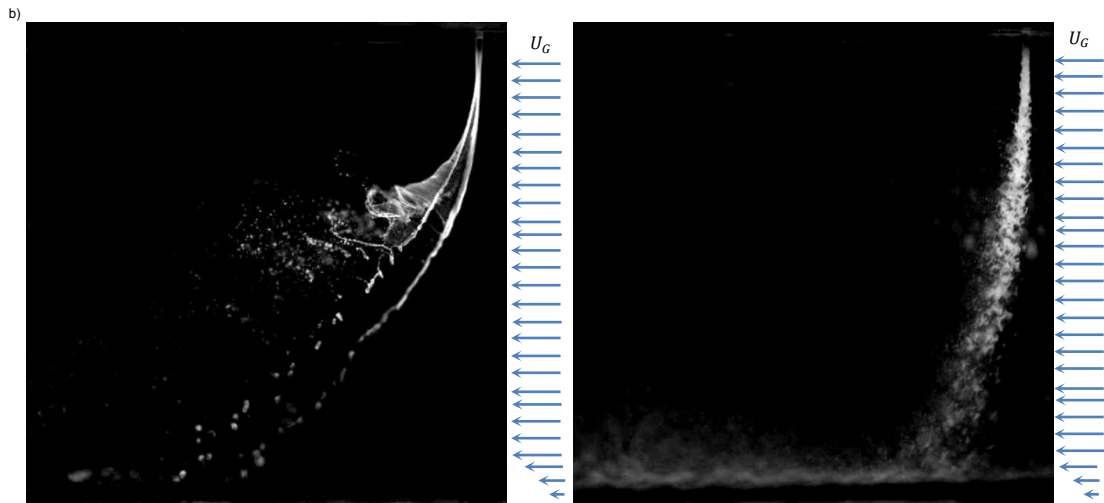


Figure 4-3 Suspension flows under cross-flow testing at GLRs of a) 0, b) 2.6%, and flowrate of $Q=800$ ml/m, $Re_L=2574$ $We_L= 2179$, $We_G=2300$

Bibliography

- [1] S. A. Esfarjani and A. Dolatabadi, "A 3D simulation of Two-Phase Flow in an Effervescent Atomizer for suspension plasma spray," *Surface and Coating Technology*, vol. 203, pp. 2074-2080, 2009.
- [2] A. Ibrahim, "Comprehensive study of internal flow field and linear and nonlinear instability of an annular liquid sheet emanating from an atomizer," University of Cincinnati, OH, 2006.
- [3] C. Weber, "On the breakdown of a fluid jet", *Zum Zerfall eines Flüssigkeitsstrahles. Z. Angew.*, *Math and Mech.* 11, 136-154, Angew, 1931.
- [4] N. Ashgriz, *Handbook of Atomization and Spray (Theory and Applications)*, N. Ashgriz, Ed., Toronto, Ontario: Springer, New York, 2011, pp. 4-5.
- [5] H. Berger, *Ultrasonic Liquid Atomization: Theory and Application*, 2nd ed., Hyde Park, Partridge Hill: Partridge Hill, 2006.
- [6] A. Lefebvre, X. Wang and C. Martin, "Spray characteristics of aerated-liquid pressure atomizers," *AIAA J. Prop Power*, vol. 4, pp. 293-8, 1988.
- [7] A. Lefebvre, "A novel method of atomization with potential gas turbine application," *Indian Defence J.*, vol. 38, pp. 353-62, 1988.
- [8] T. Roseler and A. Lefebvre, "Studies on aerated-liquid,," *International J. Turbo Jet Engines*, vol. 6, pp. 221-30, 1989.
- [9] J. Chin and A. Lefebvre, "A design procedure for effervescent atomizers," *J. Eng. Gas Turbines Power*, vol. Vol. 117, no. 12, pp. 266-271, 1995.
- [10] L. A. H., "Some recent developments in twin-fluid atomization, ., Vol. ., .," *Part. Part. Syst. Charact*, vol. 13, no. 3, pp. 205-216, 1996.
- [11] X. Wang , J. Chin and A. Lefebvre, "Influence of gas injector geometry on atomization performance of aerated-liquid nozzles," *Int J Turbo Jet Engines*,, vol. 6, no. 3-4, pp. 271-80, 1989.
- [12] B. Mulhem, G. Schulte and U. Fritching, ""Solid-liquid separation in suspension atomization." , " *Chemical engineering science*, vol. 61, no. 8, pp. 2582-2589., 2006.
- [13] A. Lefebvre, *Atomization and Sprays*, Hemisphere, 1989.

- [14] J. Schelling and R. Lothar, "Influence of atomiser design and coaxial gas velocity on gas," *Chemical Engineering and Processing*, vol. 38, no. 4, pp. 383-393, 1999.
- [15] J. Ponstein, "Instability of rotating cylindrical jets," *Appl. Sci. Res*, vol. 8, no. 6, p. 425-456, 1959.
- [16] J. Ponstein and P. Saffnab, "The number of waves on unstable vortex rings.," *J. Fluid Mech.*, vol. 84, no. 4, p. 625-639, 1978.
- [17] A. Robert and A. K. Gupta, "GAS PROPERTY EFFECTS ON DROPLET ATOMIZATION AND COMBUSTION," *Twenty-Sixth Symposium (International) on Combustion/The Combustion Institute*, p. 1645-1651, 1996.
- [18] A. Kufferah, B. Wende and W. Leuckel, "Influence of liquid flow conditions on spray characteristics of," *International Journal of Heat and Fluid Flow*, vol. 200, no. 5, p. 513-519, 1999.
- [19] H. Empie and D. Loebker, "Independency controlled drop size in black liquor sprays using effervescent atomization," *Institute of Paper science and Technology*, 2002.
- [20] L. Broniarz-Press, M. Ochowiak, J. Rozanski and S. Woziwodzki, "The atomization of water-oil emulsions," *Experimental Thermal and Fluid Science*, vol. 33, p. 955-962, 2009.
- [21] S. Nukiyama and Y. Tanasawa, "Experiments on the atomization of liquids in an air," *Transactions of the Society of Mechanical Engineers*, vol. 5, pp. 68-75, 1939.
- [22] C. Ejim, M. Rahman, A. Amirfazli and B. Fleck, "Effects of liquid viscosity and surface tension on atomization in two-phase.," *Fuel*, vol. 89, p. 1872-1882, 2010.
- [23] A. Einstein, "On the movement of small particles suspended in stationary liquids required by the molecular-kinetic theory of heat," *Annalen der Physik*, vol. 17, pp. 549-560, 1905.
- [24] M. Pavlik, "The dependence of suspension viscosity on particle size, shear rate and solvent viscosity," *Theses and Dissertations*, Chicago, 2011.
- [25] S. Bhattacharji and P. Savic, "Proc Heat Transfer and Fluid Mechanics," in *Proc Heat Transfer and Fluid Mechanics*, 1965.
- [26] F. Schmidt and D. Mewes, "MEASURING FLOW VELOCITY AND FLOW PATTERN OF A SUSPENSION-GAS MIXTURE," in *ASME Joint U.S. European Fluids Engineering Summer Meeting*, Miami, 2006.
- [27] C. Capes, "Solid-liquid separation of suspensions by atomization within twin-fluid

- atomizers," in *Elsevier, Amsterdam, Fifth International Conference on Multiphase Flow, ICMF'04*, Yokohama, 1980.
- [28] "Viscosity of Aqueous Glycerine solutions," Midland, 2009. [Online]. Available: <http://www.dow.com/glycerine/resources/table18.htm>. [Accessed 2009].
- [29] T. Young, P. Jilios and R. Trans, "Contact angle Measurements," London, 1805.
- [30] P. C. Hiemenz and R. Rajagopalan, "Principles of Colloid and Surface Chemistry," in *CRC Press: Boca Raton, FL, 1997*.
- [31] F. Dmdarevic, "Optical Spray Pattern Analysis in a Domestic Oil Burner Flame," Queens University, 2002.
- [32] G. Stephen and R. Dale, "OPTICAL PATTERNATION OF FUEL SPRAYS IN A GAS TURBINE," RMC, Ottawa, 2008.
- [33] R. Sellens and G. Pasadena, "Advances in Optical Patternation for Sprays, With Applications," in *Eighth International Conference on Liquid Atomization and Spray System*, 2000.
- [34] M. Raffel, C. Willert and S. Wereley, "Particle Image Velocimetry PIV, A Practical Guide," Springe, Shoreview, MN 55126 / USA, 2007.
- [35] M. wernet, A. Subramanian, H. Mu and J. Kadambi, "Comparisoon of Particle Image Velocimetry and Laser Doppler Anemometry Measurements in Turbulent Fluid Flow," *Annals of Biomedical Engineering*, vol. 28, pp. 1393-1394, 2000,.
- [36] L. Liu, H. Zheng, L. Williams, F. Zhang and R. Wang, "Development of a custom-designed echo particle image velocimetrey system for multi-component hemodynamic measurements: system characterization and initial experimental results," *Physics in Medicine and Biology*, vol. 53, pp. 1397-1412, 2008.
- [37] TSI Incorporation, "Phase Doppler Particle Analyzer". 500 Cardigan Road / Shoreview, MN 55126 / USA Patent 1990048, November 2005.
- [38] K. Koraitem, "Characterization of Conical and Elliptical Fuel Spray Nozzles sing Non-Intrusive Laser Diagnostic Methods," Concordia University, Montreal, 2011.
- [39] G. Westerwheel and J. Rotterdam, Digital Particle Image Velocimetry, Delft University, 1993.
- [40] J. D. Schwazkopf, J. S. Shakal, Koyoto and Courtney Bonnucelli, "A new method for

minimizing volumetric flux errors associated with PDPA measurements in the dilute region of full cone swirl atomizers.," *ICLASS*, vol. 163, 2006.

- [41] J. Chin and A. Lefebvre, "Flow patterns in internal-mixing, twin-fluid atomization," *Atomization and Sprays*, vol. 3, no. 4, pp. 463-475, 1993.
- [42] H. Bai and B. Thomas, "Bubble formation during horizontal gas injection into downward flowing liquid," *Metallurgical and Materials Transactions*, vol. 32(B), no. 6, pp. 1143-1159, 2001.
- [43] J. Sutherland, P. Sojka and M. Plesniak, "Entrainment by ligament- controlled effervescent atomizer-produced sprays," *International Journal of Multi-phase Flow*, vol. 23, no. 5, pp. 865-884, 1997.
- [44] J. Luong and P. Sojka, "Unsteadiness in effervescent sprays," *Atomization and Sprays*, vol. 9, no. 1, pp. 87-109, 1999.
- [45] P. Santangelo and P. Sojka, "A holographic investigation of the near nozzlestructure of an effervescent atomizer-produced spray," *Atomization and Sprays*, vol. 5, no. 2, pp. 137-155, 1995.
- [46] S. Sovani, P. Sojka and A. Lefebvre, "Effervescent atomization," *Progress in energy and combustion science*, vol. 27, pp. 483-521, 2001.
- [47] "High Definition Wallpaper," 15 09 2010. [Online]. Available: high-definition-wallpapers.info.
- [48] CNphotography, "CNphotography," Flickr, 12 04 2012. [Online]. Available: www.flickr.com/photos.
- [49] S. Buzz, "Sciencebuzz.org," Freefoto.com, 02 08 2006. [Online]. Available: freefoto.com.
- [50] A. P. JT15D, "Delphi," Delphi, 22 03 2011. [Online]. Available: http://delphi.com/manufacturers/cv/powertrain/injection-systems-and-components/diesel_fuel_injectors/.
- [51] Principle of Jet Engine, "Principles of Jet Engine Operation," [Online], 21 03 2011. [Online]. Available: <http://www.leitemlane.com/jetoperation.htm>.
- [52] Łatka and Leszek, "Mechanical properties of suspension plasma sprayed hydroxyapatite coatings submitted to simulated body fluid," *Surface and Coatings Technology*, vol. 205, no. 4, pp. 954-960, 2010.

Appendix

Appendix A

Flow metering:

P SINGLE TUBE FLOW METERS

INTERCHANGEABLE

Designed for low flow rates, the **Model P** flow meter is a precision instrument embodying the inherent simplicity, versatility and economy of the classical rotameter. It is particularly suitable for metering carrier gases in chromatography, indicating and controlling gases in manufacturing processes, liquid and gas measurement in laboratories, pilot plants, flow and level indicating, etc.

Shipped completely assembled, flow meters include standard mounting fittings in a choice of materials, side plates, thick protective magnifying front shield and back plate, optional built-in control valve, and flow tubes selected from the Flow Capacities tables. Panel mounting style is convertible to bench mounting through the use of the optional acrylic tripod. The tripod has a built-in spirit leveler and leveling screws.

For multiple tube meters see pages 7 and 8.

design features

- ✓ Rib-guided or fluted metering tubes facilitate stable, accurate readings.
- ✓ Magnifier lens in front shield to enhance reading resolution.
- ✓ Interchangeability of flow tubes and floats.
- ✓ Ease of installation and exchange of flow tubes.
- ✓ "Non-rotating" adapter feature - glass flow tubes are prevented from turning during the tightening phase of the assembly procedure.
- ✓ OPTIGRAD™ scales minimize parallax and eye fatigue.
- ✓ Chemical compatibility.
- ✓ Simple means of panel mounting.

126 4492

150 mm Meter with CV™ Valve

P1161-baa
a-102
-05
-Sa
-va

Wee 1 232

catalogue Pdf

P-X Technical

65 mm Meter with MFV™ Valve

5 WWW.AALBORG.COM - E-MAIL INFO@AALBORG.COM - PHONE 845.770.3000 - TOLL FREE IN U.S.A. AND CANADA 1.800.866.3837 - ORANGEBURG N.Y. U.S.A.

BUILT-IN VALVES

Meters are available with built-in needle valves (CV™), high precision metering valves (MFV™) with “non-rising stems”, or with no valves. The higher cost of MFV™ valves is justified whenever high sensitivity control and resolution are desirable particularly in conjunction with metering tubes of very low flow rates.

Generally, for gas metering it is recommended that valves are positioned at inlets (bottom) for liquids valves may be positioned either at inlets or outlets (top). For vacuum services, valves must be mounted at outlets. If unspecified at the time of ordering, meters will be shipped with valves mounted at the inlets.

Panel mounting is convertible to bench mounting through the use of an optional acrylic tripod base with spirit leveler (catalog No. TP1).

SPECIFICATIONS

| | |
|--------------------------------------|--|
| STANDARD ACCURACY | ±2% FS (mm scales) except 042 flow tubes. ±5% FS (direct reading scales) and 042 mm. |
| CALIBRATED ACCURACY | ±1% FS. |
| REPEATABILITY | ±0.25%. |
| USEFUL FLOW RANGE | 10:1 minimum with one float and better than 20:1 with combination of two floats installed in meters. |
| MAXIMUM OPERATING PRESSURE | 200 psig/13.8 bars. |
| MAXIMUM OPERATING TEMPERATURE | 250 °F/ 121 °C. |

****MATERIALS OF CONSTRUCTION**

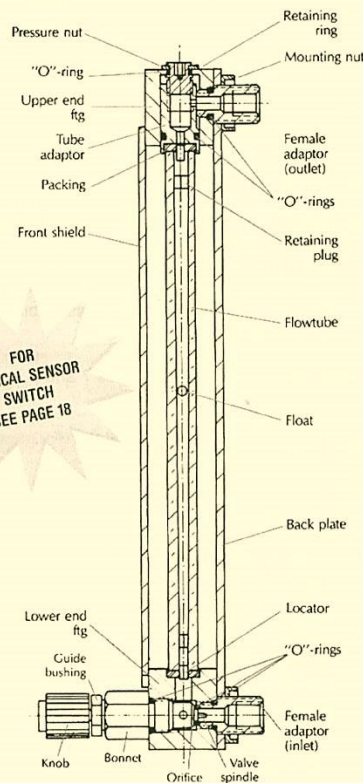
| | |
|---|--|
| FLOW TUBES | Heavy walled borosilicate glass. |
| FLOATS | Glass, Sapphire, 316 Stainless Steel, Carboly [®] and Tantalum. |
| CHOICE OF MOUNTING FITTINGS IN CONTACT WITH FLUIDS | a) Aluminum, black anodized. b) Brass, chrome plated. c) 316 stainless steel. |
| SIDE PANELS | Aluminum, black anodized. |
| FRONT SHIELD | Lexan [®] with longitudinal magnifier lens for enhanced reading resolution. |
| BACK PLATE | 1/8" thick white acrylics. |
| O-RINGS AND PACKING | Buna-N [®] o-rings in aluminum/ brass model. Viton [®] o-rings in stainless steel meters. OPTIONAL Viton [®] PTFE Kalrez [®] and EPR. |
| CONNECTIONS | 1/8" NPT female inlet and outlet connections. OPTIONAL 1/4" FNPT, hose and compression fittings are available. |

BULLETIN EN030710 P

**The selection of materials of construction, is the responsibility of the customer. The company accepts no liability.

WWW.AALBORG.COM - E-MAIL ✉ : INFO@AALBORG.COM - PHONE ☎ 845.770.3000 - TOLL FREE IN U.S.A. AND CANADA 1.800.866.3837 - ORANGEBURG N.Y. U.S.A. 6

Select flow tube consistent with requirements from flow capacity tables 6 to 23 (page 38 to 44).



Assorted flow tubes may be used in conjunction with a single mounting frame, an apparent benefit in many laboratory applications.

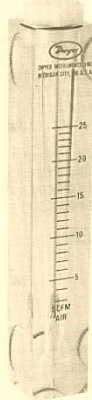
Ordering information see page 9.
Dimensional information see page 8.



VFC Series Visi-Float® Flowmeter

Bulletin F-48

Specifications - Installation and Operating Instructions



Back Connections

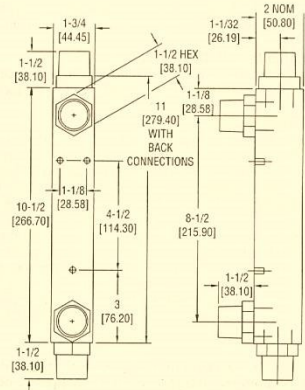
Dwyer Series VFC Visi-Float® flowmeters are available in two basic styles, either back or end connected with direct reading scales for air or water. Installation, operation, and maintenance are simple and require only a few common sense precautions to assure long, accurate, trouble-free service.

CALIBRATION

All Dwyer flowmeters are calibrated at the factory and normally will remain within their accuracy tolerance for the life of the device. If at any time you wish to re-check its calibration, do so only with instruments or equipment of certified accuracy. Do not attempt to check the Dwyer Visi-Float® flowmeter with a similar flowmeter as even minor variations in piping and back pressure can cause significant differences between the indicated and actual readings. If in doubt, your Dwyer flowmeter may be returned to the factory and checked for conformance at no charge.

LOCATION

Select a location where the flowmeter can be easily read and where the temperature will not exceed 120°F (49°C). The mounting surface and piping to the flowmeter should be free from vibration which could cause fatigue of fittings or mounting inserts. Piping must be carefully arranged and installed to avoid placing stress on fittings and/or flowmeter body. Avoid locations or applications with strong chlorine atmospheres or solvents such as benzene, acetone, carbon tetrachloride, etc. Damage due to contact with incompatible gases or liquids is not covered by warranty. Compatibility should be carefully determined before placing in service.



SPECIFICATIONS

Service: Compatible gases & liquids.

Wetted Materials:

- Body: Acrylic plastic.
- O-Ring: Buna-N (Viton® available).
- Metal Parts: Stainless steel.
- Float: Stainless steel.

Temperature & Pressure Limits: 100 psig (6.9 bar) @ 120°F (48°C).

Accuracy: 2% of full scale.

Process Connection: VFC: 1" female NPT back connections. End connections optional. VFCII: 1" male NPT back connections. End Connections optional.

Scale Length: 5" typical length.

Mounting Orientation: Mount in vertical position.

Weight: 24-25 oz (.68-.71 kg).

PIPING

Inlet Piping:

It is good practice to approach the flowmeter inlet with as few elbows, restrictions and size changes as possible. Inlet piping should be as close to the flowmeter connection size as practical to avoid turbulence which can occur with drastic size changes. The length of inlet piping has little effect on normal pressure fed flowmeters.

For vacuum service, the inlet piping should be as short and open as possible to allow operation at or near atmospheric pressure and maintain the accuracy of the device. Note that for vacuum service, any flow control valve used must be installed on the discharge side of the flowmeter.

DWYER INSTRUMENTS, INC.
P.O. BOX 373 • MICHIGAN CITY, IN 46361 U.S.A.

Phone: 219/879-8000
Fax: 219/872-9057

www.dwyer-inst.com
e-mail: info@dwyer-inst.com

Discharge Piping

Piping on the discharge side should be at least as large as the flowmeter connection. For pressure fed flowmeters on air or gas service, the piping should be as short and open as possible. This allows operation at or near atmospheric pressure and assures the accuracy of the device. This is less important on water or liquid flowmeters since the flowing medium is generally incompressible and back pressure will not affect the calibration of the instrument.

POSITION AND MOUNTING

All Visi-Float® flowmeters must be installed in a vertical position with the inlet connection at the bottom and outlet at the top.

Surface Mounting

Drill three holes in panel using dimensions shown in drawing. Holes should be large enough to accommodate #10 - 32 machine screws. If back connected model, drill two additional holes for clearance of fittings. Install mounting screws of appropriate length from rear. Mounting screws must not be longer than the panel thickness plus 1/4" (9.66 mm), or the screw will hit the plastic and may damage the meter. The screws will require additional force during the initial installation, since the insert boots are of a collapsed thread type and must be expanded into the plastic for the knurled surface to take hold. Insert boots will not have the proper 10-32 threads until the first screw has been inserted to expand the boot. Attach piping using RTV silicone sealant or Teflon® tape on threads to prevent leakage.

CAUTION: Do not overtighten fittings or piping into fittings. Maximum recommended torque is 10 ft. (lbs) (13.56 newton (meter)). Hand tighten only.

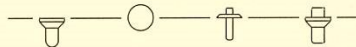
In Line Mounting

Both end connected and back connected models may be installed in-line supported only by the piping. Be sure that flowmeter is in a vertical position and that piping does not create excess stress or loading on the flowmeter fittings.

OPERATION

Once all connections are complete, introduce flow as slowly as possible to avoid possible damage. With liquids, make sure all air has been purged before taking readings. Once the float has stabilized, read flow rate by sighting across the largest diameter of the float to the scale graduations on the face of the device.

The standard technique for reading a Variable Area Flowmeter is to locate the highest point of greatest diameter on the float, and then align that with the theoretical center of the scale graduation. In the event that the float is not aligned with a grad, an extrapolation of the float location must be made by the operator as to its location between the two closest grads. The following are some sample floats shown with reference to the proper location to read the float.



Variable Area Flowmeters used for gases are typically labeled with the prefix "S" or "N", which represents "Standard" for English units or "Normal" for metric units. Use of this prefix designates that the flowmeter is calibrated to operate at a specific set of conditions, and deviation from those standard conditions will require correction for the calibration to be valid. In practice, the reading taken from the flowmeter scale must be corrected back to standard conditions to be used with the scale units. The correct location to measure the actual pressure and temperature is at the exit of the flowmeter, except under vacuum applications where they should

be measured at the flowmeter inlet. The equation to correct for nonstandard operating conditions is as follows:

$$Q_c = Q_o \times \sqrt{\frac{P_1 \times T_1}{P_2 \times T_2}}$$

Where: Q_c = Actual or Observed Flowmeter Reading
 Q_o = Standard Flow Corrected for Pressure and Temperature

P_1 = Actual Pressure (14.7 psia + Gage Pressure)

P_2 = Standard Pressure (14.7 psia, which is 0 psig)

T_1 = Actual Temperature (460 R + Temp °F)

T_2 = Standard Temperature (530 R, which is 70°F)

Example: A flowmeter with a scale of 10-100 SCFH Air. The float is sitting at the 60 grad on the flowmeter scale. Actual Pressure is measured at the exit of the meter as 5 psig. Actual Temperature is measured at the exit of the meter as 85°F.

$$Q_c = 60.0 \times \sqrt{\frac{(14.7 + 5) \times 530}{14.7 \times (460 + 85)}}$$

$$Q_c = 68.5 \text{ SCFH Air}$$

MAINTENANCE

The only maintenance normally required is occasional cleaning to assure proper operation and good float visibility.

Disassembly

The flowmeter can be completely disassembled by removing the connection fittings and top plug. When lifting out the float guide assembly, be careful not to lose the short pieces of plastic tubing on each end of the guide rod which serve as float stops.

Cleaning

The flowmeter body and all other parts can be cleaned by washing in a mild soap and water solution. A soft bristle bottle brush will simplify cleaning of the flow tube. Avoid benzene, acetone, carbon tetrachloride, gasoline, alkaline detergents, caustic soda, liquid soaps, (which may contain chlorinated solvents), etc., and avoid prolonged immersion.

Re-assembly

Install the lower fitting and then the float and float guide. Finally install the upper fitting and plug being certain that both ends of the float guide are properly engaged and the float is correctly oriented. A light coating of silicone stop cock grease or petroleum jelly on the "O" rings will help maintain a good seal as well as ease assembly.

ADDITIONAL INFORMATION

For additional flowmeter application information, conversion curves, correction factors and other data covering the entire line of Dwyer flowmeters, please request a Dwyer full-line catalog.

Appendix B

PIV and PDPA Specifications

Solo Specifications

The following tables show the Solo specifications for the different models available. Specifications are subject to change without notice.

Solo PIV Products

Solo I-15 Solo II-15 Solo II-30 Solo III-15 Solo IV-50 Solo 120XT Solo 200XT

| | | Solo I-15 | Solo II-15 | Solo II-30 | Solo III-15 | Solo IV-50 | Solo 120XT | Solo 200XT |
|------------------------------------|--------|-----------|------------|------------|-------------|------------|------------|------------|
| Repetition Rate (Hz) | | 15 | 15 | 30 | 15 | 50 | 15 | 15 |
| Energy ¹ (mJ) | 532 nm | 15 | 30 | 30 | 50 | 50 | 120 | 200 |
| | 266 nm | NA | NA | NA | NA | NA | 20 | 30 |
| Energy Stability ² (±%) | 532 nm | 4 | 4 | 4 | 4 | 6 | 4 | 4 |
| | 266 nm | NA | NA | NA | NA | NA | 9 | 9 |
| Beam Diameter (mm) | | 2.5 | 2.5 | 2.5 | 3.5 | 3.5 | 4.5 | 5.5 |
| Pulse Width ³ (ns) | | 3-5 | 3-5 | 3-5 | 3-5 | 3-5 | 3-5 | 3-5 |
| Divergence ⁴ (mrad) | | < 3 | <3 | <3 | <4 | <5 | <3 | <3 |
| Beam Pointing Stability (urad) | | <100 | <100 | <100 | <100 | <200 | <100 | <100 |
| Jitter (±ns) ⁵ | | 1 | 1 | 1 | 1 | 1 | 1 | 1 |

1. Optical losses due to optional attenuator will reduce maximum energy by 10%.
2. Pulse-to-pulse for 98% of shots after 30 minute warm up.
3. Full width half maximum.

4. Full angle for 86% of the energy, at 1/e² point.
5. From Q-Switch synchout to light pulse for 98% of 1000 shots.

Physical Characteristics

| | Laser Head* | | | Power Supply | | |
|------------------|------------------|-------------------|-----------------|-----------------|-----------------|----------------|
| | Solo I, II, III | Solo IV, 120 | Solo 200 XT | Solo I, II, III | Solo IV, 200 | Solo 120XT |
| Length | 13.775" / 350 mm | 22.4"/569 mm | 24.4"/620 mm | 18.15" / 461 mm | 22.0" / 559 mm | 20.9"/531 mm |
| Width | 7.0" / 178 mm | 9.8"/249 mm | 9.24"/235 mm | 7.75" / 194 mm | 10.8" / 275 mm | 8.7"/221 mm |
| Height | 3.187" / 81 mm | 4.86"/123 mm | 4.86"/123 mm | 14.32" / 363 mm | 15.8" / 402 mm | 15.5"/394 mm |
| Weight | 10 lbs. / 4.5 kg | 32.5 lbs./14.8 kg | 40 lbs./18.2 kg | 48 lbs. / 22 kg | 53 lbs. / 24 kg | 50.7 lbs/23 kg |
| Length Umbilical | 8 ft / 2.4 m | 10 ft / 3 m | 10 ft / 3 m | | | |

* Width and Height include mounting plate

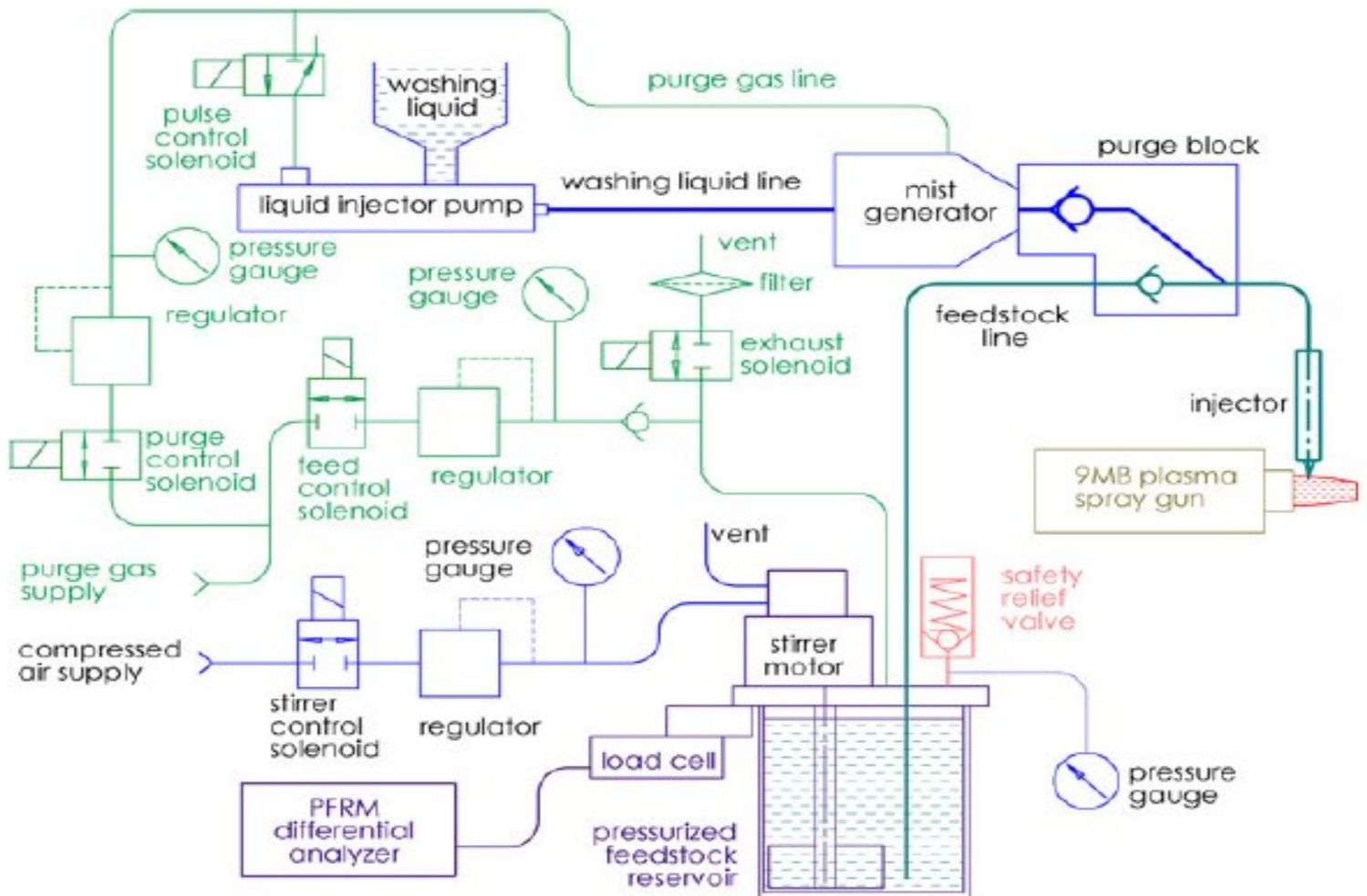
Operating Requirements

Table 2-1: Solo Performance Specifications

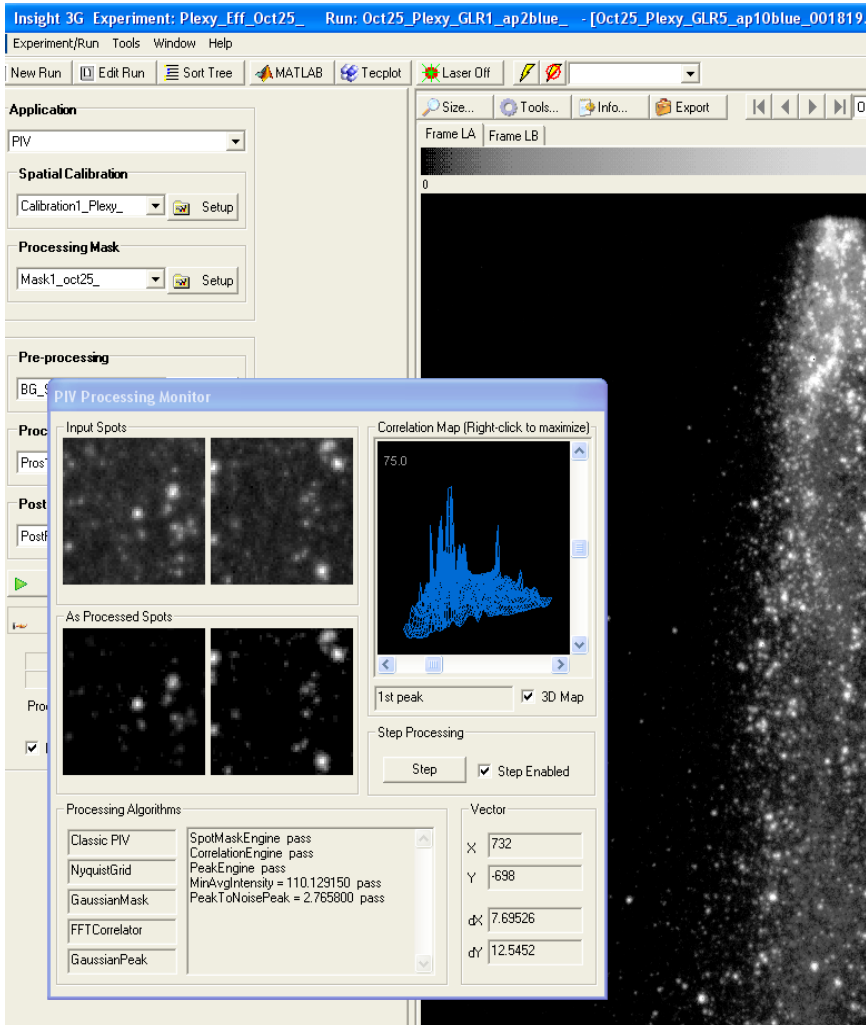
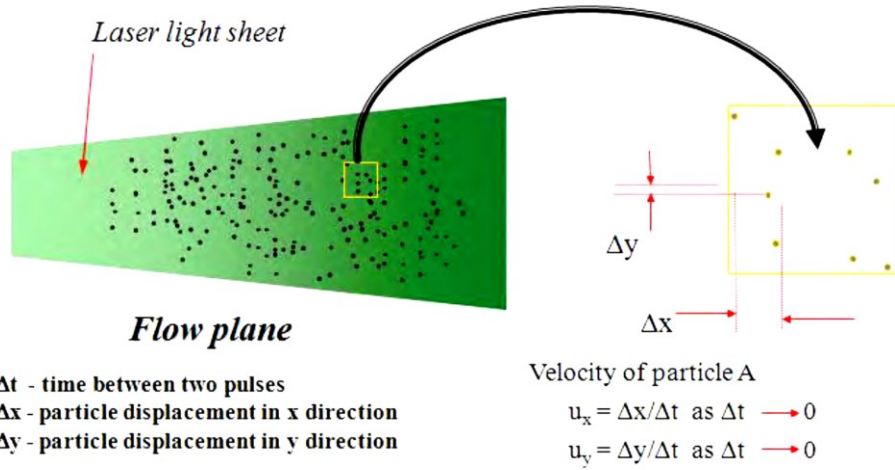
| | | |
|-------------------|------------------------------------|----------------------------------|
| Temperature | 50° – 86° ±10° F (10° – 30° ±5° C) | |
| Relative Humidity | 20—80% non-condensing | |
| Voltage | 100—240 V, 50/60 Hz | |
| Power | Solo I, II, III | 15 Hz-300 watts; 30 Hz-500 watts |
| | Solo 120XT | 1000 watts |
| | Solo IV, 200XT | 1500 watts |

Appendix B

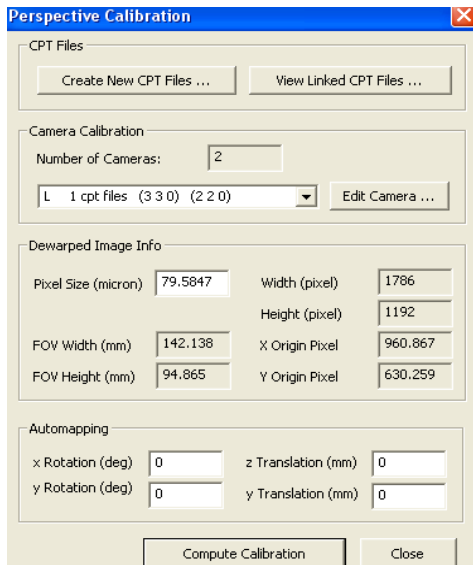
Thermal Spray Coating Setup:



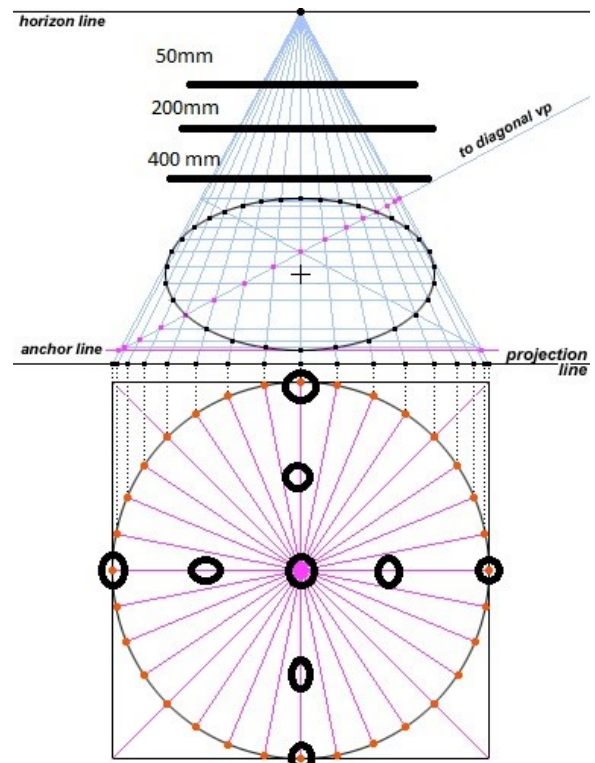
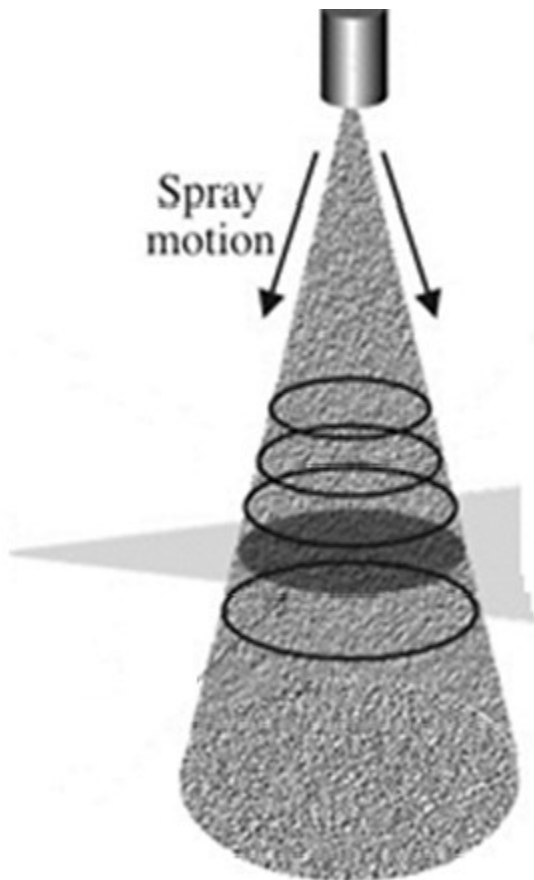
PIV Technique Fundamental Concept:



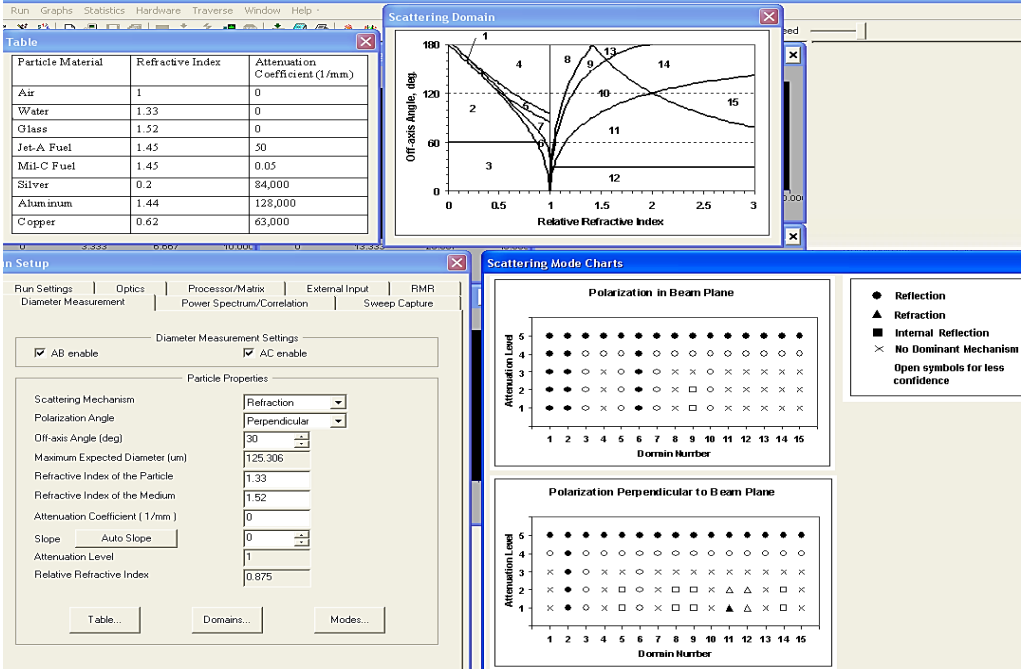
PIV Perspective Calibration Algorithm settings:



PDPA Measured Points (Position Matrix):



PDDA Diameter Measurements Settings:



Selecting an optical layout for particle diameter sizing considering refractive index and light attenuation coefficient level and standard perpendicular polarization the atomized flow

Appendix C

Tensiometer

Calibration

The calibration of the torsion wire and hence of the Surface Tensiometer has been carefully tested at the factory but should be checked before use and adjusted if necessary. The calibration is carried out so that the dial will read directly in dynes/cm.

Make sure that the torsion arm arrest mechanism is holding the arm. Hang the platinum-iridium ring on the hook at the left end of the lever. Cut a small strip of paper and fit it onto the ring to act as a platform for a weight which will be used for the calibration. Release the torsion arm, and adjust the knob on the right side of the case until the index and its image are exactly in line with the reference line of the mirror. Turn the knob beneath the main dial on the front of the instrument until the vernier reads zero on the outer scale of the dial. Arrest the torsion arm.

Place a known mass for calibration on the paper platform (600 milligrams is quite suitable and simplifies calculations). Release the torsion arm. Turn the knob on the right side of the case in a counterclockwise direction until the index and its image are again exactly in line with the reference line of the mirror. Record the dial reading to the nearest 1/10 scale division (by use of the vernier).

It is now necessary to determine the accuracy of the calibration from the reading obtained. The apparent surface tension, S , is given as follows:

$$S = \frac{Mg}{2L} \quad \text{Where:}$$

- M = The weight expressed in grams
- g = Acceleration of gravity expressed in cm/sec^2
- L = Mean circumference of the ring in cm
- S = Dial reading = Apparent Surface Tension in dynes per cm

For example, suppose that a 600 mg weight was used. The circumference of the ring is 6.00 cm and the value for g is $980 \text{ cm}/\text{sec}^2$. Then we find that:

$$S = \frac{Mg}{2L} = \frac{0.6 \times 980}{2 \times 6} = 49.00 \text{ dynes/cm}$$

If the dial reading differs from the calculated value, then

Converting Scale Readings

The Surface Tensiomat measures apparent surface tension and apparent interfacial tension. In order to obtain the true surface tension or true interfacial tension, the relationship:

$$S = P \times F$$

is used, where S is the true value, P the apparent value as indicated by the dial reading and F a correction factor. The correction factor F is dependent on the size of the ring and the size of wire used in the ring, the apparent surface or interfacial tension and the densities of the two phases. The relationships are expressed by the following two forms, either one of which may be used in preparing a correction factor chart.

$$1. (F - a)^2 = \frac{4b}{(\pi R)^2} \times \frac{P}{D - d} + K$$
$$2. F = 0.7250 + \sqrt{\frac{0.01452 P}{C^2 (D - d)} + 0.04534 - \frac{1.679 r}{R}}$$

where:

- F = the correction factor
- R = the radius of the ring
- r = the radius of the wire of the ring
- P = the apparent value or dial reading
- D = the density of the lower phase
- d = the density of the upper phase
- K = $0.04534 - 1.679 r/R$
- C = the circumference of the ring
- a = 0.725
- b = 0.0009075

The a, b and the numerical part of K are universal constants for all rings.

The correction factor is most easily determined by reference to a chart prepared from the formula. In order to use a correction factor chart, the operator must initially calculate the value of the expression $P/(D - d)$ for each sample and know the value of R/r . For the Surface Tensiometer, the circumference of the ring is 6 cm and the radius of the wire is .007". There may be some slight variation in these dimensions, but the value of R/r is usually 53.2. Curves are shown for $R/r = 50$ and $R/r = 60$, so that correction

Appendix D

Image Processing Codes

Main functions used for image processing by Matlab toolbox are:

- 1- normxcorr2
- 2-imread, imshow, subimage
- 3- bwboundaries
- 4-adapthisteq, imnoise
- 5- stretchlim
- 6-convmetx2, fspecial,

Code 1:

```
function createfigure(cdata1)
%CREATEFIGURE(CDATA1)
% CDATA1: image cdata

% Auto-generated by MATLAB on 01-Jul-2013 20:14:09

% Create figure
figure1 = figure;
colormap('gray');

% Create axes
axes1 = axes('Visible','off','Parent',figure1,'YDir','reverse',...
    'TickDir','out',...
    'Position',[0.0966942148760331 0.066429418742586 0.805981896890988
0.898378805852115],...
    'Layer','top',...
    'DataAspectRatio',[1 1 1],...
    'CLim',[0 255]);
% Uncomment the following line to preserve the X-limits of the axes
% xlim(axes1,[0.5 1024.5]);
% Uncomment the following line to preserve the Y-limits of the axes
% ylim(axes1,[0.5 1136.5]);
box(axes1,'on');
hold(axes1,'all');

% Create image
image(cdata1,'Parent',axes1,'CDataMapping','scaled');
```

Code 2:

```
function initSize(im_handle,screen_per_image_pixel,isBorderTight)
%initSize Initialize size of axes and figure
%
%   initSize(imH,screenPerImagePixel,isBorderTight) adjusts the display
%   size of an image by using the image size and the scale factor
%   screenPerImagePixel. If screenPerImagePixel==1,then the display has
one
%   screen pixel for each image pixel. If isBorderTight is false, then
%   initSize adds gutters for displaying axes and tick labels.
%
%   Note: The code assumes that it is calculating the size for a figure
that
%   contains a single axes object with a single image. Other uicontrols
%   and uipanelns are not taken into account.

%   Copyright 1993-2008 The MathWorks, Inc.
%   $Revision: 1.1.8.6 $   $Date: 2008/11/24 14:58:41 $

ax_handle = ancestor(im_handle,'axes');
fig_handle = ancestor(ax_handle,'figure');

ax_units = get(ax_handle, 'Units');
fig_units = get(fig_handle, 'Units');
root_units = get(0, 'Units');

image_width = getImWidth(im_handle);
image_height = getImHeight(im_handle);

if (image_width * image_height == 0)
    % Don't try to handle the degenerate case.
    return;
end

% Work in pixels
set(ax_handle, 'Units', 'pixels');
set(fig_handle, 'Units', 'pixels');
set(0, 'Units', 'pixels');

ax_pos = get(ax_handle, 'Position');
fig_pos = get(fig_handle, 'Position');

orig_fig_width = fig_pos(3);
orig_fig_height = fig_pos(4);

% Declare so they're in function scope
on_screen_image_width = [];
on_screen_image_height = [];
new_fig_width = [];
new_fig_height = [];
```

```

is_width_bigger_than_screen = false;
is_height_bigger_than_screen = false;

% get the size of the screen area available for display
% excludes areas used by OS for taskbar, dock, etc.
wa = getWorkArea;
screen_width = wa.width;
screen_height = wa.height;

% get figure properties
p = figparams;

% to initialize dimensions
calculateDimensions

% adjust size until the figure fits on the screen
warn_about_mag = false;
while (is_width_bigger_than_screen || is_height_bigger_than_screen)
    screen_per_image_pixel =
findZoomMag('out', screen_per_image_pixel);
    warn_about_mag = true;
    calculateDimensions % to update dimensions
end

if warn_about_mag
    wid = sprintf('Images:%s:adjustingMag', mfilename);
    warning(wid, ...
        'Image is too big to fit on screen; displaying at
%d%%', ...
        round(screen_per_image_pixel*100));
end

% Don't try to display a figure smaller than this:
min_fig_width = 128;
min_fig_height = 128;
new_fig_width = max(new_fig_width, min_fig_width);
new_fig_height = max(new_fig_height, min_fig_height);

% Figure out where to place the axes object in the resized figure.
ax_pos(1) = getAxesX;
ax_pos(2) = getAxesY;
ax_pos(3) = max(on_screen_image_width, 1);
ax_pos(4) = max(on_screen_image_height, 1);

% Calculate new figure position
fig_pos(1) = max(1, fig_pos(1) - floor((new_fig_width -
orig_fig_width)/2));
fig_pos(2) = max(1, fig_pos(2) - floor((new_fig_height -
orig_fig_height)/2));

fig_pos(3) = new_fig_width;
fig_pos(4) = new_fig_height;

% Translate figure position if necessary, using size of work area,
% figure decoration sizes and figure position

```

```

dx = (screen_width - p.RightDecoration) - (fig_pos(1) + fig_pos(3));
if (dx < 0)
    fig_pos(1) = fig_pos(1) + dx;
end
dy = (screen_height - p.TopDecoration) - (fig_pos(2) + fig_pos(4));
if (dy < 0)
    fig_pos(2) = fig_pos(2) + dy;
end

set(fig_handle, 'Position', fig_pos)
set(ax_handle, 'Position', ax_pos);

% Restore the units
set(fig_handle, 'Units', fig_units);
set(ax_handle, 'Units', ax_units);
set(0, 'Units', root_units);

constrainToWorkArea(fig_handle);

%-----
function calculateDimensions
    on_screen_image_width = image_width * screen_per_image_pixel;
    on_screen_image_height = image_height * screen_per_image_pixel;

    new_fig_width = on_screen_image_width + getGutterWidth;
    new_fig_height = on_screen_image_height + getGutterHeight;

    is_width_bigger_than_screen = ...
        (new_fig_width + p.horizontalDecorations) > screen_width;
    is_height_bigger_than_screen = ...
        (new_fig_height + p.verticalDecorations) > screen_height;
end

%-----
function w = getGutterWidth

    if isBorderTight
        w = 0;
    else
        w = p.looseBorderWidth;
    end

end

%-----
function h = getGutterHeight

    if isBorderTight
        h = 0;
    else
        h = p.looseBorderHeight;
    end

end

end

```

```

%-----
function x = getAxesX

    if isBorderTight
        x = 1;
        % If the on screen image width is less than the new figure
width,
        % need to recenter the axes. This occurs for small images
        % displayed with less than 128 pixels in width.
        if new_fig_width > on_screen_image_width
            extra_width_in_pixels = new_fig_width -
on_screen_image_width;
            x = extra_width_in_pixels / 2;
        end

    else
        x = p.YLabelWidth + 1;
    end

end

%-----
function y = getAxesY

    if isBorderTight
        y = 1;
        % If the on screen image height is less than the new figure
height,
        % need to recenter the axes. This occurs for small images
        % displayed with less than 128 pixels in height.
        if new_fig_height > on_screen_image_height
            extra_height_in_pixels = new_fig_height -
on_screen_image_height;
            y = extra_height_in_pixels / 2;
        end

    else
        y = p.XLabelHeight + 1;
    end

end

```